CHEVVA, HARISH, Ph.D. Solid-State Synthesis of Silver Nanowires by Green Chemistry and Mechanistic Aspects Influencing Nanowire Growth and Plasmonic Study in Au Thin Film/MoS_2 Heterostructures for Surface Enhanced Raman Spectroscopy. (2019) Directed by Dr. Jianjun Wei. 148 pp.

This thesis has a research focus on novel nanomaterials synthesis, fabrication and the fundamental understanding of the process and properties regarding surface enhanced Raman spectroscopy application. The two projects are: 1) a novel solid-state growth of silver nanowires (AgNWs), and 2) fabrication of 2D layered MoS_2 on gold film for surface enhanced Raman spectroscopy (SERS).

Solid-state and bottom-up growth of nanowires-based research has been specific to semi-conductor nanowires, with rare research reports on the growth of metal nanowires in the similar manner. Synthesis of AgNWs has been around in the research filed for more than a decade. Most of the synthesis processes reported till now were all solution-based processes involving complex synthesis set-up employing harsh conditions for good yield. This research presents a solid-state green synthesis of AgNWs with detailed growth analysis, reporting key factors influencing the self-growth of the nanowires. Our synthesis process is simple, performed at room temperatures and uses bio-compatible chitosan polymer as base for silver nanoparticles (AgNPs) synthesis and AgNWs growth. A new way of blocking oxygen by thin film coating, to avoid oxidative etching of Ag atoms which hinders growth of AgNWs, is investigated. Role of Cl^- ions and influence of its concentration to initiate the growth AgNWs is examined thoroughly with the help of UV-Vis, XRD and EDS analysis. Finally, role of time in the continuous growth of AgNWs is studied for seven weeks long under SEM. AgNWs/Chitosan

polymer platform is directly employed in SERS application to detect Raman active probe Rhodamine 6G (R6G) at a detection limit of 10^{-7}M. This report, for the first time, presents an inexpensive synthetic and growth mechanism for solid-state and bottom-up growth of metal nanowires. This research helps in paving a new way for research involved with Ag nanowires.

2D materials other than graphene which made their presence strong in research field are transition metal dichalcogenides (TMDCs). Among a range of TMD materials, Molybdenum disulfide (MoS_2) has shown promising impact in various fields like optoelectronics, SERS based biosensors, photonics and electrochemistry. SERS enhancement observed in semiconductor (1.8ev) monolayer MoS_2 is due to various factors like surface plasmons, excitons and charge transfer. But, monolayer MoS_2 exhibit a modest Raman enhancement (<100) when compared to other 2D materials like graphene. Multilayer MoS_2 which have lower bandgap (1.4ev to 1.6ev) exhibits no SERS enhancement due to increase in the thickness of the material. Lower SERS enhancement property of monolayer MoS_2 is addressed by incorporation of nanoparticles on the surface of MoS_2 and with the combination of MoS_2 and metal nanostructures. But, there are very less reports on dealing with few layers MoS_2 SERS enhancement. Here, in this report we observed raise in intensity of primary Raman signals E_{2g}^1 and A_{1g} of few layer MoS_2 with respect to change in thickness of Au film substrates on which MoS_2 is deposited. Thorough optical and Raman analysis proved that along with monolayer MoS_2, few layers MoS_2 which are deposited on gold film also exhibit promising results in showing SERS enhancement for the detection of Raman active probe R6G. Further,

thickness dependence of underneath Au film influencing the SERS property of particularly few layers of MoS_2 is validated using Raman analysis supported by FDTD simulation data. The results proved thickness of 150nm Au showing highest enhancement in both increasing the intensity of MoS_2 Raman peaks and in detection of R6G molecule at the concentration of 10^{-6}M. These findings and understanding of the behavior of few layer MoS_2/gold film expand the use of MoS_2 on wide range of SERS applications.

SOLID-STATE SYNTHESIS OF SILVER NANOWIRES BY GREEN CHEMISTRY AND MECHANISTIC ASPECTS INFLUENCING NANOWIRE GROWTH AND PLASMONIC STUDY IN AU THIN FILM/MOS_2 HETEROSTRUCTURES FOR SURFACE ENHANCED RAMAN SPECTROSCOPY

by

Harish Chevva

A Dissertation Submitted to
the Faculty of The Graduate School at
The University of North Carolina at Greensboro
in Partial Fulfillment
of the Requirements for the Degree
Doctor of Philosophy

Greensboro
2019

Approved by

_____

Committee Chair

To my late. Dad, beloved Mom, Grand Parents, Sister, Uncle & Family, Friends and to my loving Wife & Family – Who Have all Supported My Endeavors to this point.

APPROVAL PAGE

This dissertation written by Harish Chevva has been approved by the following committee of the Faculty of The Graduate School at The University of North Carolina at Greensboro.

Committee Chair _____

Jianjun Wei

Committee Members

_____

Dennis R. LaJeunesse

_____

Joseph Starobin

_____

Tetyana Ignatova

_____

Date of Acceptance by Committee

_____

Date of Final Oral Examination

TABLE OF CONTENTS

Page

LIST OF TABLES

Page

LIST OF FIGURES

Page

CHAPTER I

INTRODUCTION

Silver nanowires synthesis procedures has been in the research field for more than a decade. Most common method employed for the growth of silver nanowires is polyol method[1], which is a solution based process. This process primarly uses PVP as stabilizing agent and ethlyne glycol as reducing agent to convert silver precursor to silver nanoparticles and eventually to silver nanowires when subjected to additional chemical and mechanistic conditons[2]. Once the silver nanowires of desired aspect ratio are obtained, using series of filteration and cleaning processes nanowires are separated from polymer solution and trasfered to various substrates for employing them in for different applications[3].

The prime motive of this study lies in establishing a completely new way of synthesizing silver nanowires in solid-state and investigating science behind the reported growth[4]. Synthetic and mechanistic parameters influencing the growth of silver nanowires has been reported. Chitosan polymer which is abundantly avaialble in nature[5] and is also a bio-compatible polymer is used as both reducing and stabilizing agent in our study to form silver nanoparticles. Chitosan ploymer and halide additive NaCl incorporated in the form of AgCl nanoparticles inside the ploymer matrix forms base for the growth of silver nanowires in the solid state. Time lapse studies on the Ag/Chitosan film shows the gradual self growth of AgNWs from the film, demosntrating

the basic science of slow relase of Ag^+ ions from the AgCl nanoparticles insdie the chitosan polymer helping to form AgNWs

MoS_2, a new age 2 D material which belongs to Transition metal dichalcogenides (TMDs) family generated wide interest in research community in recent times[6]. This is due to its tunable bandgap property, where MoS_2 have a direct bandgap of 1.8ev when the material is in monolayer form and an indirect bandgap of 1.2ev when it is in bulk form[7]. Three primary methods avaliable for fabricating monolayer and few layers of MoS_2 are: 1. chemical vapor deposition[8], which uses Molybdenum trioxide and Sulfur powder as surfacants in high temparature furnace to obtain large area mono layer MoS_2, 2. Chemical exfoliation of bulk MoS_2 by lithium ion intercalation between layers of MoS_2 and followed by dissciaition of layers to obtain monolayer of MoS_2 in solution[9], 3. Traditional mechanical exfoliation method, executed by using scotch tape and peeling off the layers and transfering on to the desired substrates[10]. With extensive research on monolayer MoS_2 direct band gap property, many researchers have reported unique optical properties of monolayer MoS_2.

In our study, we investigated the behavior of few layer MoS_2 in terms of its Raman enahncement when tranfered on to the Au film using mechanical exfoliation method. This phenomenon is reported to be observed due to the plasmons generated on the surface of the Au thin film. Which is stongly supported by FDTD simulation results under similar expermentation conditons. Further SERS enhancement is obtained for the detection of Raman probe molecule on the surface of few layers MoS_2/Au thin film

heterostructure, which is higher when compared to similar number layers deposited on glass substrate.

1.1 Synthesis of Silver Nanowires in Solid-State

1.1.1 Synthesis Methods of Silver Nanoparticles

Silver metal nanomaterials are synthesized by a variety of different methods including photochemical approaches that utilize the light sensitive aspects of precursor materials, standard chemical approaches using citrate or borate reducing agents, and "green" approaches that use a biological material in at least step of the synthesis process[11-13]. Nanoparticle synthetic processes involve several steps that include the reduction of a metal ion in solution into an insoluble precipitate; the formation of a nucleation site either from individual precipitated nanoparticles or through the aggregation of these particles; the stabilization of the nascent particle, which is followed by the nanoparticle growth[11, 12, 14]. Control of each of these steps has enabled the control over the size, crystallinity and morphology of the nanomaterial products from specific synthetic reactions[15, 16].

Several green synthetic methods for generating silver nanoparticles (AgNPs) have also been developed which use biomolecules such as proteins and polysaccharides to stabilize and promote nucleation[14, 17]. Environmentally friendly "green" methods of nanoparticle synthesis often take advantage of biological self-assembling system or catalysis such as living organism or biopolymers[18, 19]. A polysaccharide AgNP synthetic method uses starch as the capping agent and monomeric β-D-glucose as the reducing agent in an aqueous solution[18]. Extracts of various plants and microorganisms

have also been demonstrated to promote the formation of silver nanoparticles through the participation of protein/peptides in the reduction, nucleation, and stabilization steps[18]. Recently a chitosan photochemical AgNP synthetic method has been described that enables the formation AgNP of different morphology and crystallinity in a wavelength dependent manner[11]. Synthetic processes that generate highly anistropically shaped particles are especially desirable in many applications due to the enhancement of specific optical properties such as surface Plasmon resonance[16].

1.1.2 Synthetic Strategies of Silver Nanowires

Growth of silver nanowires emerges from the controlled conditions subjected to the synthesis process of silver nanoparticles. There are different mechanisms proposed in this process, both in soft chemical synthesis procedures and hard template synthesis procedures. But, due to extensive research and due to the complex mechanisms involved in hard template method (Klaus peppler et al.)[20], synthesis of silver nanowires and study of its mechanistic growth aspects are majorly reported in solution processes which are discussed below.

There are different solution processes for the synthesis of AgNWs as listed by Rycenga et al. [21], such as citrate reduction, silver mirror reaction, polyol synthesis, seed-mediated growth and light-mediated growth. Primary difference between all the listed processes is the reaction energy generation for reducing silver precursor $AgNO_3$ to form AgNPs and eventually AgNWs. Lee and Meisel first reported the synthesis of Ag colloids in solution by reducing $AgNO_3$ with the help of citrate ions. Popular synthetic method to achieve desired growth of Ag nanostructures is seed-mediated growth, where

synthesized nanocrystals are used as seeds for further growth of AgNWs [22]. Likewise, making use of silver interaction with light, photochemical approach is introduced to synthesize high quality Ag nanostructures[23]. Out of all the proposed synthetic methods for AgNPs and AgNWs synthesis most researched method is polyol method, where with specific controls employed into the reaction process high aspect ratio of AgNWs are obtained [1]. Understanding the process of polyol synthesis of AgNWs forms as based for our proposed mechanism for the growth. Detailed discussion on polyol synthesis is presented in next section.

1.1.3 Polyol Synthesis of Silver Nanowires

Polyol synthesis is known for its high degree of control in shaping different structures of silver. By varying different conditions, such as temperature, reagent concentration and inclusion of different halide materials in the reaction system, this synthesis process achieves high throughput of silver nanowires growth. Typically, Ethylene glycol acts as both a solvent and reducing agent, PVP polymer acts as stabilizing agent[24], which promotes the growth of AgNWs and NaCl halide material acts as nucleation points for the growth of AgNWs[25].

At the initial stage of the reduction process, Ag atoms form small clusters of fluctuating structure. As the Ag cluster grow larger, they become more stable and emerge to one of the three predominant structures: single crystalline, single twinned, and multiply twinned. Here, if the reaction system is directed towards formation of single twinned structures, they aggregate together to form AgNPs which are more in spherical shaped. If more of multiply twinned structures are formed, the growth will occur more rapidly at the

twin defects of the seed, resulting in the formation of wires with a pentagonal cross section[26].

Factors that influence the growth of AgNWs in polyol synthesis include, oxidative etching[27], role of Cl^- ions and other kinetic properties related to the external reaction conditions. Multiply twinned structures, which are base for formation of AgNWs are unstable structures, which can be dissociated quickly to form single crystals. Oxygen from air, during the reaction, reacts with the defect sites of multiply twinned structures and dissociates them to single crystals and leads to formation of more spherical structures of Ag. The depiction of the reaction is shown in Figure 1. To avoid the effect of reported oxidative etching, use of Fe^{2+}/ Fe^{3+} in the reaction can reduce the extent of oxidative etching, further performing the reaction in non-oxygen environment to helps in growth of AgNWs. Inclusion of halide ions like Cl^- and Br^-, react with silver precursor in the reaction system and tend to form AgCl compound, where AgCl slowly releases Ag ions into the reaction avoiding quick deformation of multiply twinned structures and helping in the growth of AgNWs. Finally, list of external factors, which helps in formation of AgNWs include, control of reaction temperature, rate of silver precursor injection into the reaction and stirring rate of the reaction system.

With this through background of polyol synthesis for growth of AgNWs, we propose our soli-state growth of AgNWs and present the influencing conditions on the proposed growth.

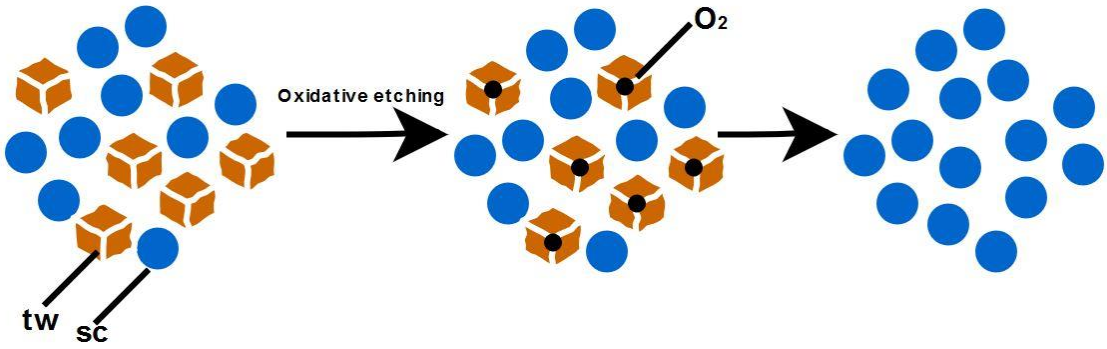

Figure 1. Schematic of Oxidative Etching Process Leading to the Formation of AgNPs

1.1.4 Solid-State Growth of Semiconducting Nanowires

Nanomaterials with dimension of 1-100nm in their lateral dimension are considered as 1D. 1D nanomaterials exist in various forms like wires[28-30], rods[31, 32], ribbons[33-35] and tubes[36-38]. Although there are many potential applications of 1D nanomaterials as both interconnects and functional units in fabrication of electronic devices[39], electrochemical[40, 41], and optical nanodevices[42, 43], when compared to 0D and 2D materials, far less work has been performed in the 1D materials, because of the complexity involved in fabricating of 1D nanomaterials. However, recently, the development of advanced techniques like Vapor-Liquid-Solid (VLS)[44, 45], CVD[46, 47] and many novel chemical methods[48-50], rapid and desired growth has enabled the systematic and consisted generation of new 1D nanomaterials are obtained.

The other methods of synthesizing 1D nanostructures as well as the growth mechanisms underlying these processes have been studied [51-53] and are mainly

divided into two strategies: bottom-up methods, and top-down methods [54, 55]. In all bottom-up methods, the fabrication of the material is controlled at the level of the individual atom thus enabling the arrangement of these atoms to form specific 1D nanostructures such as nanowires. Prominent existing bottom-up methods for 1D nanomaterial synthesis include Vapor-Liquid- Solid (VLS) synthetic methods that has been used to fabricate semiconducting nanowires, and Chemical Vapor Deposition (CVD) methods which has been used to synthesize carbon nanotubes (CNTs). These two methods are solid-state growth of 1D nanostructures; however, there are wet chemical synthesis or solution synthesis methods other that are used for the bottom-up synthesis of 1D nanomaterials including [56] Templated growth with 1D morphologies to direct the formation of 1D nanostructures [57]; Use of super saturation control to modify the growth habit of a seed; Use of appropriate capping agents to kinetically control the growth rates of various facets of a seed [58], and Self-assembly of 0D nanostructures [59, 60]. While bottom-up approaches have been used to generate a wide variety of 1D nanomaterials only a few approaches have been used to generate metallic 1D nanomaterials and none of these methods involves a solid-state approach. To the best of our knowledge, there are no reported research articles under solid-state bottom-up fabrication of 1D metal nanostructures.

1.1.5 Top-down Growth of Silver Nanowires

Top-down method of forming silver nanowires involve extraction of a nanowire from a bulk sample through processes such as electron-beam lithography or mechanical reduction [61]. Currently the only available method to synthesize solid state

semiconducting nanowires [62-64] and metal nanowires [65-67] involve top-down methods in which 1D nanostructures are fabricated using advance laboratory lithographic techniques like E-Beam, Focus Ion Beam (FIB), UV lithography and Reactive Ion Etching (RIE). This form of fabrication is much more labor intensive and economically expensive when compared to current bottom-up approach but have advantages in their uniformity and controls [55, 68].

1.1.6 Bottom-up and Solid-State Growth of Silver Nanowires

Bottom-up growth of silver nanowires classification is done based on their growth through chemical or molecular assembly or by template-assisted electrodeposition. Chemical synthesis is typical polyol synthesis, which we have discussed in previous section. Template-assisted electrodeposition method of AgNWs growth involves complex mechanisms for careful preparation of desired template, which forms base for the growth of AgNWs. Silicon templates with porous alumina membrane containing varying thickness of pores forms as a base for nanowires growth, when electrodeposition of silver sulfide is processed over the templated structure [69]. This mechanism primarily depends on the reaction rate in the electrochemical system for deposition of silver onto the porous membrane and to further grow nanowires from the pores. This template-assisted growth of silver nanowires is considered as potential bottom-up method except for its need of complex process involved template fabrication.

Still, with all the methods discussed in previous sections, there is no specific established method reported till now proposing the growth of AgNWs in both solid-state and bottom-up manner.

This area of research paves a way for new paths of findings in applications involving AgNWs.

1.1.7 Applications of Solid-State Silver Nanowires

Three main fields of applications silver nanowires proved to play important role are, Transparent conductive film electrode[70], Surface plasmon resonance applications[71-76] and their use in anti-bacterial activity[77]. Electronic industry needs transparent conductive films for their use in applications like solar cells, liquid crystal displays and photodiodes. Currently most used transparent conductive material is ITO, which can be efficiently replaced a network of AgNWs. Since, AgNWs show high level of transparency and conductive at the same time.

Surface Plasmon Resonance approach is employed over the detection of biological sample to enhance the existing detection signal. This principle basically works in the presence of Nano particles and Nano Structures mostly made by coin age metals like Ag and Au. When the optical light is shined on to these Nano structured metal platform, the free electrons on the surface of the metal will start oscillating and generates a travelling resonant wave called surface Plasmon resonance. This resonant signal will constructively be added to the existing single molecule detection signal and a significant enhancement in the detection signal is obtained. Important property of SPR, which is related to our current research is Surface Enhanced Raman Spectroscopy (SERS). Many kinds of silver nanostructures are employed for this need [78-80]. In current research, we use in-situ grown silver nanowires (AgNWs) as SERS enhancement material and chitosan polymer matrix as Raman signal generator, of which the enhancement is

measured and monitored due to the presence of mentioned AgNWs. The unique factor and key advantage in current platform are in-situ and self-growth of AgNWs in chitosan polymer matrix film and no fluorophore use of the platform for instant verification of SERS.

Silver has been in use in vast number of consumer products both in the form of engineered material and as nanomaterial. Through understanding is available on the behavior of bulk silver and its anti-bacterial property, which might not directly relate to the behavior of nano silver. Marambio-Jones and Hoek proposed three mechanisms in which silver nanoparticles and wires contribute in anti-bacterial activity. First one is most agreed mechanism where, silver ions from the metallic silver that forms silver nanowires plays role in inhibiting the bacteria, second mechanism discusses on the possibility of Reactive oxygen species (ROS) generation by silver nanowires and their effect on bacteria and final mechanism being direct physical damage by AgNWs adhering to the surface of bacterial cells[81].

1.2 MoS_2/Au Fabrication Methods and its Optical Properties

1.2.1 Fabrication Methods for MoS_2

Graphene like two-dimensional (2D) transition metal dichalcogenides (TMDCs) have been attracting a wide range of research interest. MoS_2 particular direct band gap of 1.8 ev in monolayer and layer dependence of band structure tackle the gapless problems of graphene[82-86].

In single layer of MoS_2 films, Mo (+4) and S (-2) are arranged to a sandwich structure by covalent bonds in a sequence of S-Mo-S as shown below[87-89]. Monolayer

MoS_2 with trigonal prismatic polytype is found to be semiconducting (2H ((trigonal prismatic D_{3h})), while that with octahedral crystal symmetry configuration (1T (octahedral Oh)) is metallic[90].

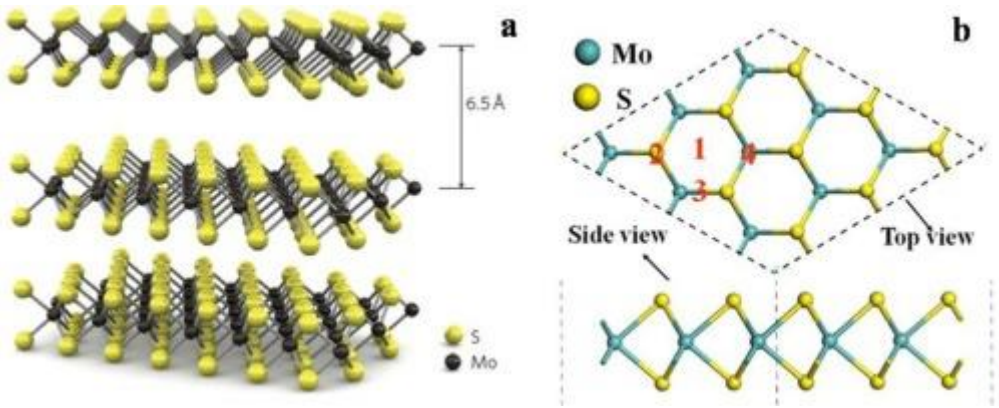

Figure 2. MoS_2 Structural Overview with a Layer of Mo and Other of S Bonded Together.[91]

There are three most used ways to obtain few layers to monolayer MoS_2, that are primitive Mechanical exfoliation[10, 92, 93], Liquid Exfoliation[94-97] and Chemical Vapor Deposition (CVD)[98-102] in which I have opted for Mechanical exfoliation, since this method produces pristine level MoS_2 layers, it is simple process and is extremely comfortable method to opt for laboratory research and prototype design. The schematic below shows the working of listed three methods for fabricating MoS_2

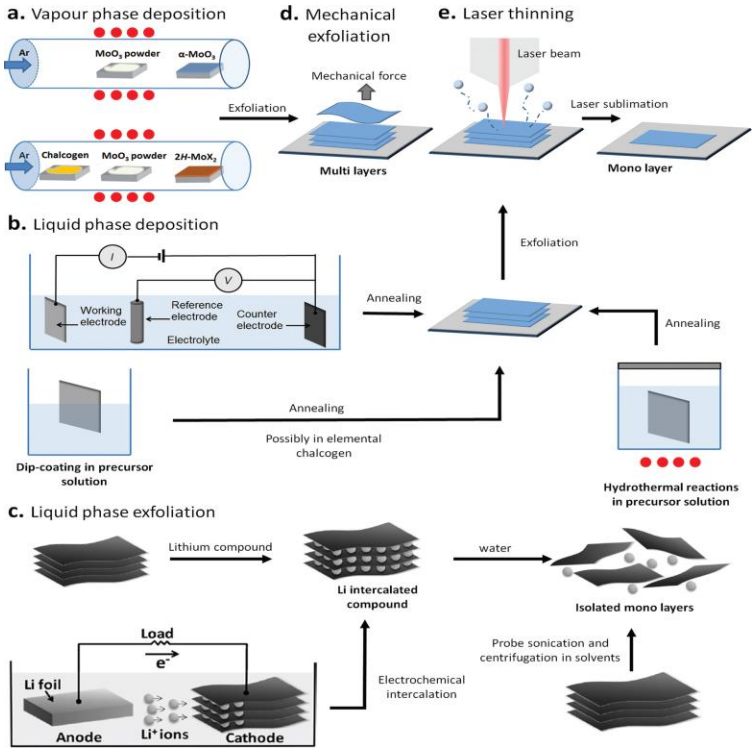

Figure 3. Schematic Representation of Different Methods for Fabricating MoS_2 Layers. [103]

1.2.2 Characterization Techniques Associated with MoS_2

With the properties of MoS_2 and its methods of fabrication, which are listed in previous section it is evident that monolayer MoS_2 have superior properties to use in specific applications. So, need for characterization tools, by which precise differentiation between number of layers of MoS_2 can be presented along with the properties associated with the same.

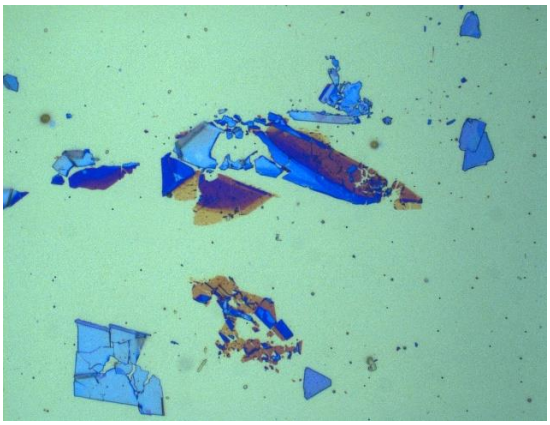

Figure 4. Optical Image of MoS_2 Deposited on the Au Film

In line with my work for finding the optical properties associated with monolayer to few layers of MoS_2 when associated with Au thin films, I have extensively made use of optical microscope and Raman spectroscopy. Optical microscopy is proved to use on 2D materials for finding number of layers associated with the material based on the optical contrast it shows when illuminated under white light, which is shown if Figure 4. Raman spectroscopy is more robust technique used in finding details like number of layers, stress induced in the material and doping details of the material. Further, to verify the role of Au thin film in generation of plasmons with varying in its thickness, Fourier transfer time domain (FDTD) analysis has been performed on the modeled system.

1.2.3 MoS_2 Layer Number Dependency on Optical Properties

Importance of employing characterization tools on MoS_2 mainly lies in determining number of layers that are prepared from the employed method. A few tools using which we can determine the count of layers are Atomic Force Microscopy (AFM)[104], Raman Spectroscopy[85] and Photo Luminance tool (PL)[105].

The monolayer width of MoS_2 is 0.75 nm[106], this can be precisely determined by subjecting the same to AFM analysis. As discussed in the introduction, monolayer MoS_2 have direct band gap of 1.8ev which can be confirmed by using PL tool. Finally, most easy method employed for determining the count of layers is Raman spectroscopy, where MoS_2 consists of two dominant Raman peaks i.e. $Eg^1{}_{2g}$ and A_{1g} [107]. The difference in wavenumber of these two peaks determines the count of layers[108] like, if the difference is of ~19 cm^{-1} it corresponds to monolayer and further increase in this difference like 20 cm^{-1}, 21 cm^{-1}, 22 cm^{-1}, 23 cm^{-1} and 24 cm^{-1} corresponds to 2, 3, 4 layers respectively. If the difference of wavenumber is more than 25 the characterized MoS_2 is noted as bulk.

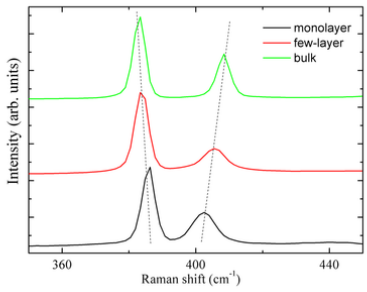

Figure 5. MoS_2 Layer Dependence on Change in Intensity and Wavenumber Shift

1.2.4 Heterostructure MoS_2/Au Platforms

In past three years optical analysis of MoS_2 and Au thin film heterostructures became widely popular in understanding linear and non-linear optical behavior of MoS_2 when deposited on Au thin film. Jia et al. investigated theoretically the behavior of MoS_2 on Au thin film under 20nm thickness reporting drastic modification in the excitonic optical properties of MoS_2 monolayer because of Au thin film[109]. Zeng et al. presented

his research findings on Au thin film influence on secondary harmonic peak intensity raise of few layers MoS_2, which is due to strong localized field induced by Au thin film[110]. Photoluminescence (PL) is one of the important optical property of MoS_2 that is being constantly investigated for its intensity and quantum yield associated with direct bandgap monolayer MoS_2. Le Yu et al. claims that gap plasmons induced by their Au thin film and nanoparticle structure improved PL of monolayer MoS_2 by 4 times[111]. Haifeng Xu in his research report proved that with the inclusion of gold mirror layer between the dielectric layer and the substrate enhances overall PL intensity by 4 times of monolayer MoS_2 because of enhanced optical absorption[112]. Buscema et al. reports in detail the role and effect of the substrate on the PL and Raman signal of mono layer MoS_2. On all his studied substrates including Au thin film, single-layer MoS_2 shows a factor of ~4 enhancement of PL efficiency, relative to commonly used SiO2 substrate, which is reported due to radiative decay rates of neutral and charged excitons, which is different from previous claims[113]. Robison et al. with the help of Raman spectroscopy and scanning Kelvin probe microscopy (SKPM) investigated the effect of Au substrate on optical and electrostatic properties of monolayer MoS_2. The increase in the Raman peak enhancement of monolayer MoS_2, when on Au thin film is claimed to be associated to SERS like enhancement shown by the nanoscale-textured metallic surfaces[114]. Different shapes of Au nanostructures influence monolayer MoS_2 for enhance in optical absorption due to surface plasmons[115-117], shows ultrafast plasmonic hot electron transfer from Au nanostructures to MoS_2 and exhibits plasmonic pumping of excitonic photoluminescence. Other metal surfaces and nanostructures reported to induce plasmons

into MoS_2 for change in its optical properties are Aluminum[118] and Silver[119]. Raman peak intensities change is mostly influenced by number of layers of MoS_2 with raise in intensity is directly propositional to raise in number layers[120-123]. This phenomenon is same for all preparation methods of MoS_2 and irrespective of substrate on which MoS_2 is deposited. The primary reason presented for this observation is the optical scattering taking place in the number of layers of the material[124], which is observed in the case of graphene too[125]. Monolayer MoS_2 deposited on Au film and on insulating films like PVP, it observed to have higher Raman peak intensities compared to its deposition on semiconducting substrate silicon. This phenomenon is supported by argument of electron transfer property taking place between Au and MoS_2[113] along with capability of band alignment induced by underneath Au film onto MoS_2.

In present study, I have investigated the behavior of monolayer to few layers of MoS_2 deposited on different thickness of gold thin films. Change in Raman intensities of the material due to the thickness of Au film and influence of surface plasmons generated by Au thin film of specific thickness in effecting the SERS property of few layers MoS_2 is presented.

1.2.5 SERS Property Analysis of MoS_2

Optical absorption and surface plasmon generation properties of MoS_2 has been widely investigated in terms of Raman peak enhancements due to incident light scattering with change in number of layers of MoS_2 [126, 127], and moderate SERS generation of free standing monolayer MoS_2 and its enhancement with combination of metal nanoparticles and metal nanostructures with MoS_2 [128]. Recently, there is increase in

research interest on improving the SERS property of semiconducting MoS_2, combining it with metal nanoparticles and nanostructures, especially understanding the behavior of MoS_2 when combined with Au metal. Many research findings claimed change in linear and non-linear property changes seen in monolayer MoS_2 and Au heterostructures. But, there is still room in investigation of plasmonic role of Au thin film induced in few layers of MoS_2 both in its optical properties related to Raman peak intensity change and in increasing SERS enhancement property associated with few layers of MoS_2.

CHAPTER II

SYNTHESIS OF SILVER NANOPARTICLES (AGNPS) USING CHITOSAN POLYMER

2.1 Introduction

Chemical synthesis of silver nanoparticles other the use of PVP polymer and ethylene glycol is rarely investigated, since its proven that, additional capping agent like PVP helps in good control of the shape of nanoparticle. But, with ethylene glycol being heated to high temperature for initiating reduction process of silver precursor $AgNO_3$ and longer hours reaction time for obtaining desired shape and size of AgNPs, there is need for investigation for new, simple synthesis processes of AgNPs. Additionally, with the inclusion of PVP in the reaction system, synthesized AgNPs are not advisable to be used in biomedical applications.

To address the above short comes of the traditional synthesis process for AgNPs, we report the green synthesis of AgNPs and AgNWs using chitosan/chitin-based polymer as both reducing and stabilizing agent and without using any toxic chemicals. Chitosan / chitin is a polysaccharide that occurs naturally. They are investigated as a natural cationic biopolymer because of its known excellent biocompatibility, biodegradability, nontoxicity, bioactivity, and multifunctional groups from years of research. It is also extensively being studied for food packaging film, bone substitutes, artificial skin, and pH sensitive drug delivery among others due to several great properties it possesses[129].

2.2 General Methods

500 mg of chitosan (32.7mM) low molecular weight (bought form Sigma Aldrich) is dissolved completely (magnetic stirring) in 10ml of water along with 1% wt (1ml) of pure Acetic acid. Acetic acid (AA) helps chitosan dissolve in water. The stirring is continued till chitosan peaks are completely dissolved in the water.

$AgNO_3$ (>99 %) was purchased from Sigma Aldrich chemicals and its solution of 10^{-2}M was prepared. Chitosan (0.5 g, dissolved in 10 mL of 1% v/v acetic acid solution) and 0.2M NaCl in 5mL solution is added drop by drop. Mixtures of chitosan and $AgNO_3$ solution were prepared with a ratio of 1:5 (by volume). The mixed sample solutions were kept for ultra-sonication for 3-4 h for formation of monodispersed nanoparticles.
The optical absorptions of chitosan and mixtures of colloidal solution of $AgNO_3$ (sample solutions) were evaluated in 10 mm optical path length quartz cuvettes of the ultraviolet-visible spectroscopy (UV-Vis spectroscopy, Varian Cary 6000i), followed with Fourier transform infrared spectroscopy (FTIR, Varian 670) measurements. To get the size of the synthesized AgNPs, transmission electron microscope (TEM, Carl Zeiss Libra 120 Plus) is used. For getting the results, the copper grid was plasma treated and a drop of sample solution was kept on a copper grid and dried under a vacuum drier, before scanning the sample under TEM. Morphology including shape and size of nanoparticles, was viewed under Scanning electron microscope. Sample preparation and imaging for morphology study: The samples are placed on SEM sample pug. After drying, the samples had a 4 nm thickness of gold layer applied using a Leica EM ACE200 with a real time thickness monitoring quartz crystal microbalance (QCM). The scanning electron micrographs were

obtained using a Zeiss Auriga FIB/SEM. Scale bars were added using ImageJ software, followed with energy-dispersive X-ray spectroscopy (EDS) (Hitachi S-4800-I FESEM w/Backscattered Detector & EDX) performed to verify the presence of Ag.

2.3 Results

2.3.1 Description of the Synthetic Process

Chitosan polymer solution was prepared by continuous stirring and dissolving the same in water solvent along with addition of acetic acid, which helped chitosan dissolving in water. Silver Nitrate solution was added to the prepared chitosan polymer solution and was subjected to low power sonication till the color of the solution was changed to green color as shown in Figure 6, indicating the formation of silver in the chitosan polymer matrix.

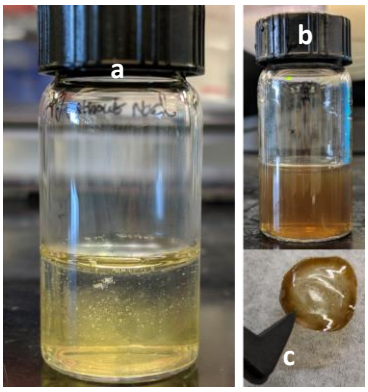

Figure 6. Synthesis of AgNPs in Chitosan Polymer Solution

UV-Visible analysis of the synthesized solution which is seen in green color, shows clear plasmonic peak of absorption related to metal Ag nanoparticles at a wavelength of ~420nm.

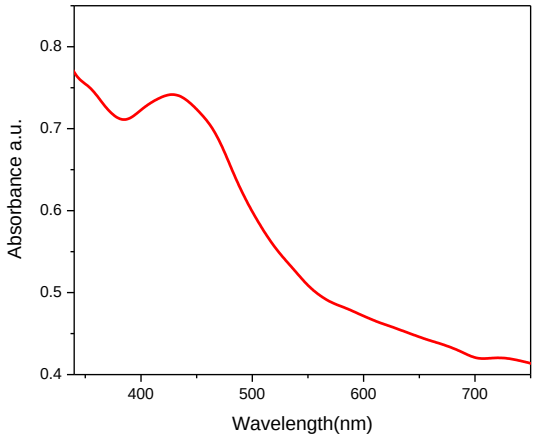

Figure 7. Absorption Peak of AgNPs Obtained at ~420nm

The obtained solution of Ag/Chitosan is drop casted on to the PET substrate and then dried at 50^0C. The obtained film is shown in Figure 6c, PET substrate is used mainly due to ease of peeling of the film from the substrate. Further, for understanding the crystal structure of metallic Ag, X-ray diffraction tool is used, where Ag peaks with dominant (111) peak corresponds to cubic structure of Ag, as shown in Figure 8 below, which are matching with the peaks listed in literature.

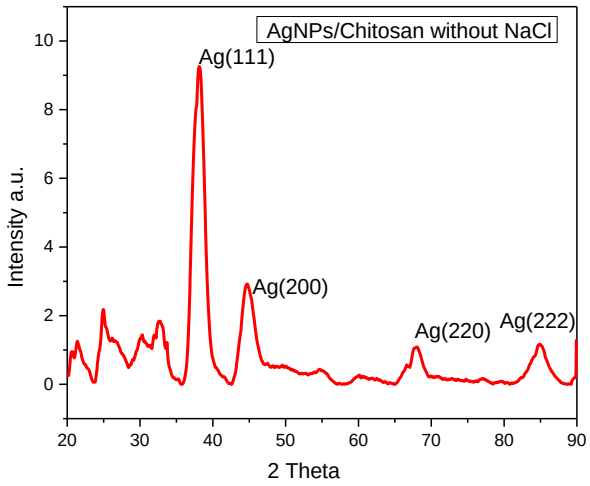

Figure 8. XRD Analysis of AgNPs/Chitosan Film, Showing Dominant (111) Phase

Infrared analysis of as such chitosan polymer matrix film was performed with the help of standard IR laser and ZnSe source. In a typical case of pure chitosan, similar to various research articles the standard peaks observed are: peaks in broad bands between 3360 cm^{-1} and 3295 cm^{-1} correspond to amine (N-H) and hydroxyl (O-H) stretching vibrations; further dominant peak at 2870 cm^{-1} corresponds to asymmetric stretching vibrations of CH_3 and CH_2 of chitosan polymer. Absorption peak at 1560 cm^{-1} corresponds to bending vibration of amine N-H (N acetylated amide II band). Peak at 1420 cm^{-1} typically corresponds to amide III (N-H) stretching vibrations. The peaks observed at 1060 cm^{-1} and 1030 cm^{-1} are corresponding to the vibrations of secondary hydroxyl group and primary hydroxyl group, which also correspond to carbonyl stretch. Significant stretch in these two peaks with respect to pure chitosan peaks were observed in Ag-Chitosan composite film IR peak, however with different intensities, this is

because silver particles are bonded by chitosan, which served as a stabilizing agent that helps in reducing $AgNO_3$ ions to Silver NPs. Clear depiction of this stretch is seen in the inset Figure 9.

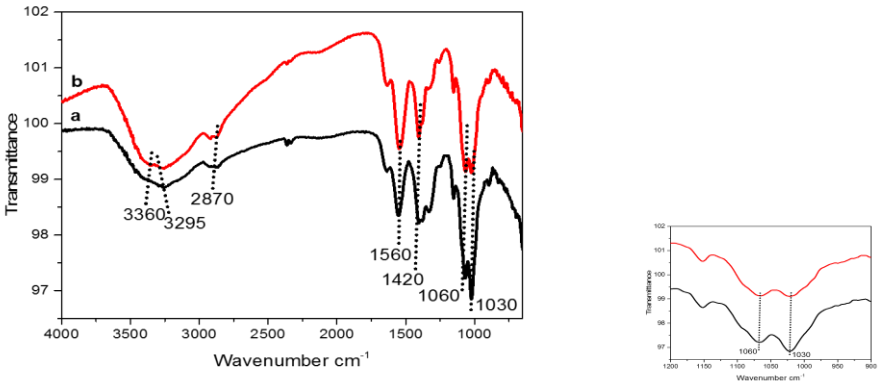

Figure 9. FTIR Spectrum of Ag/Chitosan

Particle size, concentration and distribution are important factors to reflect the mechanism of particle formation. Particle size and distribution were determined by DLS (Dynamic Light Scattering). Figure 10. shows the graphs of volume (%) vs size (d.nm). It is observed that the particles are mono-dispersed as it is represented by having single peak and lesser PDI (poly-dispersity index). The average particle size is around ~180 nm which is indicating a comparable population of Ag nanoparticles around this size. Three measurements are taken continuously, to average the obtained size of the particles.

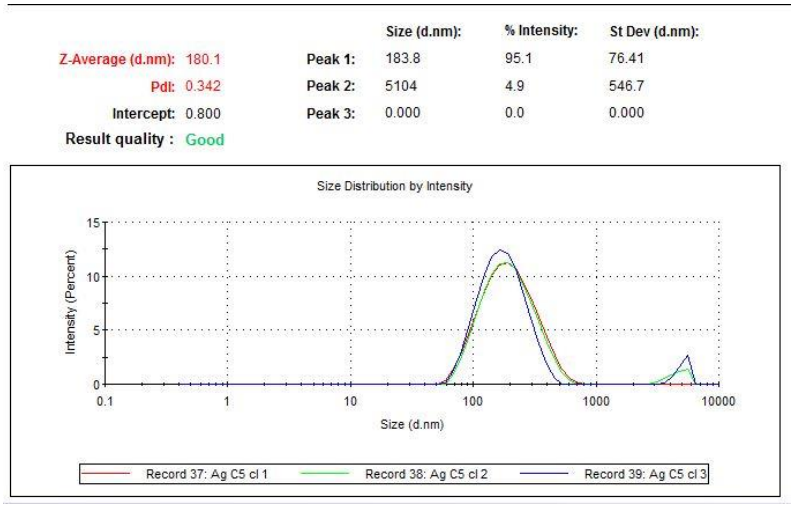

Figure 10. DLS Analysis of AgNPs in Ag/Chitosan Solution

To verify the surface morphology and distribution of AgNPs on the Ag/Chitosan film, SEM characterization is done on the film. Below Figure 11 shows the SEM image of the film shown in Figure 6c, it is seen on the film that AgNPs of spherical shape are distributed all over the film, with size approximately being around ~150nm.

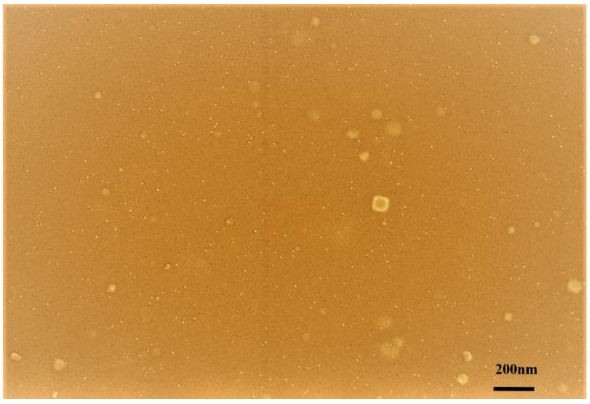

Figure 11. SEM Image of Ag/Chitosan Film Showing the Spherical Shape of AgNPs

EDS characterization is performed on the Ag/Chitosan film to know the composition of materials on the surface of the film. This result is line with all the above characterizations for proving the formation of AgNPs, with major weight percentage of material composition is coming from Ag i.e. 50% Wt, as seen in Figure 12.

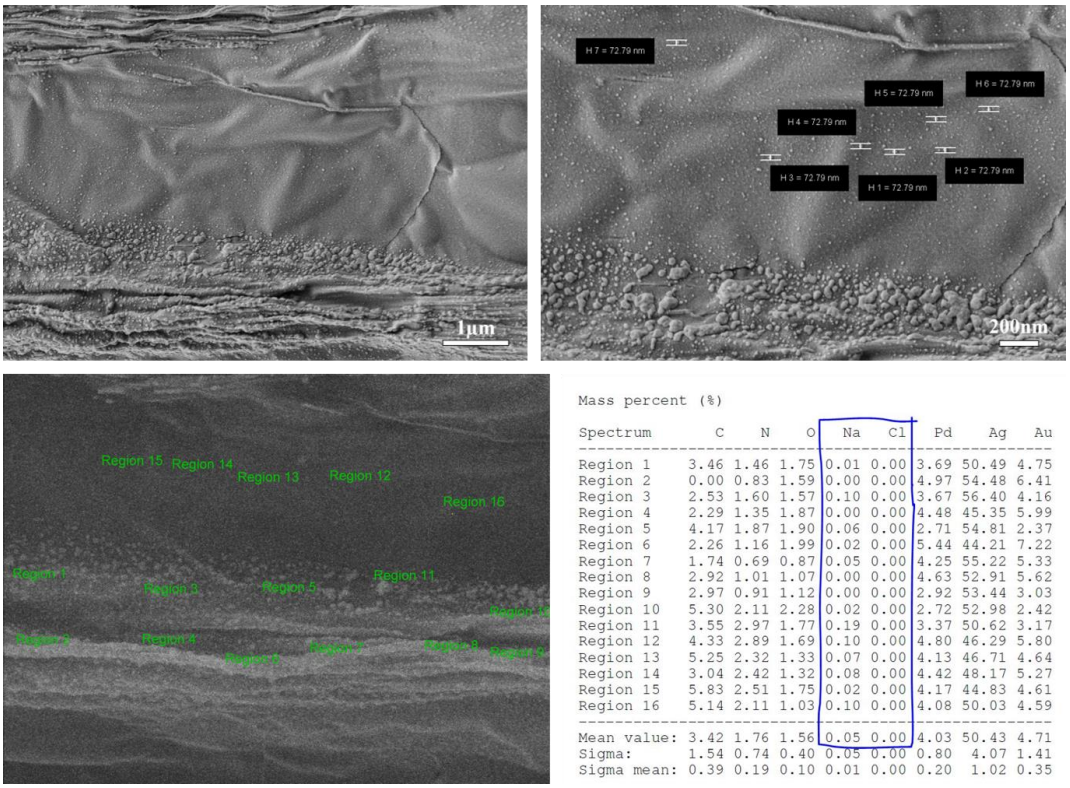

Mass percent (%)

Spectrum	C	N	O	Na	Cl	Pd	Ag	Au
Region 1	3.46	1.46	1.75	0.01	0.00	3.69	50.49	4.75
Region 2	0.00	0.83	1.59	0.00	0.00	4.97	54.48	6.41
Region 3	2.53	1.60	1.57	0.10	0.00	3.67	56.40	4.16
Region 4	2.29	1.35	1.87	0.00	0.00	4.48	45.35	5.99
Region 5	4.17	1.87	1.90	0.06	0.00	2.71	54.81	2.37
Region 6	2.26	1.16	1.99	0.02	0.00	5.44	44.21	7.22
Region 7	1.74	0.69	0.87	0.05	0.00	4.25	55.22	5.33
Region 8	2.92	1.01	1.07	0.00	0.00	4.63	52.91	5.62
Region 9	2.97	0.91	1.12	0.00	0.00	2.92	53.44	3.03
Region 10	5.30	2.11	2.28	0.02	0.00	2.72	52.98	2.42
Region 11	3.55	2.97	1.77	0.19	0.00	3.37	50.62	3.17
Region 12	4.33	2.89	1.69	0.10	0.00	4.80	46.29	5.80
Region 13	5.25	2.32	1.33	0.07	0.00	4.13	46.71	4.64
Region 14	3.04	2.42	1.32	0.08	0.00	4.42	48.17	5.27
Region 15	5.83	2.51	1.75	0.02	0.00	4.17	44.83	4.61
Region 16	5.14	2.11	1.03	0.10	0.00	4.08	50.03	4.59
Mean value:	3.42	1.76	1.56	0.05	0.00	4.03	50.43	4.71
Sigma:	1.54	0.74	0.40	0.05	0.00	0.80	4.07	1.41
Sigma mean:	0.39	0.19	0.10	0.01	0.00	0.20	1.02	0.35

Figure 12. AgNPs Distribution on the Surface of Ag/Chitosan Film and its Corresponding EDS Data

2.3.2 Concentration Evaluation of Silver Precursor $AgNO_3$

Synthesis of AgNPs with the presence of halide ions like Cl^- and Br^- is common method of reaction in polyol synthesis. NaCl is used as Cl- source in the reaction processes. Cl^- ions along with oxygen atoms in the environment tend to dissociate all

other Ag structures, that tend to form during the synthesis process. These Ag atomic structures are responsible for the formation of different shaped Ag nanostructures. So, to obtain good spherical shaped AgNPs. Inclusion of NaCl and investigation of different Ag concentrations in the synthesis process, need to be investigated to get understanding of the behavior of Cl^- ions when reacted with different concentrations of $AgNO_3$.

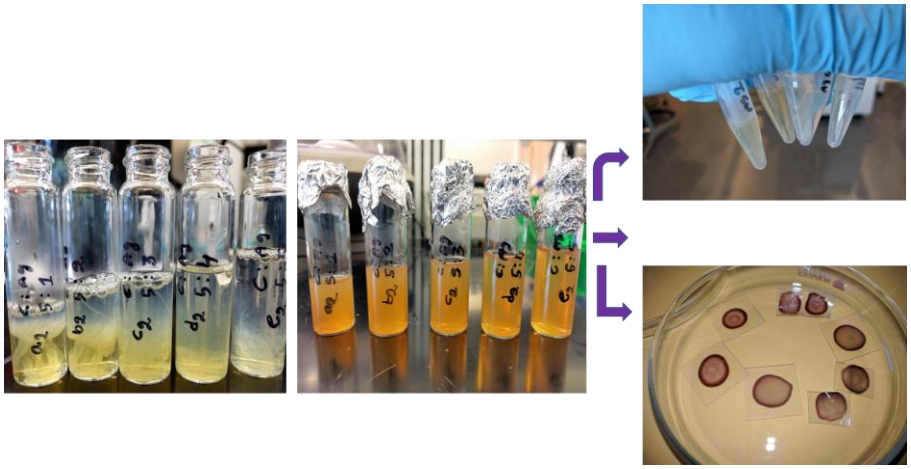

Figure 13. Depiction of Dissolving $AgNO_3$ in NaCl Included Chitosan Solution and Formation of AgNPs

NaCl when reacted with $AgNO_3$ forms a white precipitate indicating formation of AgCl in the solution. In polyol synthesis, the AgCl acts as slow release agent for Ag ions, which further join to form Ag nanostructures. This formation of AgCl have other advantage of avoiding oxidative etching in the solution, which dissociates the formation of desired shape Ag nanostructures. In this section, I have used different concentrations of silver precursor, $AgNO_3$ in the synthesis process as listed in Table 1.

Table 1. Table Listing the Sample Notations and List of Different Volume Concentrations Change of $AgNO_3$

Notation	**Concentration of Chitosan: $AgNO_3$ (vol by ml)**
Ag sample 'a'	5:1
Ag Sample 'b'	5:2
Ag Sample 'c'	5:3
Ag Sample 'd'	5:4
Ag Sample 'e'	5:5

The change in concentration of $AgNO_3$ is by volume, where chitosan of 100mM concentration of 5ml by volume and $AgNO_3$ of 58mM is taken in volumes of 1ml to 5ml in intervals of 1ml as shown in Table 1. When the solutions of $AgNO_3$ and chitosan are subjected to the ultrasonication, plasmonic color change of the solution is seen, which corresponds to the formation of metallic Ag in the solution. Further, these solutions are filtered using centrifugation at 3500rpm and then filter papers to obtain solution of just AgNPs.

The filtered and purified AgNPs dispersed in DI water as shown in Figure 13 are characterized with SEM to verify the change in structure of AgNPs with change in concentration of $AgNO_3$ by volume. It is seen from the SEM images listed under Figure 1 that, at the low volume concentration, AgNPs tend to form in spherical shape and with the increase in the concentration of $AgNO_3$ in the solution, there is seen in the increase in particle size and shape converting to cubic structures.

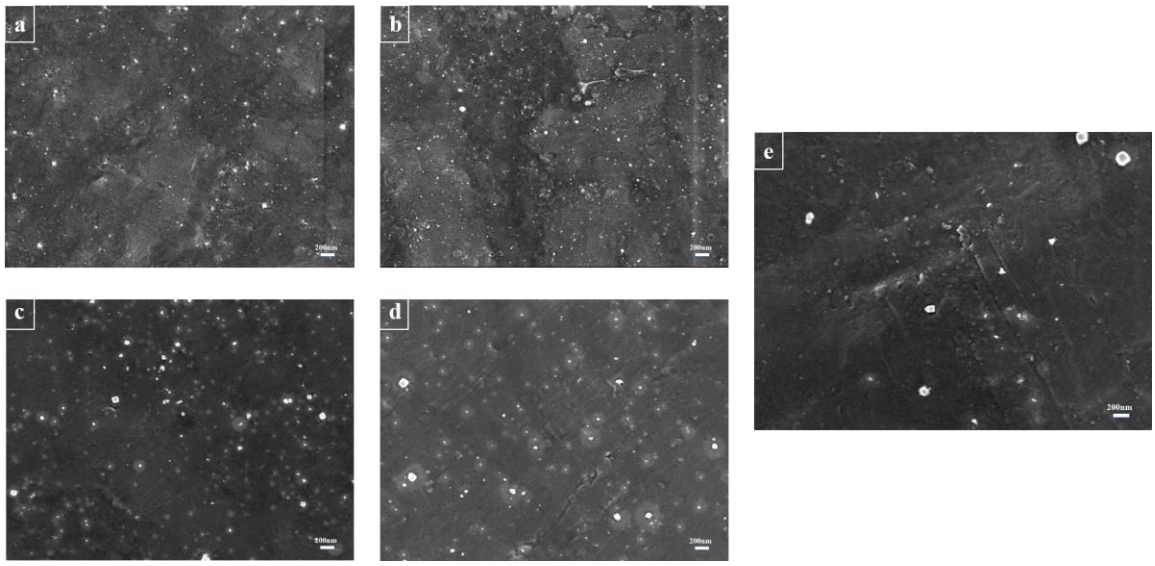

Figure 14. SEM Images of AgNPs With Change in Silver Precursor Concentration

This change in shape and size of the AgNPs is verified by UV-Visible analysis. Where, with the increase in the concentration of silver precursor, the sharp absorption peak wavelength observed at ~420nm for sample ‘a’ broadens and shifts to higher wavelengths for sample ‘e’ as shown in Figure 15. This is because of the increase in the size of AgNPs in the solution and due to the formation of cubic structures as seen in Figure 14 SEM images.

To further confirm the change in crystal structure of the AgNPs formed with the change in concentration, X-ray diffraction analysis is performed on the films formed with the Ag/Chitosan solutions at different concentrations of $AgNO_3$. XRD results showed the formation metallic Ag with the dominant phase being at (111) crystal phase. Increase in the concentration of $AgNO_3$ in the film, the growth orientation of AgNPs/NWs move from <200> plane to <111> plane. The change is shown in XRD spectra in Figure 16.

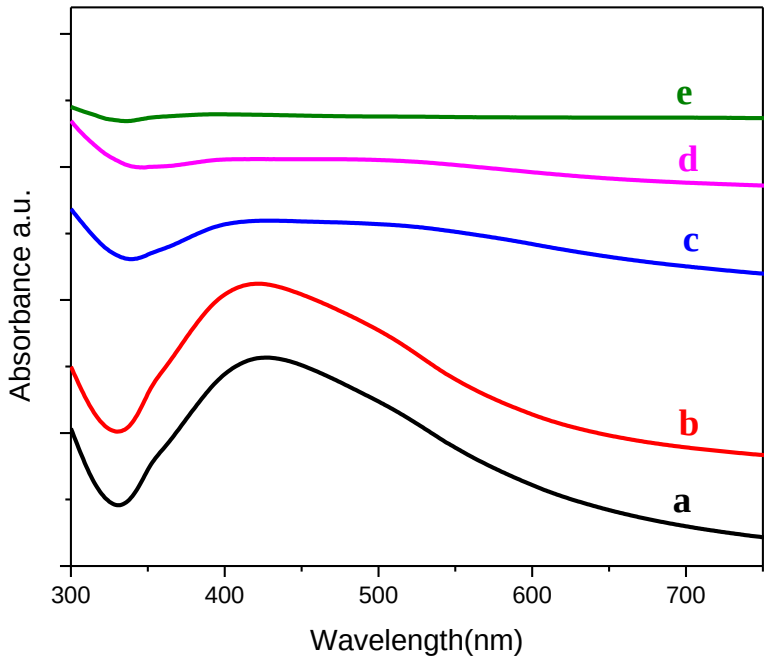

Figure 15. UV-Vis Analysis of Ag/Chitosan Solution with Varying Concentrations of $AgNO_3$

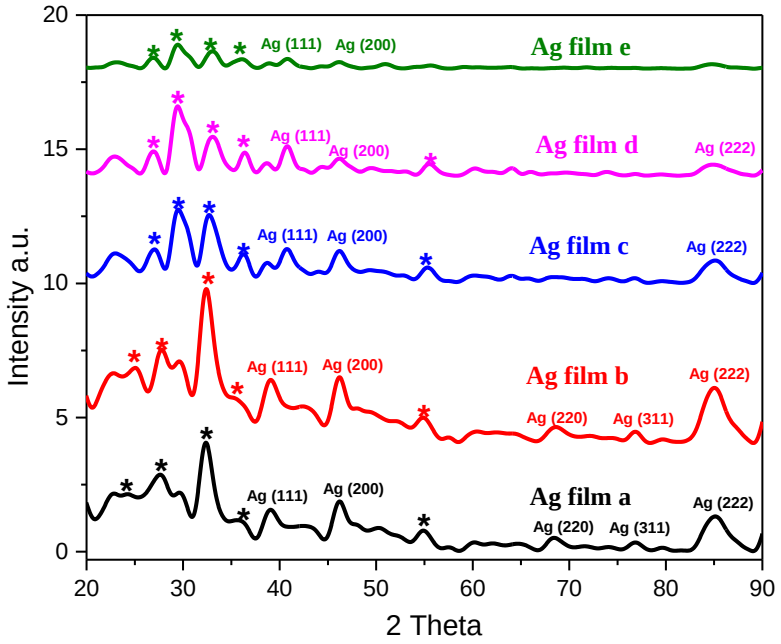

Figure 16. XRD Analysis of Ag Films Formed by Ag/Chitosan Solutions with Varied Concentrations of $AgNO_3$

At the highest concentration of $AgNO_3$, it is observed from the SEM results that, there is clear formation of cubic nanostructures. With UV-Vis analysis, and with the shift in absorption peak wavelength to longer wavelengths and broadening of its peak, it can be confirmed with the presence of large nanoparticles in the solution too. XRD of the films confirms the change in crystal phase from Ag (200) to Ag (111) for the highest concentration of $AgNO_3$. So, with these analyses, it can be concluded that for all further experiments, we use the 5:5 concentration made Ag film, i.e. sample ‘e’.

2.3.3 Distribution of Silver Nanoparticles in Chitosan Films

Since, the synthesized Ag/Chitosan solution is drop casted onto the PET substrate and then peeled off from the substrate after drying process, even after all the above presented characterizations of the film. It is still unclear that how well the nanoparticles are distributed inside the film and there is scope for investigation on plasmon generation capability of these silver nanoparticles which are imbedded inside the framework of chitosan polymer.

To analyze both the above predictions, I have made use of Raman spectroscopy to characterize the Ag film. Thickness and dimensions of the Ag film are depicted in below SEM image in Figure 17. Where thickness of the film is around ~500nm.

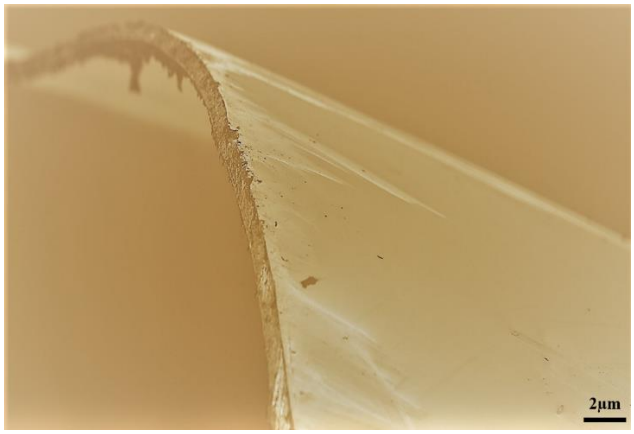

Figure 17. SEM Image of Ag Film, Showing its Cross Section

The primary reason for performing Raman analysis on Ag film, is to investigate the capability of the AgNPs which are imbedded inside the film and nanoparticles which are distributed on the film does have surface plasmon property associated to them. To verify this argument. Figure 18 displays pure chitosan polymer matrix film with basic

Raman signals of peaks at 1300 cm^{-1}, 1500 cm^{-1} and a main peak at 2800 cm^{-1}. In this analysis, pure chitosan polymer matrix film at varying laser powers i.e. using different filters (1%, 10%, 25%, 50%, 100%) for allowing laser to shine on the sample; the spectra show ascending order increase in the intensities associated to the peak 2800 cm^{-1} and less significant enhancement on rest of peaks at 1300 cm^{-1}, 1500 cm^{-1}. There is good enhancement in the dominant peak signal with the increase of laser power, however it is known that the strong light intensity of the laser power shining on the molecules will possible spoil the system of detection.

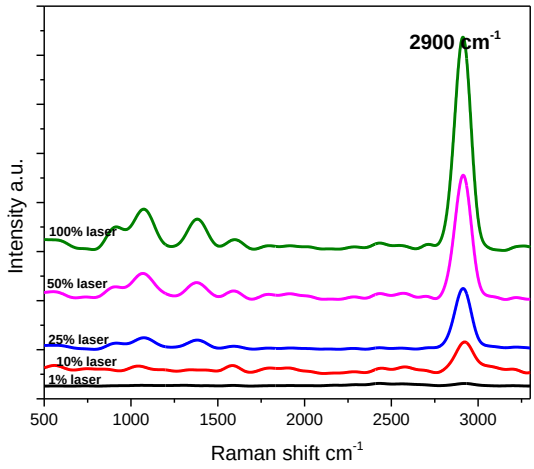

Figure 18. Raman Spectrum of Pure Chitosan at Different Laser Powers

To verify the distribution of the AgNPs in the polymer matrix and to evaluate the surface plasmon property of imbedded nanoparticles, Raman analysis on Ag film with different concentrations of $AgNO_3$ is performed. Figure 19 gives the obtained Raman spectrum of chitosan film imbedded with AgNPs at different concentrations. This

analysis of Raman spectrum is performed at lowest laser power of 1%. When compared to the 1% laser power Raman spectrum of pure chitosan to the Ag films, there is a clear difference in the intensity of the detection of the polymer. This is precisely due to the presence of AgNPs in the matrix of the polymer and surface plasmon property shown by the metal nanoparticles. This phenomenon is further supported by analysis of chitosan peak intensity raise with the increase in the concentration of Ag in the films. For the sample 'e', which is of highest concentration, Raman spectrum of the chitosan is obtained equally better than its Raman peak, when measured at 100% laser power.

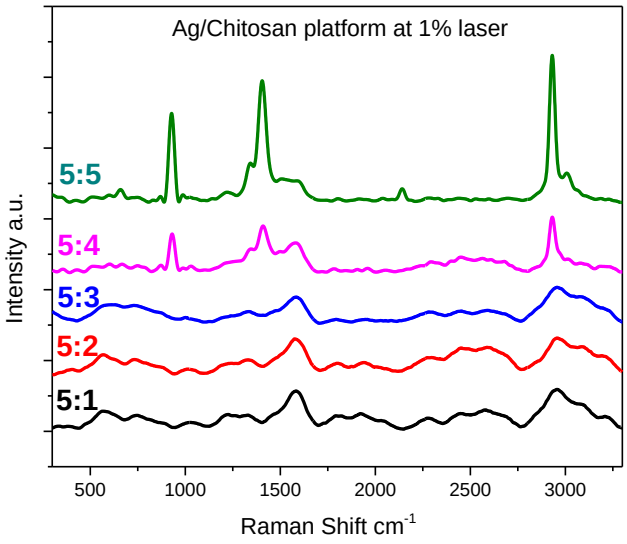

Figure 19. Raman Peak Analysis of Chitosan Polymer with Different Concentrations of AgNPs

With the above two analysis experiments, it is proved that, AgNPs are widely distributed inside the polymer matrix and even when imbedded in the polymer, AgNPs can generate surface plasmons.

2.4 Discussion

Few observations that support the role of NaCl and the concentration of silver precursor play role in change of shape and size of synthesized AgNPs in the presented novel green synthesis method of AgNPs are: 1. AgNPs which are formed when no NaCl is added to the reaction solution are clearly of spherical shape with strong plasmon absorption peak shown at ~420nm. 2. Addition of NaCl in the solution immediately forms AgCl white precipitate, which is observed visually during experiments, this for AgCl slowly releases Ag ions to form AgNPs. 3. With varying concentration of $AgNO_3$ in NaCl included chitosan solution, synthesis of AgNPs is not affected but, size and shape of the nanoparticles obtained differed, which is proved from SEM images, UV-vis analysis and XRD analysis. 4. Irrespective of the concentration of AgNPs imbedded inside the film of Ag/Chitosan solution, distribution of the AgNPs in polymer matrix is uniform and thick, which is verified by unique Raman experiments.

In the current work, AgNPs synthesis using novel green synthesis method is presented, where chitosan polymer dissolved in water using trace amounts of acetic acid acts as both reducing and stabilizing agent for the synthesis of AgNPs. Except for the ultrasonication no other harsh external forces are imposed on the synthesis process. Further, investigations on the change in concentration of the $AgNO_3$ addition into the chitosan solution by volume is shown to give varied size and shape of the AgNPs. Synthesized solution of Ag/Chitosan is made into a thin film under room temperature drying.

This novel AgNPs imbedded polymer matrix platform is successfully presented to be used as SERS generating platform by presenting the raise in intensity of pure chitosan Raman peaks at the highest concentration of AgNPs imbedded in the surface of the film.

2.5 Conclusion

In summary of this work, presented a new way of AgNPs synthesis using only chitosan polymer and silver precursor followed by ultrasonication of the solution to obtain plasmonic color solution. This work further investigated the effect of $AgNO_3$ concentration on the size and shape of the AgNPs, with observation of forming cubic nanostructures at the highest concentration of $AgNO_3$ in the reaction system. Finally, proved that AgNPs imbedded chitosan film can be used as SERS platform with good detection capability.

CHAPTER III

SOLID – STATE SYNTHESIS OF SILVER NANOWIRES USING BIOPOLYMER THIN FILMS

3.1 Introduction

Several green synthetic methods for generating silver nanoparticles (AgNPs) have also been developed which use biomolecules such as proteins and polysaccharides to stabilize and promote nucleation. Environmentally friendly "green" methods of nanoparticle synthesis often take advantage of biological self-assembling system or catalysis such as living organism or biopolymers. A polysaccharide AgNP synthetic method uses starch as the capping agent and monomeric α-D-glucose as the reducing agent in an aqueous solution. Extracts of various plants and microorganisms have also been demonstrated to promote the formation of silver nanoparticles through the participation of protein/peptides in the reduction, nucleation, and stabilization steps. Recently a chitosan photochemical AgNP synthetic method has been described that enables the formation AgNP of different morphology and crystallinity in a wavelength dependent manner. Synthetic processes that generate highly anistropically shaped particles are especially desirable in many applications due to the enhancement of specific optical properties such as surface Plasmon resonance.

There are fewer methods for the synthesis of silver nanowires (AgNWs)which is predominantly performed using a polyol method and most AgNW synthesis

processes are energetically and environmental costly. Recently, there has been an increased interest in the identification and fabrication of novel nanocomposite materials that consist of metallic or metal oxide nanoparticles with another nanoscale material. By combining the properties of two nanomaterials there is often a synergetic effect that extends, enhances, and/or increases the properties of one or more of the constituents of the nanocomposite. However, fabrication methods of such multicomponent nanomaterials often rely on a multistep process, relying on post-fabrication mixing or combining of the individual nanoscale components, which often results in a product that is not ideal in composition and/or non-scalable.

In this section, we describe a novel, single step process that promotes the self-growth of AgNW within thin films of the polysaccharides chitosan. To our best knowledge this is first time reporting this kind of AgNWs growth form bio-polymer. The resulting material is a flexible conductive biopolymer nanocomposite that has potential in several applications.

3.2 General Methods

The chitosan stabilized/synthesized AgNP solution was drop cast onto a flat clean glass substrate which upon drying to produce a 1- 2 μm purplish thin film which contained cuboidal AgNPs. Chitosan thin films lacking AgNPs were clear and topologically smooth. After several days of incubation at room temperature, SEM analysis of the AgNP-containing chitosan thin films demonstrated the presence of long, irregular silver nanowires (AgNWs) that erupted from the surface of the chitosan thin film. AgNWs were only observed on chitosan thin films that contained AgNPs that had

been starved of oxygen either via smothering with a sputtered layer of gold or a layer gold deposited by plasma vapor deposition, or incubation of the AgNP/Chitosan thin film in a vacuum. Oxidation of the cuboidal AgNP within the chitosan film via methanol wash resulted in a complete lack of AgNW formation further supporting this observation. Analysis of SEM micrographs demonstrate that the AgNWs emerge from within the chitosan thin film. Unlike the silver nanowires generated by previously described methods such as PVP mediated synthesis, which exhibit uniform 100nm symmetric pentagonal rods, chitosan-grown AgNWs display an irregular twisting/wandering morphology which display self–growth and bottom up mechanisms commonly seen for semiconductor NWs growth using ultra high vacuum and complex systems. Most processes that involve the formation of nanoparticle thin films or composite materials require two steps: the synthesis of the particle, followed by a compositing step; the AgNW/chitosan nanocomposite material generated by this single pot, a self-seeding synthetic process is green, simpler, and far more cost-effective than previously described nanocomposite synthetic methods. As discussed in previous chapter, at the highest concentration of $AgNO_3$ inclusion in the reaction system, formation of cubic nanoparticles are seen all over the film, eventually when films are stored for longer times, growth of Ag nanowires from bottom-up mode is seen from the film. The schematic of the observed growth of AgNWs is shown in Figure 20 below.

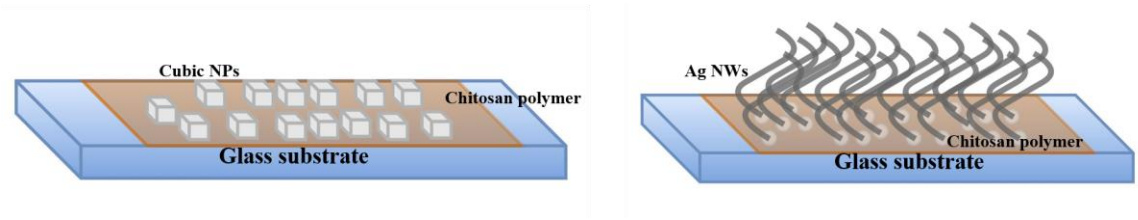

Figure 20. Schematic of Growth of AgNWs from the Cubic Nanostructures

3.3 Synthesis of Solid-State Silver Nanowires

It is well known that chemical reduction is a common method for preparing nanoparticles. For example, sodium borohydride solution is used for nucleation of Ag nanoparticles as follows:

$$AgNO_3 + NaBH_4 \rightarrow Ag + 1/2\ H_2 + 1/2\ B_2H_6 + NaNO_3$$

In the above reaction, it is the electrostatic force among the Ag nanoparticles, which keep them suspended in the colloidal solution. As the reaction proceeds, more borohydride layers are formed around them and particles grow in size. Some authors have used PVA (Polyvinyl alcohol) and other polymers for stabilization of nanoparticles. In the present investigation, Ag nanoparticles are reduced by chitosan and chitin biopolymer with its amine group and also the self-assembling polymer acts as a stabilizing agent, which provides the dual purpose for the formation of the Ag nanoparticles.

The colloids in liquid are charged particles. These particles acquire charge through the composition of colloidal material. As soon as they are exposed to liquid, ions of opposite charges accumulate around them. The accumulation of ions leads to formation of electric double layer. The ions move under the phenomena of brownian

motion and form a dynamic double layer around them which is loosely bound. Stability of colloids can be increased by increasing the stearic repulsion (hindrance), which occurs by adsorption of some layers of different materials on colloidal particle. Adsorption of organic molecules on inorganic colloidal particle e.g., Ag nanoparticle, is possible to reduce the attractive forces by addition of adsorbed layers. Consequently, the effective size of the particle changes, which helps them to stay at a larger distance due to reduction of the attractive interaction.

In this process, the biosynthesis of the Ag nanoparticles is formed by self-assembling of the chitosan/chitin biopolymer during the reduction process. Charge transfer takes place from the amine groups present in the biopolymer, resulting in the nucleation of Ag nanoparticles. Further, this is followed by condensation, surface reduction and electrostatic stabilization by oxalic acid molecule layer.

Chitosan polymer have the amine and acetylamine functional group, where the acetamide of chitin makes it less soluble in water and more de-acetylated form of chitin is chitosan is soluble in water under mild acidic condition. The structure of the alpha chitin orientation, which creates the socket for the Ag nanoparticles to get stabilized and also grow AgNWs as show in Figure 21. On subsequent stages of reaction, the above molecules structure of the polymer, get adsorbed to the Ag nanoparticle under influence of coulomb force (electrostatic double layer) resulting in formation of layers of the polymer side chain with the layer of reducing agent.

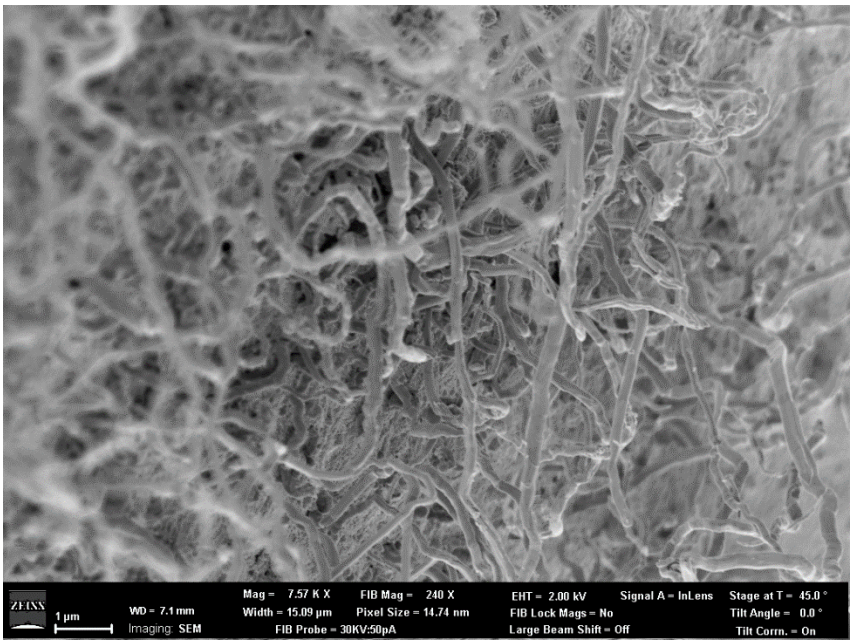

Figure 21. Growth of AgNWs from Chitosan Polymer Base is Shown through SEM Image

In the similar way of the formation of the AgNPs, the formation of the AgNWs arises through the surface of the polymer and the individual AgNPs assembles as a bottom-up processes to form the AgNWs and the structure of the polymer plays a major role in the AgNWs formation at the room temperature. The oriented attachment and growth of the AgNPs can lead to the formation of AgNW. The structure of the α-chitin orientation and the de-acetylated form chitosan can create the socket for the AgNPs to get stabilized and AgNWs formation could occur based on the crystal orientation. Morphology comparison of plane chitosan, AgNPs loaded chitosan and AgNWs grown chitosan polymer surface is depicted in Figure 22 below.

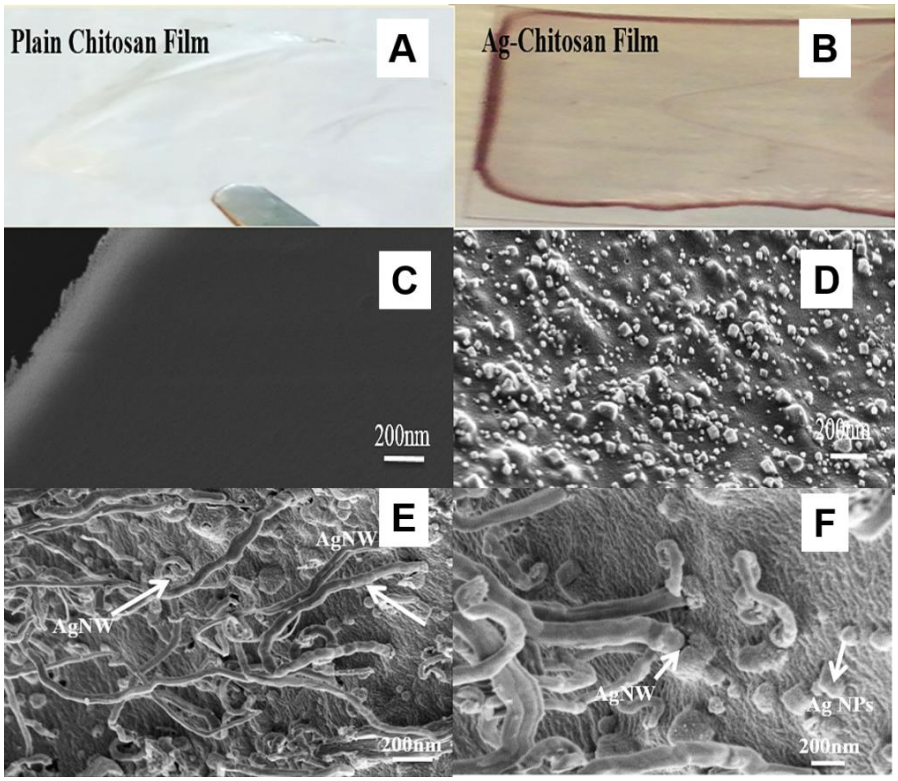

Figure 22. Optical and SEM Images Depicting the Surface of Plane Chitosan, AgNPs Loaded Chitosan and AgNWs Grown Chitosan

3.4 Results

3.4.1 Growth Evaluation of AgNWs at Different Concentrations of $AgNO_3$ using SEM

Analysis of AgNPs size and shape with the change in concentration of $AgNO_3$ has been presented in section 2.3.2. This section is the follow up research of the Ag/Chitosan films with same concentrations as listed in Table 2 for the growth of AgNWs on the surface of the film. Prime goal of this work it to find the optimized concentration of $AgNO_3$ in combination with chitosan solution gives good growth of AgNWs on the surface of the film.

Ag/Chitosan solution obtained for different concentrations, without any filtration or purification is made into films with the same procedure as discussed in chapter 2. The films are directly subjected to SEM imaging to see the possible growth of AgNWs on the surface of the polymer film. To get clear images of the surface of the film and to scavenge oxygen to react on the film surface, a 5nm Au/Pd sputter coated onto the polymer film. Figure 23 shows the SEM images of the Ag films, where it is seen that, at the lower concentration of $AgNO_3$ in the reaction solution, Figure 23a shows small buds of AgNWs trying to grow from the polymer surface. With increase in the concentration of $AgNO_3$, AgNWs growth initiation is increased and for the highest concentration sample film, highest growth of AgNWs is seen, with good aspect ratio. It is interesting to observe that, on high concentration Ag film, AgNWs popped out from the polymer matrix similar as seen Figure 23d.

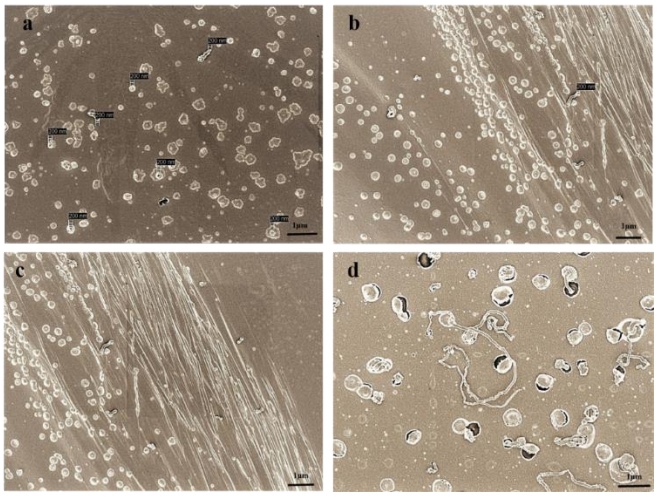

Figure 23. SEM Images of Growth of AgNWs from the Surface of the Chitosan Polymer

Since, only at the concentration 5:5 by volume of the Ag and chitosan solution, good growth of AgNWs is observed as per the SEM analysis. For all further experiments sample ‘e’ film is used. To understand the density of AgNWs growth on the film, SEM imaging of sample ‘e’ film is performed. Below in Figure 24, where high density of nanowires growth is seen at different locations of the film and at different magnification of SEM imaging.

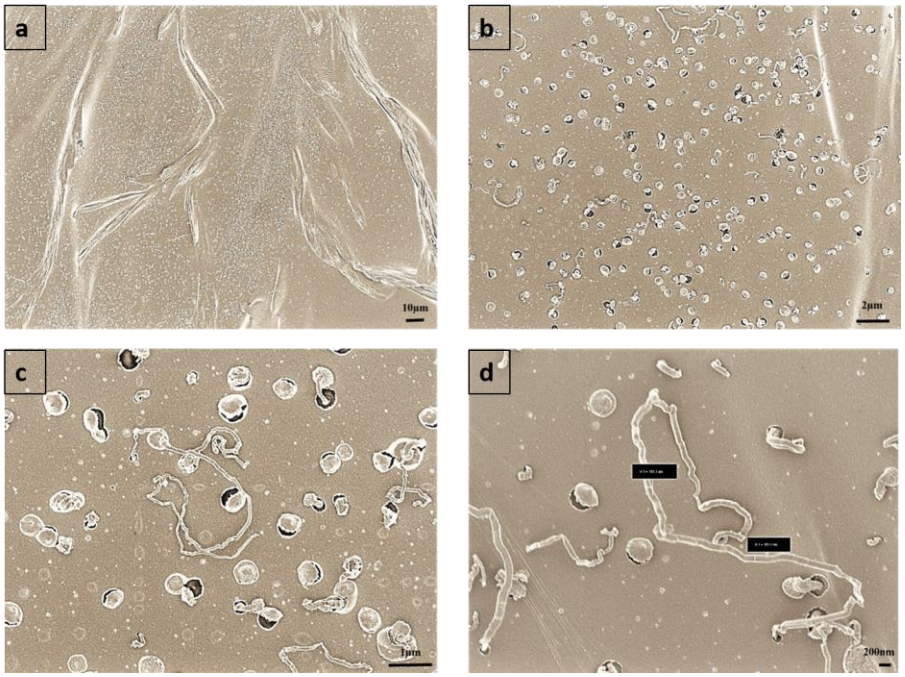

Figure 24. SEM Images of Ag Film ‘e’ at Different Magnifications

To investigate the surface composition of polymer film and match the presence of Ag on the surface with respect to the added concentration, EDS analysis is performed on the surface of the polymer. Figure 25 shows the EDS data of the films with just AgNPs compared to the films with cubic nanostructures and the short growth of AgNWs and to

fully grown AgNWs. It is observed that, for the film with no possibility of wire growth and is covered with just AgNPs, weight percentage of material composition is obtained as 50%. For the film covered with cubic nanostructures weight % of Ag is obtained just 18%, further when film is characterized at short growth of nanowires, it is obtained as 35% and, finally weight percentage of Ag for fully grown AgNWs is shown as 56%.

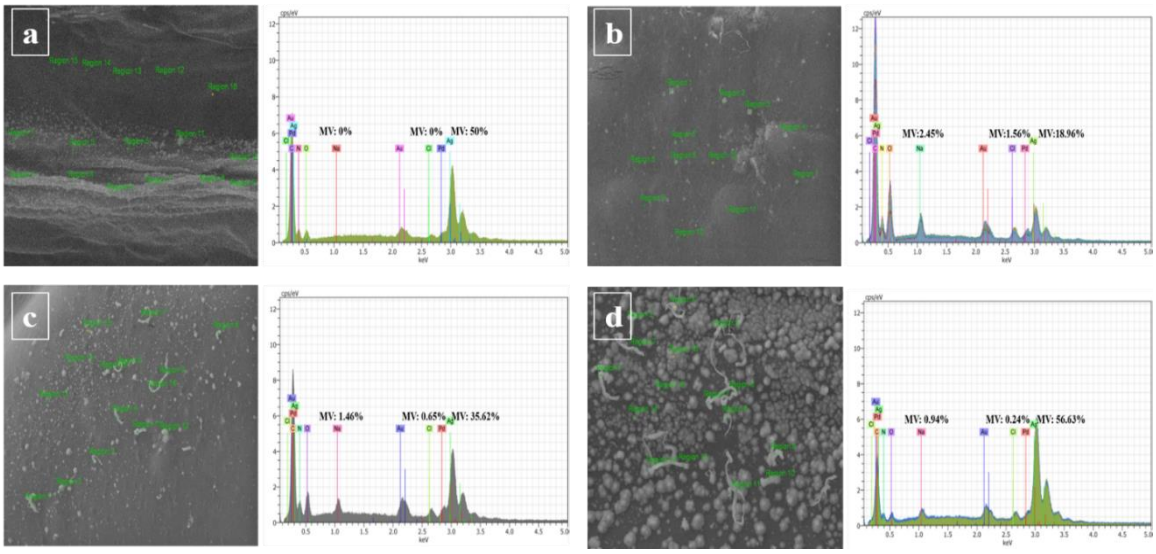

Figure 25. EDS Data of Ag Film at Different Growth Times

3.4.2 PH Dependence of Chitosan Polymer Solution for AgNWs Growth

In my synthesis process of AgNPs and eventually growth of AgNWs, Chitosan polymer plays key role in the reaction system. As discussed in general methods section of chapter 2, chitosan polymer is dissolved in water with the addition of trace amounts of acetic acid and by magnetic stirring of the solution till chitosan completely dissolves in water. The obtained solution is further used in the synthesis of AgNPs and acts as a base, when dried, for the growth of AgNWs.

In this section, I have investigated the dependence of PH of this chitosan solution on the formation of AgNPs and AgNWs. Series of experiments are performed after the end solution of Ag/Chitosan is formed with change in PH to find the composition of the end product.

PH measurements is done by traditional PH paper color change monitoring. As synthesized chitosan solution PH is measured to be slightly acidic i.e. PH 5 and the proposed investigation with the change in PH is attempted by adding 1ml of NaOH solution to the reaction process to make the PH of the solution to 8 i.e. base and 1ml of acetic acid is further added to the solution to make it more acidic i.e. to PH 1. The final reaction solution turned more diluted with the addition of acetic acid and it turned to jelly form when NaOH is added to the solution. It can be visually observed as presented in the Figure 26.

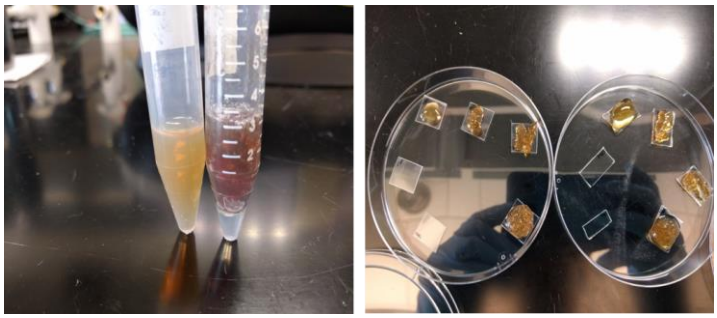

Figure 26. Photographic Image Depicting the Formation of Ag/Chitosan Solutions

Characterization analysis on more acidic solution of Ag/Chitosan is performed, where it behaves like the as synthesized PH5 solution of chitosan, except for the observation in SEM of no formation of AgNWs on the film. So, all other characterization

investigations presented here are of Ag/Chitosan PH 8 solution. The jelly form solution obtained as seen in Figure27, prepared at different concentrations of $AgNO_3$ as shown in Table 2 below are dried in similar process as mentioned in previous chapters and subjected to UV- vis, XRD analysis and SEM analysis.

Table 2. Different Concentrations of Basic Ag/Chitosan Solution Varied by Volume

Notation	**Concentration** **Chitosan:** $AgNO_3$
Ag sample 'Bc'	**Plane chitosan**
Ag sample 'B1'	**1:0.2**
Ag sample 'B2'	**1:0.4**
Ag sample 'B3'	**1:0.6**
Ag sample 'B4'	**1:0.8**
Ag sample 'B5'	**1:1**

UV-Vis analysis is performed on the films, formed using jelly form of the basic solution of Ag/Chitosan. Sharp absorption plasmonic peak is obtained for all the concentrations with slight broadening of the peak, which is associated to increase in the concentration of silver precursor. The UV-Vis plot is presented in Figure 27 below.

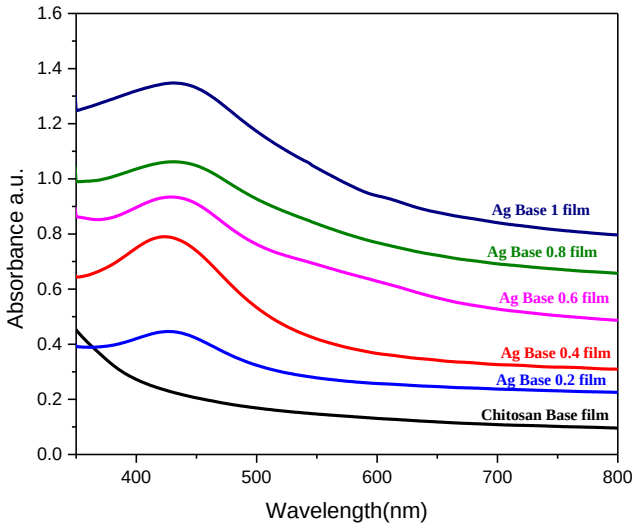

Figure 27. UV-Vis Plot of the PH 8 Ag Solution at Different Concentrations of $AgNO_3$

Interesting results are obtained in XRD analysis on the jelly films at different concentrations as listed in Table 3. At the lowest concentration of $AgNO_3$ added to the reaction solution, in this case there are no dominant metallic Ag peaks corresponding to Ag (111) is seen. But, with the increase in the concentration, till the highest concentration, intensity of Ag (111) is seen to increase. The XRD plots of the discussed films are given below in Figure 28.

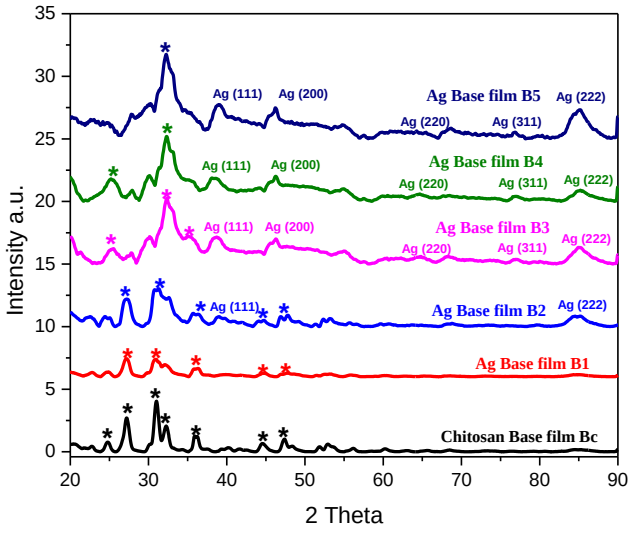

Figure 28. XRD Combined Plot of the PH 8 Solution Films

SEM imaging of the PH 8 based Ag/Chitosan films is performed and observed the structure of Ag formed when the solution is turned into base is of rod shaped. This rod-shaped Ag is observed only for the equal concentrations of Ag and chitosan solution, rest all other concentrations are either distorted due to jelly shape of the material or not suitable for imaging using SEM. SEM image of the film showing the rod structure of Ag is shown in Figure 29 below.

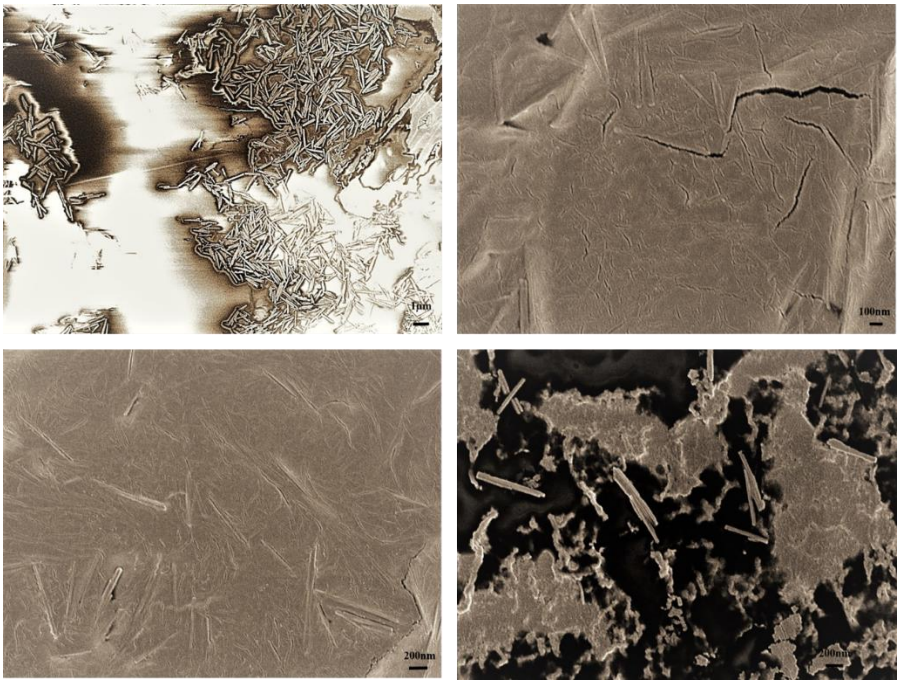

Figure 29. SEM Images of Ag Film at Highest Concentration Showing the Rod Structure

3.5 Discussion

Key observations and understandings presented in this chapter regarding the growth of AgNWs in the solid state are: 1. AgNWs are successfully seen grown from the polymer surface when incubated in the oxygen starving condition and in the presence of highest concentration of $AgNO_3$ in the synthesis process. 2. EDS analysis proved that, Ag weight percentage on the film is seen to increase in percentage with the growth of AgNWs in length from the surface of the film. 3. Chitosan solution is key for the reduction and stabilization of the Ag nanostructures formed in the synthesis process. when the PH of this solution is changed to basic i.e. to PH 8, it is observed that instead of forming plane film, jelly kind of film is formed and Ag nanorods are imbedded in the film rather than AgNPs and growth of AgNWs.

In the current work and in current chapter, growth of AgNWs from the films which are imbedded with AgNPs is presented with strong support of SEM imaging at each stage of growth process. It is confirmed that the equal volume concentrations of Ag and chitosan gives high density growth of AgNWs. Material composition on the surface of AgNWs film is measured using electro dispersion spectroscopy, which gave clear indication of the AgNWs growth is happening from the surface of the chitosan film. Since, with growth in length of AgNWs on the surface, it is seen increase in the raise of Ag weight percentage on the surface of the film. This clearly indicate the formation of the AgNWs is due to the source of Ag coming from inside the film. Additionally, it is seen that PH of the solution too have affect on shaping the AgNPs to form AgNWs or not. When, the solution PH is made basic by adding NaOH i.e. to PH 8, the chitosan polymer inside the synthesized solution breaks down its structure and it forms into jelly like form. When the jelly solution is made into films and characterized with UV-Vis, XRD and SEM, it is observed that, there is no sign in the formation of AgNWs, which is seen to form in the films which contain as synthesized chitosan solution. With this PH experiment, it is understood that, chitosan solution structure plays major role in the formation of AgNWs.

3.6 Conclusion

In summary of this work, Solid-state growth of AgNWs is presented for the first time. Growth of AgNWs is shown when the Ag/Chitosan film is completely dried and characterized for the presence of AgNPs covering the surface of the film. With extensive SEM and EDS characterizations, it is proposed that, the presence of Ag source inside the

polymer matrix, which is proven to exist in the previous chapter under Silver NPs distribution section is responsible for the growth of AgNWs from the surface of the chitosan polymer. With change in the structure of the chitosan polymer by changing the PH of the solution, growth process of AgNWs from the polymer is completely stopped and formation of Ag nanorods is seen.

CHAPTER IV

SOLID-STATE GROWTH OF AG NANOWIRES AND ANALYSIS OF SELF-GROWING PROCESS

4.1 Introduction

Our current research report of growth mechanism of AgNWs at solid-state is unique and different from above discussed established methods. We propose a simple method for solid-state bottom-up growth of AgNWs on chitosan bio-polymer film. Most of the research reports regarding syntheses of silver NPs/NWs use PVP as reducing and stabilizing agent in solution syntheses process. There are less reports, where chitosan polymer is used for syntheses of AgNPs. Among those few reports, our published work is the simplest method to syntheses AgNPs and eventually grow solid-state AgNWs on the chitosan film. Here in this article, we report the science behind this growth process and employed conditions for the successful growth of AgNWs.

Growth mechanism for AgNWs in solution form relies on influencing factors like a. Oxidative etching, b. Role of Cl- ions, c. Thermodynamics factor i.e. temperature at which syntheses reaction is performed and d. Kinetics of reaction system i.e. stirring speed and time of stirring. For solution processing of AgNWs, Oxidative etching is proposed to be blocked by three ways (i) Purging Ar gas into the reaction solution. (ii) Introducing oxygen scavenging ions like FeIII/FeII, CuII/CuI[83]. (iii) Protecting dissociation of AgNWs source, the multi twined Ag seeds by using capping agents like

citrate, which avoids the adsorption of oxygen atoms on to the seeds. With the introduction of Cl^- ions into the reaction solution, Ag^+ ions combine with Cl^- ions to form AgCl, which further helpful in releasing Ag^+ ions slowly avoiding the faster dissociation of multi twined Ag seeds, additionally in few reports it is reported that formed AgCl converts to cubic structures which again forms as nucleation sites for growth of AgNWs in solution. Typical temperature at which solution-based growth reactions are carried is around ~200^0 C, where temperature acts as catalyst to form more multi twined seeds and eventually AgNWs. Lastly, kinetics of reaction system is seen to affect the growth of AgNWs in some research articles, where the sonication time of reaction [130] and stirring speed reported to play key role in homogenous growth of AgNWs.

As current report is for growth of AgNWs at solid-state, above discussed growth factors differ in their applicability and functionality for the current system. Modified blocking of oxygen on to the system for AgNWs growth is discussed. Role of Cl^- ions is studied thoroughly in solid-state system. Thermodynamic factor for AgNWs growth after film formation is reported. Other factors specific to solid state growth of AgNWs is reported. Such as volume ratio of $AgNO_3$ and chitosan, growth time of AgNWs and Volume of Ag/Chitosan solution to make Ag film. All of the above conditions are thoroughly discussed in this research.

Ag Nanostructures have many potential applications. One such field of our interest in current study is to use AgNWs platform for Antibacterial testing. There are good number of research articles presenting anti-bacterial property of chitosan combined AgNPs in solution form.

But our experimental results are first to report the study of anti-bacterial property using AgNWs grown on chitosan film.

4.2 Experimental

4.2.1 General Methods

Chitosan (MW: molecular weight: 150,000, 1.5% w/v), $AgNO_3$(>99%), Acetic acid (70% diluted solution) and NaCl are bought of ultra-pure grade from Sigma-Aldrich. Morphology including the shape and size of nanoparticles was viewed under a scanning electron microscope (SEM). Sample preparation and imaging for morphology study: The samples were placed on SEM sample pug. After drying, a 4-nm-thick gold-palladium (Au/Pd) layer was deposited on the samples using a Leica EM ACE200 with a real-time thickness monitoring quartz crystal microbalance. The SEM images were obtained using a Zeiss Auriga FIB/SEM. Scale bars were added using ImageJ software, followed by energy-dispersive X-ray spectroscopy analysis (Hitachi S-4800-I FESEM w/Backscattered Detector & EDX) to verify the presence of AgNPs/AgNWs. Optical properties of Ag film and solution is evaluated by ultraviolet-visible spectroscopy (UV-Vis spectroscopy, Varian Cary 6000i), XRD(Aligent) is used for structural analysis of Ag film.

Chitosan flakes (500mg) are dissolved in 10ml of water with the help of 1% wt acetic acid (500µL) and diluted 1% wt acetic acid (1 ml) with trace amounts of NaCl in the same. Trance amounts of NaCl is added to the solution. The solution is kept for magnetic stirring for 24hrs till complete flakes of chitosan are dissolved to form a thick solution of the same. $AgNO_3$ (50nM) is dissolved completely in 5ml of water. Once the

chitosan solution is available, dissolved $AgNO_3$ is flushed into 5ml of chitosan solution in glass vial in orders of 1ml at a time till 5ml. A white path is seen in the way of $AgNO_3$ flush in chitosan solution indicating the start of reduction of $AgNO_3$. Following which the obtained solution is kept for ultrasonication for few hours till the color changes to plasmonic colors. In this research case, the white color turns to immediate yellow and then to pinkish brown. Once the color change to pinkish brown the ultrasonication is stopped and stored the same for further characterizations.

In our previous work [131], the characterization results for the solution formed are presented thoroughly. Here with varying volume concentrations of $AgNO_3$ i.e. 1 ml, 2 ml, 3 ml, 4 ml and 5 ml in constant 5 ml of chitosan polymer solution are subjected to characterizations to deduce and understand the growth conditions of AgNWs on the formed chitosan/Ag composite films. Further in the paper the above mixture ratios of chitosan and $AgNO_3$ are noted as ‘sample a’ (5:1), ‘sample b’ (5:2), ‘sample c’ (5:3), ‘sample d’ (5:4) and ‘sample e’ (5:5) respectively for all the characterizations performed.

Chitosan/Ag composite films are formed by drop casting 300 µL of solution on PET films and kept for drying the same at 50^0 C till the chitosan/Ag film peels itself off from the PET. Main intension of using the PET base is to peel off the film to characterize the same as standalone film.

4.2.2 Growth Factors Evaluation

4.2.2.1 Oxidative Etching

In literature of solution processing synthesis of AgNWs, role of oxidative etching in hindering the AgNWs growth is explained in detail[132]. In brief, multiply twinned

seeds (MTS) which are source for AgNWs growth are thermodynamically stable and are at higher in energy relative to single crystals. So, the oxygen atoms attack these MTS structures and dissolve them to form single crystal seeds as shown in Figure 30. This effect is not seen with single-crystal seeds as they are more resistant to oxidative etching as they don't have twin boundary defects on their surface.

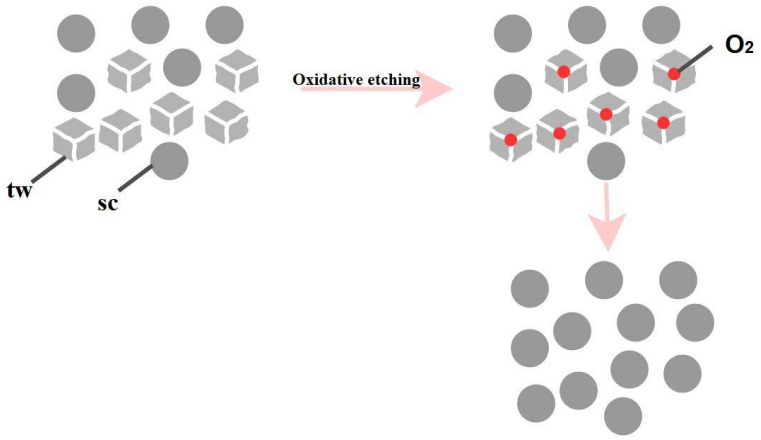

Figure 30. Schematic of Oxidative Etching Process in Solution Processing

So, considering saving the dissociation of MT seeds from the system, inhibiting oxygen from the reaction system is important to form AgNWs. In solution process, three ways that are proposed to inhibit oxygen are: a. Removing O_2 from the reaction system by bubbling inert gas through, b. Blocking oxygen adsorption to the seeds through the selection of suitable capping agents (eg. Citrate), c. Diminishing the role of oxidative etching by scavenging oxygen in the solution with a redox pair (eg. Fe III/I or Cu II/I salts). Since the current study and growth process of AgNWs is in solid state, we propose a new and fourth way of blocking oxygen from the as dried and peeled Ag film from the PET. That is, Sputtering of Au/Pd film of 3nm thickness on the solid Ag film proved to

block oxygen from the system and paves a way for AgNWs growth. This growth process of AgNWs with oxygen blocking is verified using FE-SEM

4.2.2.2 Role of Cl^- Ions

The role of Cl^- ions in the AgNWs growth system is one other important factor in the NW growth process analysis. Many research articles[25, 133] have reported this factor in solution process of AgNWs growth. Most used Cl- ions source in the reaction system as an additive for the growth of AgNWs is NaCl, which can be easily dissociated to Cl^- ions. In typical polyol synthesis, PVP reacts with NaCl to form Cl^- ions as shown in the article[25]. These free Cl^- ions combines with free Ag^+ ions in the reaction solution to form AgCl, which further releases Ag^+ ions in slow pace avoiding the fast dissociation of formed multiply twinned seeds under oxygen influence thus helping in formation of AgNWs.

4.2.2.3 Time

Influence of oxidative etching on AgNWs growth and inclusion of Cl^- ions for AgNWs growth are reported and discussed in many research articles previously. Baring condition that all the growth is in solution processing. We, in previous two sections of this article reported thoroughly on these conditions for the growth of solid state AgNWs. The third important condition influencing this solid-state growth of AgNWs is time of AgNWs growth. This influencing factor is unique and importantly specific to solid state growth. Since this factor is never observed or discussed before in solution processing of AgNWs.

There are research articles, where varying time factor of synthesis factor reported the growth change in silver nanowires in solution processing[134]. But our discussion is on self-growth of AgNWs, under no active reaction conditions imposed on the Ag/Chitosan film.

4.2.2.4 Temperature

In solution synthesis of AgNWs, one key factor considered for uniform growth of AgNWs is the reaction temperature, i.e. the temperature at which polyol reaction to form AgNWs is carried out. Typically, this temperature ranges from 100 to 150^0 C. This influence factor is studied as thermodynamic effect in the solution reaction system. Here in our AgNWs growth system, since the synthesis of AgNPs is carried out at room temperature. The thermodynamics factor is introduced at the stage of AgNPs/Chitosan film drying process. Typical opted temperature for drying the films on PET is 50^0 C and dried for extended time of 8hrs, this temperature is chosen to avoid distortion of PET substrate when subjected to higher temperatures for longer times. The optimization of drying time is verified based on the SEM characterizations and analysis of AgNWs growth at different drying times.

4.2.2.5 Volume of Film Formation

This section discusses the last growth effecting factor. Which is the volume of AgNPs/Chitosan solution needing to be used to form a film to observe good growth of AgNWs. This factor is verified, reported and discussed in this section. After many trial and errors in choosing right volume of solution for good AgNWs growth, we ended up in concluding it to 400µL.

4.3 Results

4.3.1 Ag Nanowires Growth Analysis by New Way of Blocking Oxidative Etching Method

In this manuscript, we demonstrate a new method of reducing oxidation from the polymer-based AgNW reaction system which we call smothering. In previous reports of the chitosan film synthesis of AgNWs, the films of chitosan that contained silver nanoparticles were sputtered coated by a thin Au/Pd film. The metal coated chitosan film resulted in the AgNW growth, while those left uncovered did not. To determine whether a nm thickness layer of Au/Pd was sufficient to prevent exposure to oxygen and to determine whether the present of oxygen was inhibitory to solid state AgNW growth. We performed the following experiment (Figure 31). A single thin film of chitosan containing silver nanoparticles was prepared as described earlier and divided into four pieces: quadrant '1' was coated with 3 nm of Au/Pd, quadrant '2' was coated with 8 nm of Au/Pd; quadrant '3' was treated with an oxygen plasma to promote oxidation, and quadrant '4' was unprocessed. All the treated film quadrants are denoted as '1^1', '2^1' and '3^1' respectively as shown in Figure 31 below. The samples were then stored in dry air and examined after one day and then a week after for the growth of Ag NW.

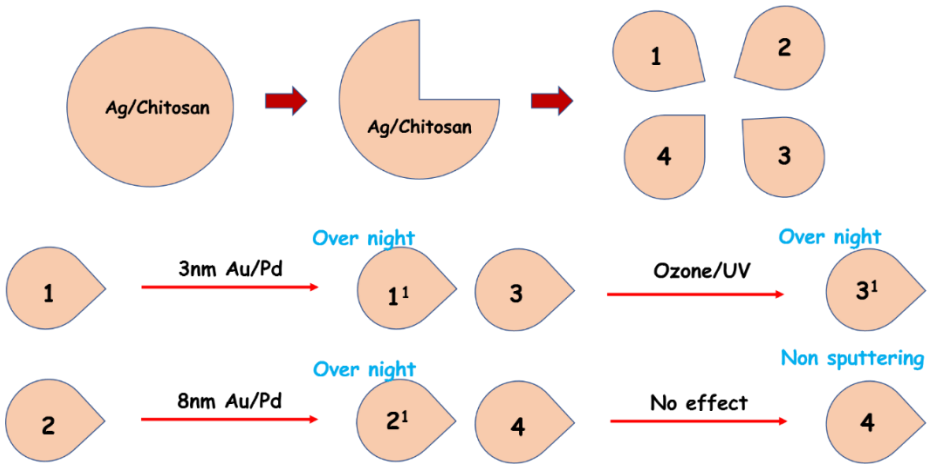

Figure 31. Schematic of Experiment Performed on Single Ag/Chitosan Film

Since our hypothesis is that oxygen will inhibit AgNW growth in the solid state, it is expected that the thin films that are uncoated (‘4’) or plasma etched with an oxygen etch (‘3^{1}’) should have little or no AgNWs after a week of growth, while the thin films coated with varying amounts of Au/Pd metal (‘1^{1} & 2^{1}’) will have AgNW. To verify this, SEM was taken to characterize the films as presented in Figure 32.

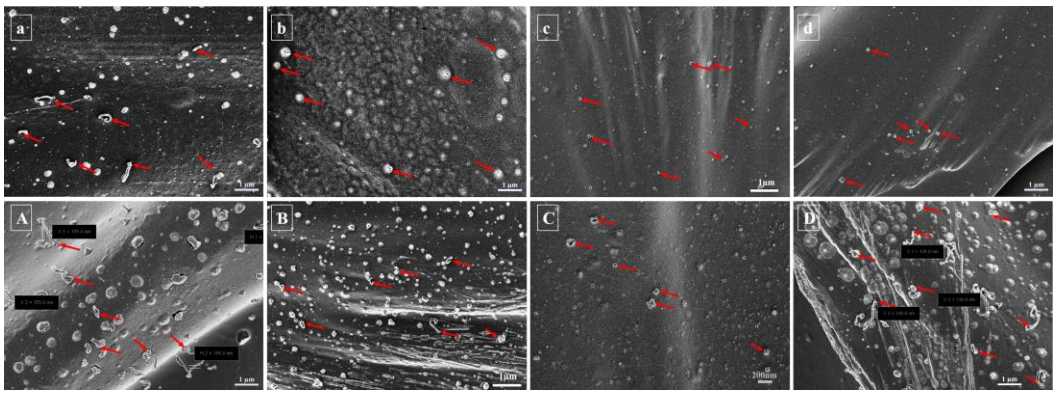

Figure 32. SEM Images of Above Experimented Films of Four Sections of Film

As expected, we observed the growth of AgNWs on the film with 3 nm coating of Au/Pd and stored overnight at room temperature (Figure 32a, with pointed arrows indicating growth initiation of AgNW). The one-day old AgNWs are small with an average diameter of 90±10 nm and average length of 500±50 nm. For the films with 8 nm coating of Au/Pd and stored the same way (Figure 32b), AgNW growth initiation was also observed by small protrusions of AgNWs from the film (Figure 32b, arrows). Note the thickness of the 8 nm Au/Pd coating obscures much of the details of the wire. However, there is no growth of AgNWs on the film treated with oxygen plasma (Figure 32c), in fact we observed the breakage of the cubic particles on the film surface. For the untreated film in quadrant 4, we only observe the cubic particles within the chitosan film surface (Figure 32d). This indicates that ambient oxygen can inhibit the AgNW growth on the film (‘4’).

In the samples stored for one week, we observe a similar trend further increase in the size AgNWs (Figure 32A). The Ag NW on the film with 3 nm coating of Au/Pd had an average length of 3±1 μm and average diameter of 150±10 nm. In the film with 8nm coating of Au/Pd, Ag NW growing out of the film is clearly observed (Figure 32B). On week old AgNWs have an increased aspect ratio when compare to one day old AgNWs, demonstrating that these wires grow laterally as well as longitudinally. This is distinct form solution-based AgNW growth processes where the AgNWs mainly grow longitudinally. The chitosan films that exposed to the oxygen plasma, even after a week time, show no trace of Ag NW growth (Figure 32C). This proves the hypothesis regarding the effect of oxygen on the surface of the film in hindering the growth of

AgNWs. Coming to the case of quadrant ‘4’ film, initially when it is exposed to oxygen in the air for one day, no growth of AgNWs (Fig 32d) was observed. But the same section 4 of film coated with Au/Pd for after a week SEM characterization, clear growth of AgNWs is seen on the film (Fig 32D) though shorter than sample 1 and 2. This proves that even slight amount of oxygen on the surface of the film will hinder the growth of AgNWs.

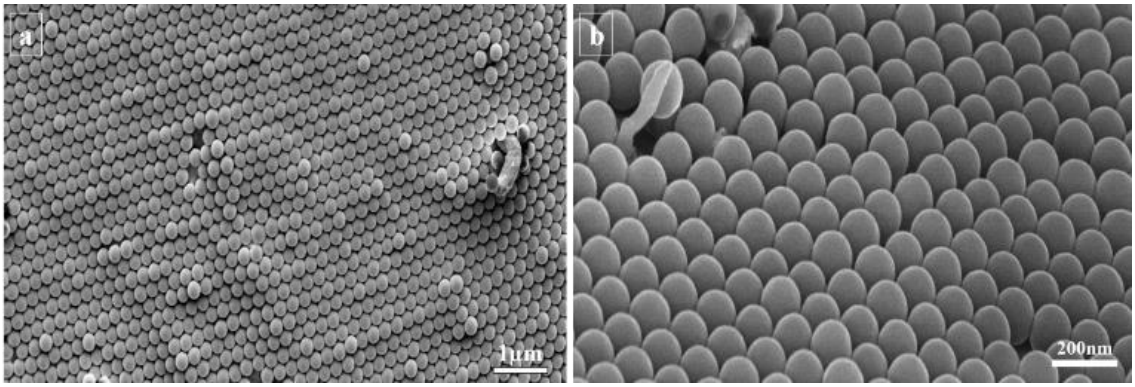

Figure 33. SEM Images of Ag/Chitosan Film Coated with Self-Assembled Polymer Beads

We extended this study further by examining the smothering of chitosan thin film with a PVD deposition of a 5 nm Au layer Figure 34 and and a self-assembled monolayer of 400 nm polystyrene beads shown in Figure 33 [135] Similar to the sputter coated samples, , the initiation of AgNWs from the corners of cubic Ag nanoparticles were observed from the PVD Au coated chitosan thin films and later the AgNWs grown into longer and thicker. For 400 nm beads covered films, AgNWs sprout out from the bottom of the beads by pushing beads away (Figure 33 b). These experiments further prove that blocking oxidative etching is necessary in solid state growth of AgNWs.

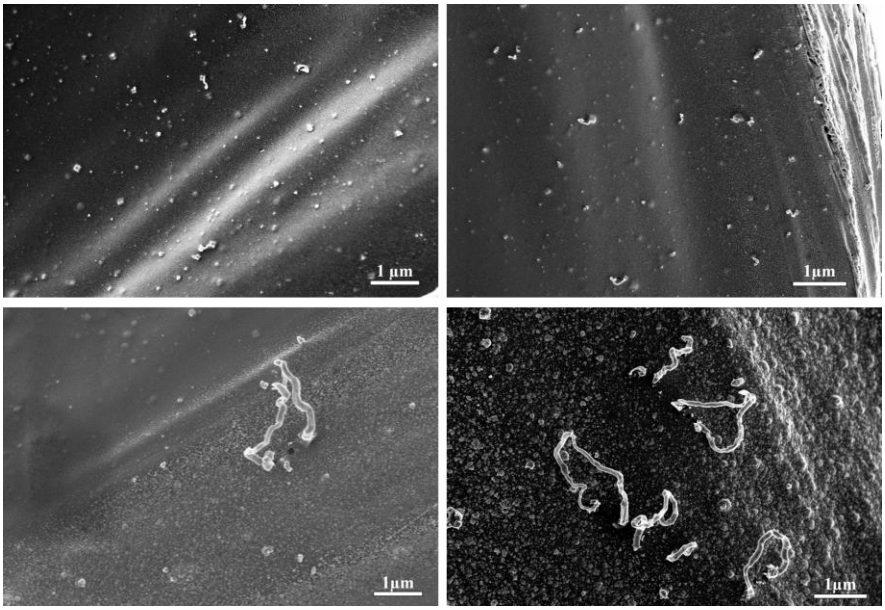

Figure 34. Growth of AgNWs through the PVD Coated Au Thin Film of 5nm Thickness

4.3.2 NaCl Concentration Evaluation for AgNWs Growth Initiation

Description of synthesis process, and AgNWs growth studies as in previous studies [136], NaCl was used as key additive during the synthesis process for the growth initiation of AgNWs on the chitosan polymer film. Concentration of NaCl used in all our previous studies was 100mM mixed in base chitosan solution along with the addition of $AgNO_3$ precursor. Immediate formation of white precipitate with the addition of precursor indicates the formation of AgCl in the solution. Under ultrasonication conditions, the solution converts into plasmonic color, indicating the formation of AgNPs.

In this research, we varied the concentration of NaCl added to the synthesis process as shown in the Table 3. Sample names indicated in the table are continued forward to be used in characterizations results reported below.

Table 3. List of Concentrations of NaCl Varied in the Reaction Solution

Sample	Concentration (mM)
No NaCl	0
Sample a	1
Sample b	5
Sample c	10
Sample d	25
Sample e	50
Sample f	100

Varying concentration of NaCl in the synthesis process yielded different plasmonic color products of AgNPs solution as shown in Figure 35. Figure 35 depicts chitosan solution with the addition of $AgNO_3$ precursor and Chitosan/AgNPs solution of varied colors after ultrasonication. AgCl precipitate formation is clearly seen with the increase in the concentration of NaCl. To further understand the effect of varying concentration of NaCl on AgNPs and AgNWs formation, UV-Vis analysis is separately performed both on Ag solution depicted in Figure 35 and Ag Films are made from the solutions respectively.

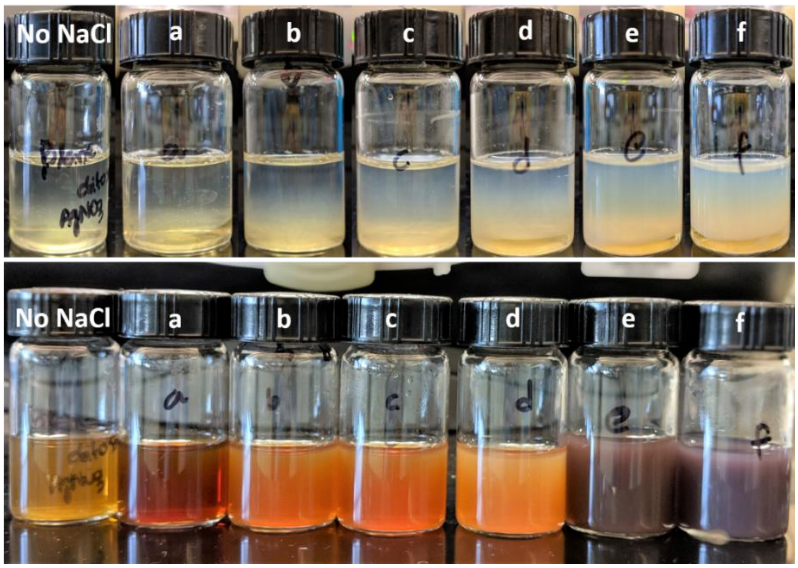

Figure 35. Synthesis Process with Varying Addition of NaCl Concentrations

UV visible spectroscopy peaks of AgNPs solutions depicted in Figure 35 are presented in Figure 36. Clear peak of metallic Ag at ~420nm is obtained for 'no NaCl' and 'Sample a' solutions. With increase in the concentration of NaCl in the synthesis process, more number of AgCl NPs are formed in the solution along with AgNPs. This effect is clearly seen by the change in the broadness of UV peak of the samples 'b', 'c', 'd', 'e' and 'f' along with blue shift of the peak.

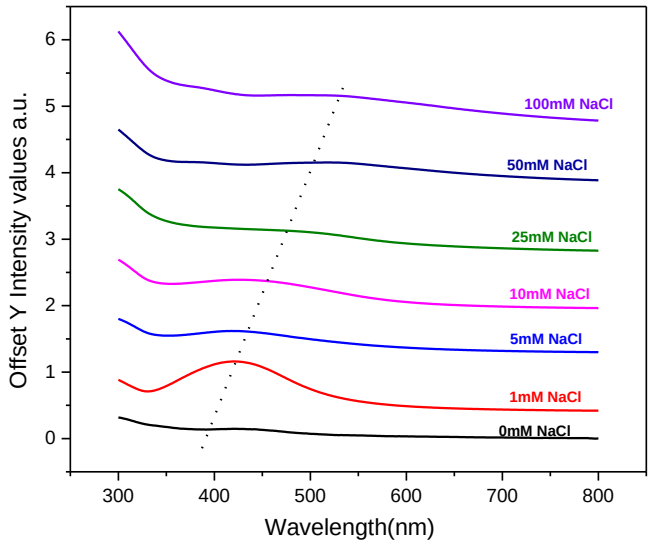

Figure 36. UV-Vis Spectrum of AgNPs Solution with Varying Concentration of NaCl

The AgNPs/Chitosan solutions indicated in table 1 are made into films and are subjected to XRD characterization. XRD patterns indicate the formation of (111) dominant phase Ag on the film with 'no NaCl' addition. With increase in the addition of NaCl to the reaction process, AgCl Nano cubes are formed and eventually distributed all over the chitosan film, acting as nucleation points for the growth of AgNWs. This formation of AgNWs and presence of AgCl Nano cubes are shown up in the XRD patterns shown in Figure 37. For all the sample films, AgNWs phase remain same at (111) peak. But, additional peaks of AgCl are visible clearly as indicated in Figure 37. This result proves the presence of AgCl nucleation sites in the film, which are key for AgNWs growth. FTIR peaks of the Ag solutions of Figure 35 adds up to the support of the UV-Vis and XRD characterizations in terms of indication of change in chemical

properties of the solution with the addition of more and more NaCl into the reaction process. Figure 38 shows the FTIR pattern of all the sample solutions compared with plane chitosan FTIR peaks. With addition of NaCl and with formation of AgCl, two additional peaks in the FTIR pattern is observed for samples from ‘a’ to ‘f’ as indicated by dotted lines in the Figure 38.

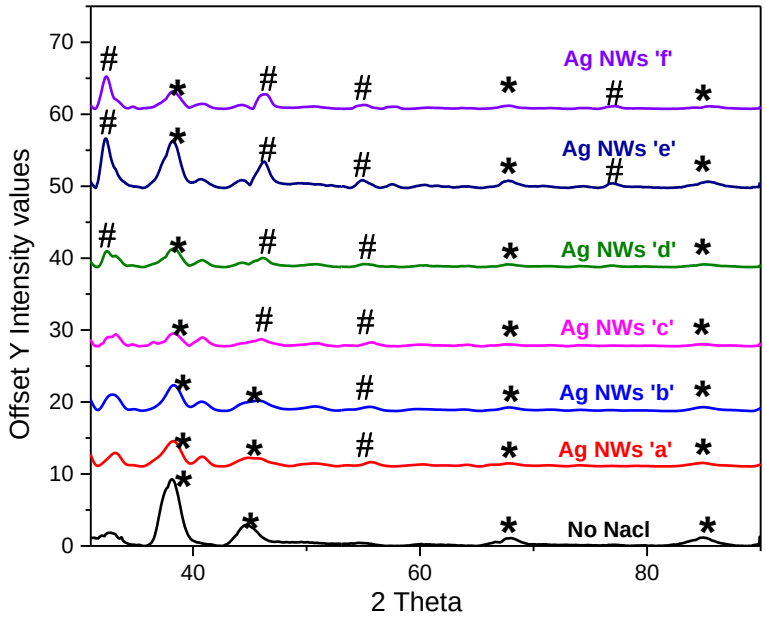

Figure 37. XRD Pattern of Ag Film with no NaCl to 100mM NaCl

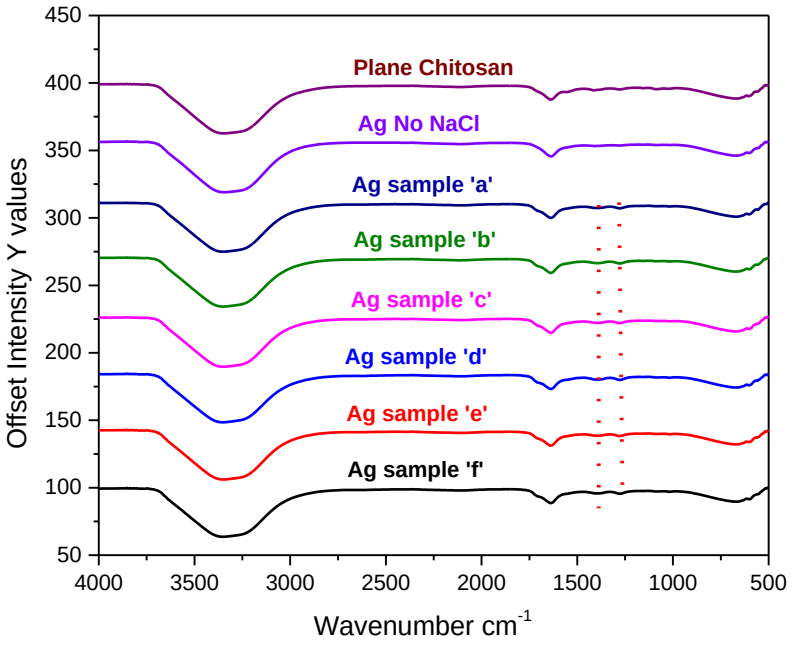

Figure 38. FTIR Patterns of All the Samples Compared with Chitosan FTIR Peaks

The key goal of this research is to find the right concentration of NaCl required for the initiation of AgNWs growth on the chitosan film. In our previous research, we took 100mM uniform concentration for all the research findings reported. Where, good growth of AgNWs is observed all over the film. SEM images are presented for all the samples indicated in Table 3 in Figure 39, which are taken immediately after the formation of the film. In line with our previous research SEM results [137], Figure 39a shows SEM image of Ag film with ‘no NaCl’, where the film looks plane with few spherical AgNPs on the surface. For sample ‘a’, 1mM of NaCl is added to the reaction solution and Figure 39b shows SEM image of sample ‘a’ film, where clear formation of AgCl Nano cubes in the solution and their distribution on the surface of the film is seen.

There is no indication of initiation of AgNWs growth is observed for 1mM concentration of NaCl. Further NaCl concentration is increased to 5mM for sample ‘b’ and respective SEM image of the film is presented in Figure 39c. Small buds are visible on film of sample ‘b’, indicating the possibility of growth of AgNWs. Figure 39d indicates the SEM image of sample ‘c’, where large bud areas are observed all along the surface of the film. Since the concentration of NaCl is raised to 10mM, Ag source i.e. AgCl availability is more in this care, so larger buds are formed on the film. Still this is not considered as growth initiating concentration. For sample ‘d’, having 25mM NaCl concentration, SEM image is presented in Figure 39e. From the SEM image it can be observed that, at this concentration, there is clear growth initiation point for AgNWs with the previously seen buds being broken open, making a way for AgNWs growth. With further increase in NaCl concentration to 50mM i.e. sample ‘e’. Small growth of AgNWs on the surface of the film is observed, as shown in SEM image of Figure 39f. But, the growth is not seen all over the film. Figure 40g indicates the SEM image of the film with highest concentration of NaCl i.e. 100mM. It is seen that, at this concentration, growth of AgNWs is ideal. AgNWs are grown out good from the polymer surface.

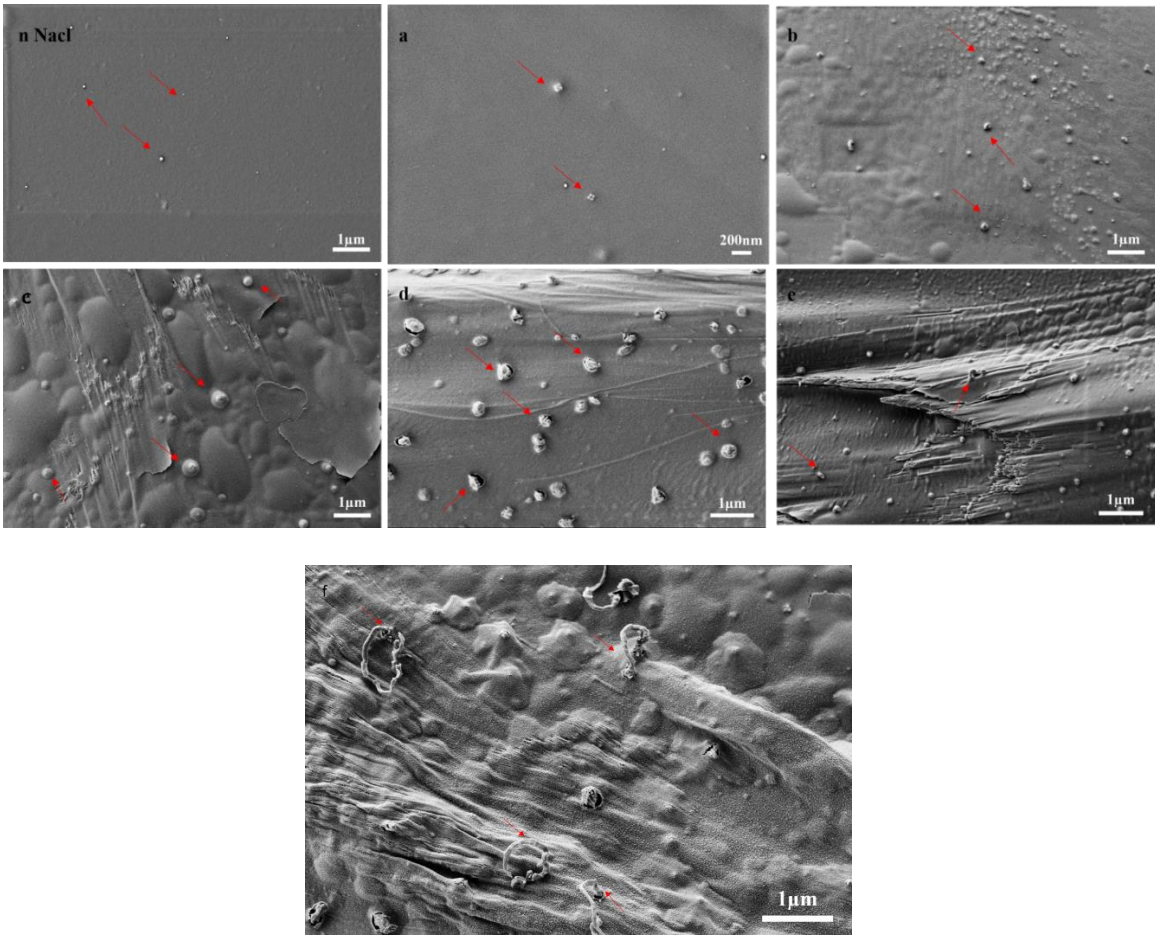

Figure 39. SEM Images of Ag Films with Different Concentrations of NaCl

As per our previous report [137], growth of AgNWs on the surface of the film depends on the time. So, we have taken SEM images of the above samples after a week time. Results are provided in Figure 40. For all the samples except for the samples ‘d’, ‘e’ and ‘f’ there is no change on the film is observed with respect to the growth of AgNWs. But for the films ‘d’, ‘e’ and ‘f’ increase in the growth of AgNWs is clearly seen both in terms of aspect ratio and density of the wires on the surface of the film. This factor depends on the availability of the Ag source in the film with respect to the storage time.

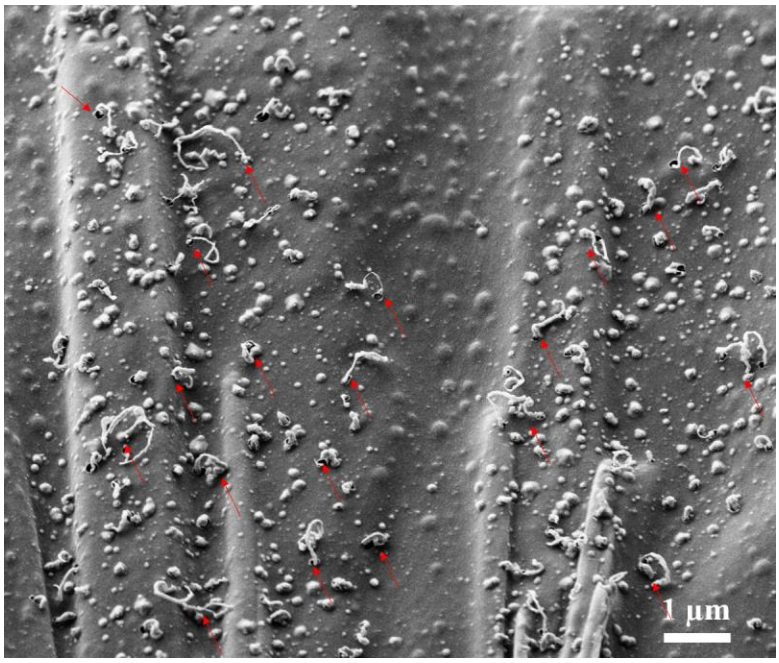

Figure 40. SEM Image of Ag Film at the Highest Concentration of NaCl, Growth of Wires is After a Week.

Additionally, chemical elemental analysis EDS is carried out on the sample films shown in Figure 39. Which indicate the amount of Cl present in the film with the change in NaCl concentration. The result data is provided in Figure 41. Further on the aged film corresponding to sample ‘f’, where good growth of AgNWs is seen.

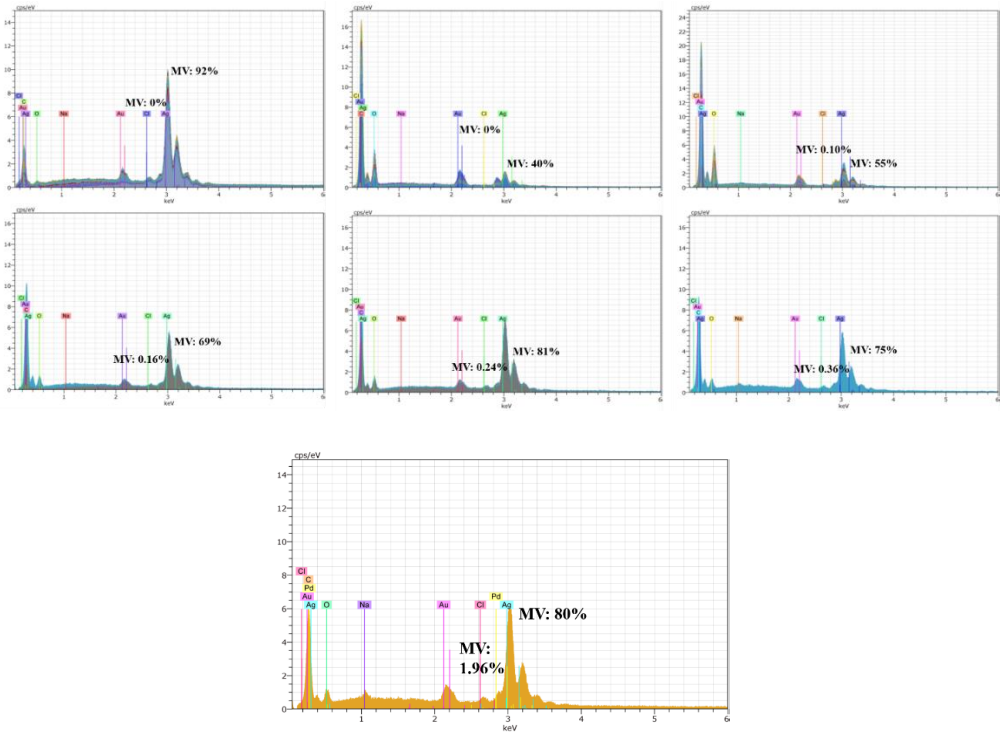

Figure 41. EDS Analysis of Ag Films with Varying Concentrations of NaCl

In second part of this section we investigated the role of cubic AgCl nanoparticles serving as a nucleation points for the solid-state growth of AgNWs. In polyol synthesis of AgNWs, cuboidal AgCl nanoparticles function as the supreme nucleation sites for heterogeneous growth of AgNWs. In this system, AgNW growth depends on the secondary addition of silver precursor $AgNO_3$. In the chitosan thin film synthesis, AgCl nanocubes also appear to form the base for the growth of AgNWs with the growth of AgNWs occurring directly from the corners of the cube structures (Figure 42). Average diameter of the wire growing from these cubic structures is around 80 nm. SEM images of Figure 42 are the first depiction of this kind of AgCl based AgNWs growth in the solid state. The experiments of excluding addition of NaCl in the synthesis process showed no

formation of AgCl Nano cubes on the surface of the chitosan film (Figure 12) and, as a result, no growth of AgNWs on the same.

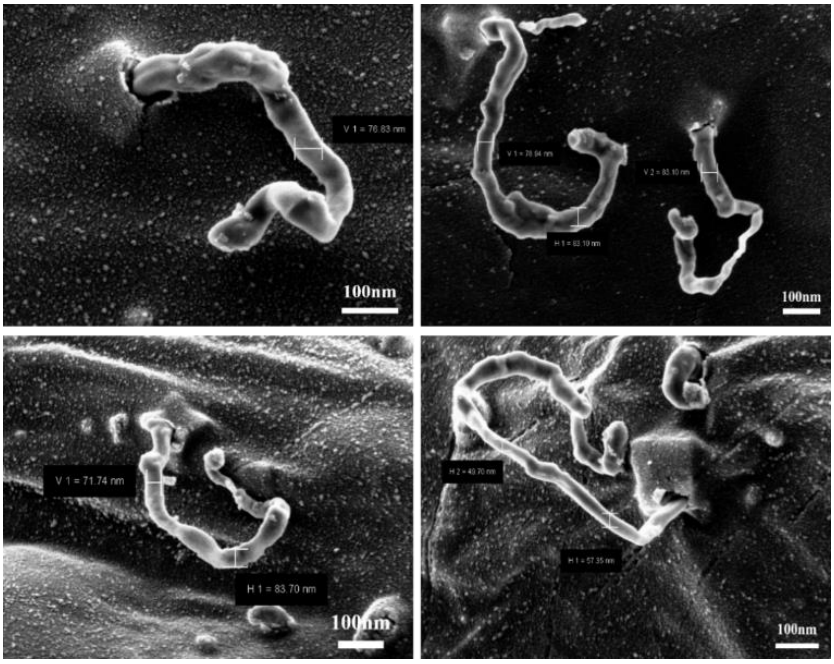

Figure 42. SEM Images of AgNWs Growth from the Corners of the Cubic AgCl Nanostructures

4.3.3 Silver Nanowires Diameter and Length Growth Kinetics w.r.t Time

There are research articles, where varying time factor of synthesis factor reported the growth change in silver nanowires in solution processing [92]. But our discussion is on self-growth of AgNWs, under no active reaction conditions imposed on the Ag/Chitosan film. Here we present our investigation of time dependence of AgNWs growth by imaging single film using SEM by varying time periods i.e. from week 0 to week 7.

Where week 0 represents immediate imaging of the film, which is coated with 5nm Au/Pd thing film to avoid oxidative etching and the synthesized solution contains NaCl.

Week by week SEM images of Ag/Chitosan film is shown in Figures 44, 45, 46, 47 and 48 corresponding to week0, week1, week2, week4 and week7 respectively. Figure 44 corresponding to week0 represents AgCl cubic particles all over the surface of the film. Additionally, small protrusions at the corners of AgCl cubes are observed, which corresponds to Ag metal as from the discussion in previous sections. Figure 45 corresponding to week1, shows initiation of growth of AgNWs from the surface of chitosan film and from the corners of the AgCl cubes. Diameter of the wires range about ~70nm. Figure 46 of week2 shows further raise in density of AgNWs on the film with increase in aspect ratio of the wires, having diameter of ~130nm. Figure 47 of Week4 shows fast shift in both density and length of AgNWs on the film, leaving width of AgNWs to not much change from previous week. Note that imaging of week3 is not presented as there is no much change in width of Ag NW is observed. Finally, Fig 48 corresponds to SEM image of AgNWs on the film which is aged beyond week4, say week7. Where, after which the growth change in nanowires is not as noticeable as previous weeks. Here, max dense and max aspect ratio of AgNWs can be noticed on the film, with width increasing to ~400nm and length to ~30µm.

Below is the Figure 43, representing growth progress of solid state AgNWs with varying time duration in weeks, form week0 to week7 as discussed above.

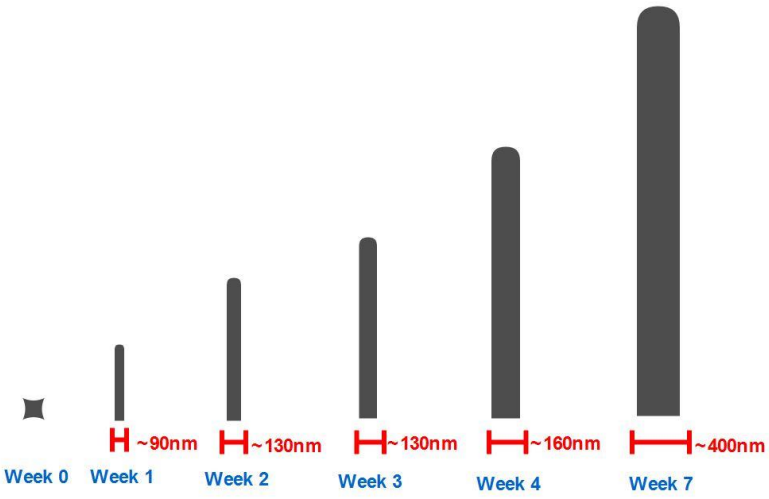

Figure 43. Schematic Representation of Growth of AgNWs w.r.t Time

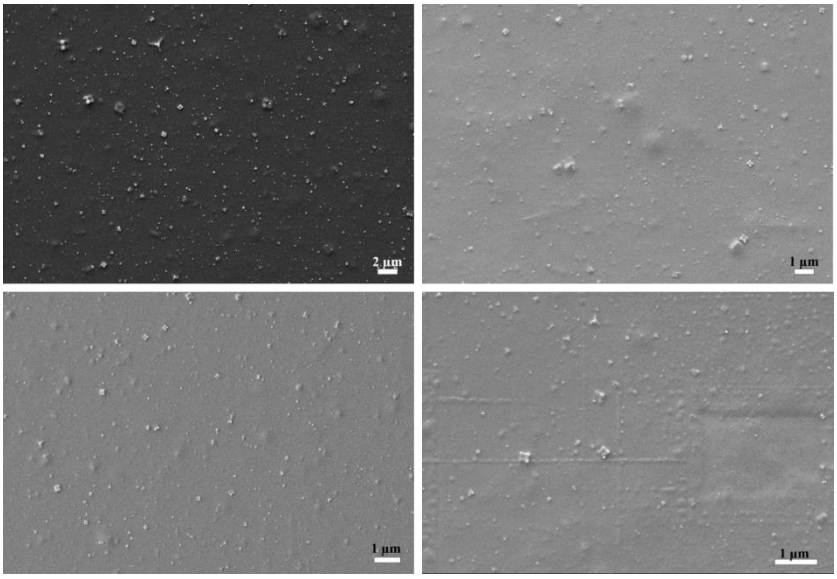

Figure 44. SEM Image of Ag/Chitosan Film at Week0.

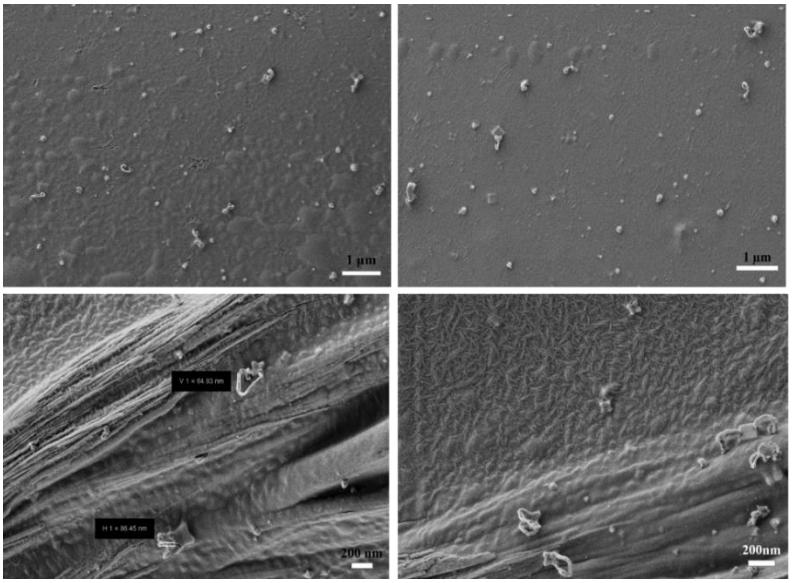

Figure 45. SEM Image of Ag/Chitosan Film at Week1.

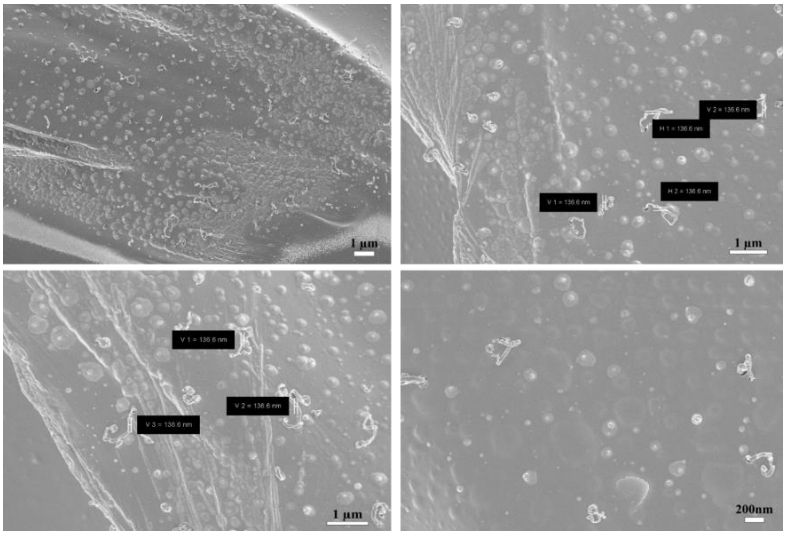

Figure 46. SEM Images of Ag/Chitosan Film at Week2.

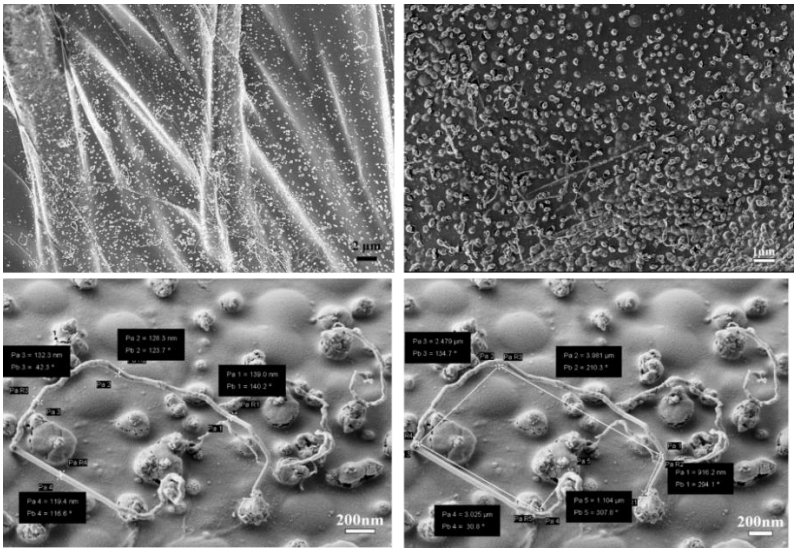

Figure 47. SEM Images of Ag/Chitosan Film at Week4.

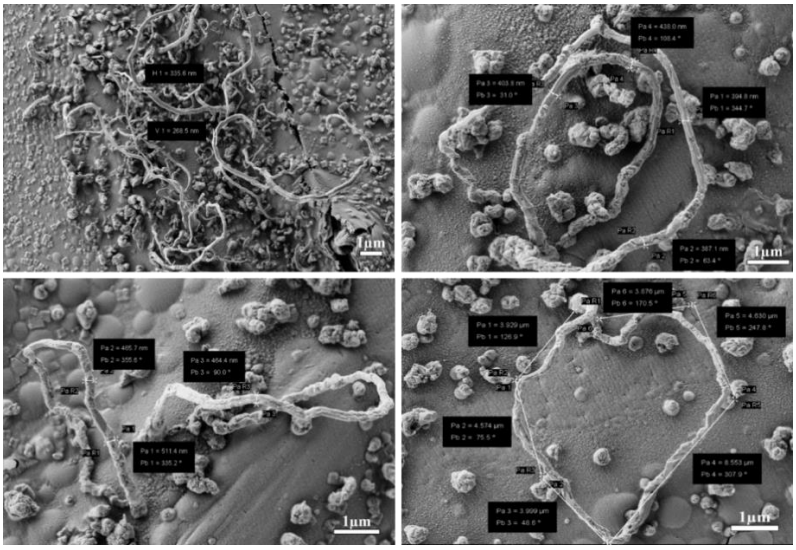

Figure 48. SEM Images of Ag/Chitosan Film at Beyond Week4.

Below Table 4 summarizes the above results of change in aspect ratio of AgNWs with change in time.

Table 4. Represents the Metrics of AgNWs Length and Width Change with Change in Time

Week0	**Week1**	**Week2**	**Week4**	**Beyond Week4**
Cubic structure	Ag NW of diameter 65nm±15nm	Ag NW of diameter 135nm±15nm	Ag NW of diameter 165nm±20nm	Ag NW of diameter 400nm±50nm
Cubic structure	Ag NW of length 500nm±50nm	Ag NW of length 4µm±1µm	Ag NW of length 9µm±1µm	Ag NW of length 28µm±2µm

To further depiction of AgNWs growth in width and length wise individually. SEM images of individual AgNWs on the film, which show clear width and length change along the growth of AgNWs are presented in Figure 49 & 50 respectively. Figure 49 represents the change in width of Ag NW along its growth process overtime. Figure 49 a shows SEM image of single vertically grown Ag NW of width ~120nm. Figure 49 b&c shows gradual increase of wire width from growth root towards tip, starting from width of ~280nm to ~50nm for Figure 49 b and from ~135nm to ~50nm for Figure 49 c. Figure 49 d show, fully grown single nanowire with uniform width ~200nm of all of its grown length.

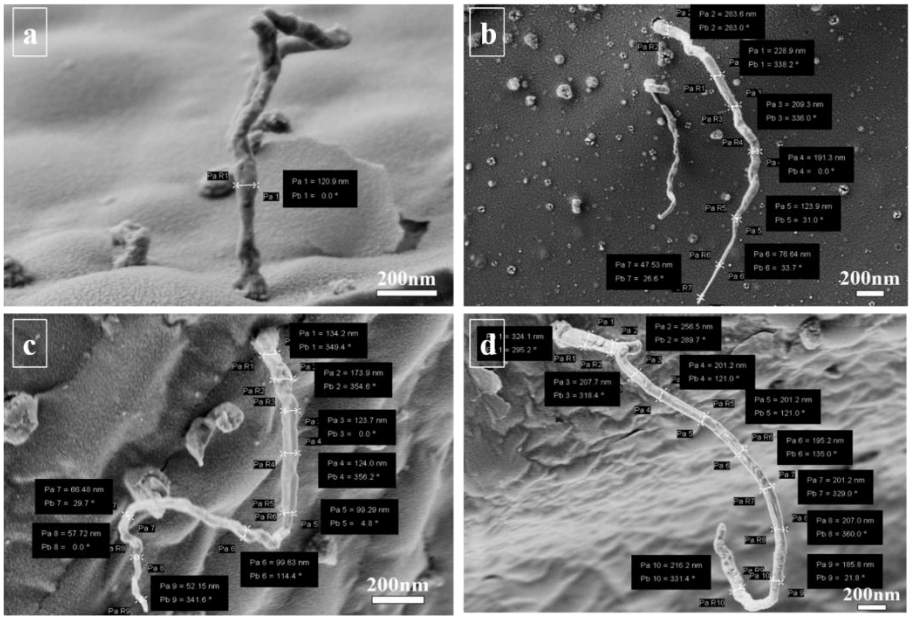

Figure 49. SEM Image Depiction of Change in AgNWs Width w.r.t Time

Coming to the growth length monitoring of Ag NW over time, Figure 50 presents SEM images of stage wise growth of AgNWs in its length. It can be clearly observed the step by step raise in AgNW length w.r.t. the presented SEM images below ranging wire length from 0nm to 20µm of length.

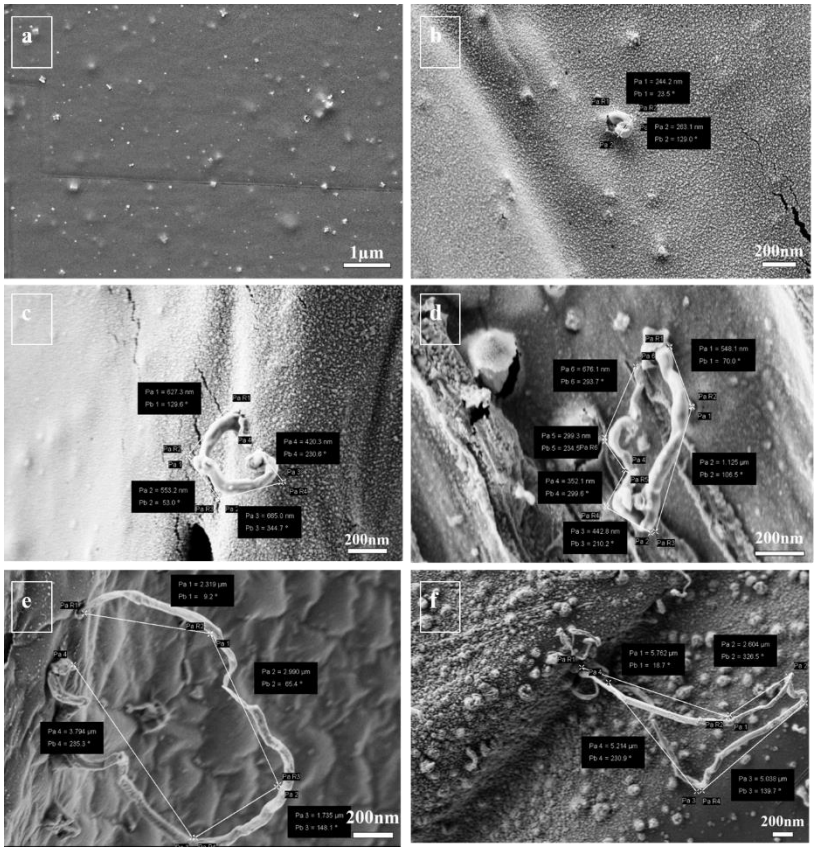

Figure 50. SEM Images of Nanowires Grown on the Chitosan Film Varying in Length w.r.t Time

The change in aspect ratio of the AgNWs with respect to time, if different phenomenon observed in my growth study. Since, in polyol synthesis of AgNWs only longitudinal growth of AgNWs is reported. Change in width of the nanowires along with the length is new observation, seen in the growth mechanism analysis of soli-state growth of AgNWs. Figure 51 shows the summarizing plot of the change in aspect ratio of the AgNWs with respect to time.

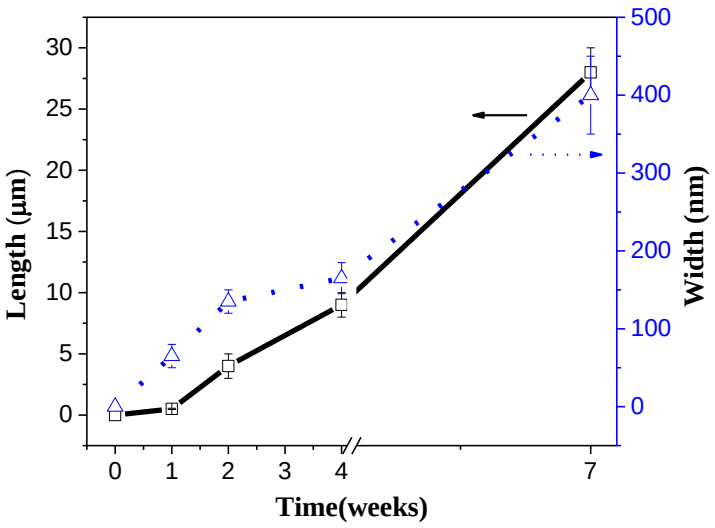

Figure 51. Summarizing Plot of Growth of AgNWs in Terms of Length and Width w.r.t Time

4.3.4 Temperature of Drying for AgNPs/Chitosan Film

Here in our AgNWs growth system, since the synthesis of AgNPs is carried out at room temperature. The thermodynamics factor is introduced at the stage of AgNPs/Chitosan film drying process. Typical opted temperature for drying the films on PET is 50^0 C and dried for extended time of 8hrs, this temperature is chosen to avoid distortion of PET substrate when subjected to higher temperatures for longer times. The optimization of drying time is verified based on the SEM characterizations and analysis of AgNWs growth at different drying times. Note that all other growth conditions discussed above are kept constant to verify this growth analysis.

Figure 52 a & b show SEM images of Ag/Chitosan film which is subjected to dry on PET substrate for 2 hours of time. Where it is observed that the film is not smooth and

cubic AgCl are not completely formed at many place, followed by very minimal sign of AgNWs growth on the surface. Figure 52 c & d show SEM images of film which is subjected to dry for 8 hours of time. Here the surface of film is smooth and perfect cubic AgCl NPs are observed on the surface, followed by good growth of AgNWs as shown. This specific experimental analysis of thermodynamics factor influence in growth of AgNWs has been repeated multiple times to obtain similar result.

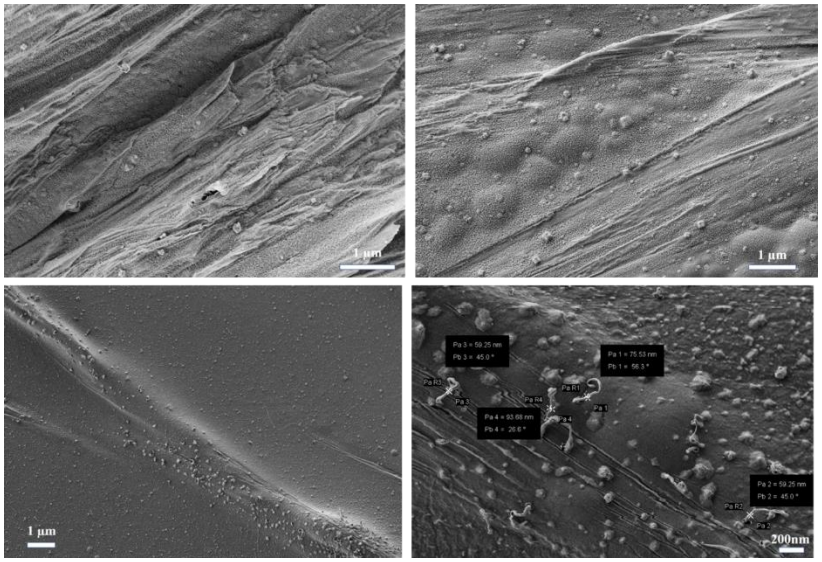

Figure 52. SEM Imaging of Ag/Chitosan Film Subjected to Longer and Optimum Drying Temperature

4.3.5 Volume Analysis of Ag/Chitosan Film Formation

After many trial and errors in choosing right volume of solution for good AgNWs growth, we ended up in concluding it to 400µL. Explanation and support for choosing this specific volume to make film for AgNW growth is presented by SEM images presented in Figure 53.

From the SEM images, 400µL volume film forms vein like structures as seen on the film where high concentration of silver is accumulated. So, at the veins on the surface of the film, good density of AgNWs growth is observed. The SEM images of other volume concentration to make film show no sign of this mentioned veins on the film surface and hence minimal growth of AgNWs on the film.

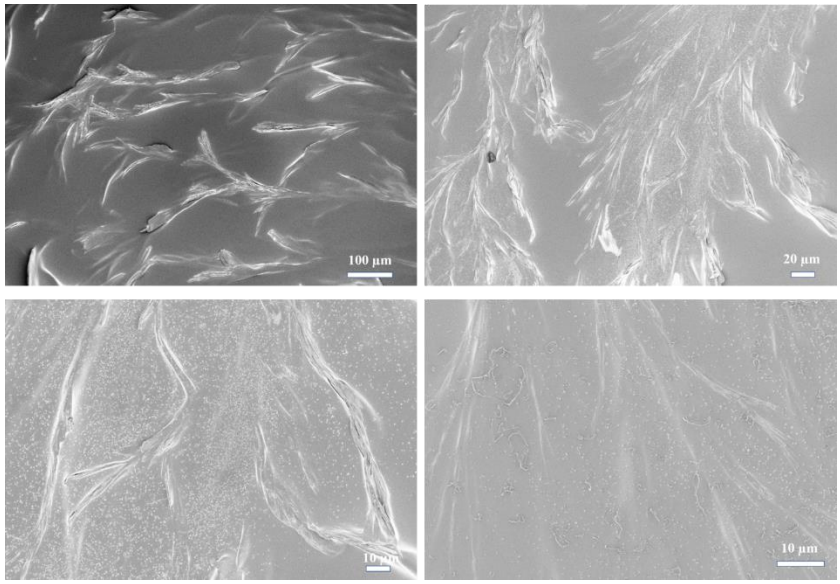

Figure 53. SEM Images of Ag/Chitosan Film Made at Right Volume of the Solution

4.3.6 SERS Applications of AgNWs/Chitosan Film

Surface enhanced Raman spectroscopy (SERS) is a powerful vibrational spectroscopy technique that allows for highly sensitive structural detection of low concentration analytes through the amplification of electromagnetic (EM) fields generated by the excitation of localized surface plasmons. In simple terms, this method enhances the existing Raman signal of the substrate material of interest with help of nanostructured materials over the same substrate. This light concentration occurs

preferentially in the gaps, crevices, or sharp features of plasmatic materials, which are traditionally noble and coinage metals (e.g., silver, gold, and copper) with preferably nanoscale features formed on the surfaces. Reproducible and robust structures that strongly enhance the EM field are most desirable for SERS. Depending on the structure of the supporting plasmonic material, EM enhancement for SERS is theoretically calculated to reach factors of ~ 10^{10} – 10^{12}. The success of SERS is highly dependent on the interaction between adsorbed molecules and the surface of plasmonic nanostructures, often the classic SERS substrates of gold (Au), silver (Ag), or copper (Cu). In general, Au and Ag are most often used as SERS substrates because they are air stable materials, while Cu is more reactive. All three metals have surface plasmon resonance (SPR) that cover most of the visible and near infrared wavelength range, where most Raman measurements occur, also making them convenient to use avoiding the biological emission range which usually hinders the accurate biomolecule detection signal measurements. Novel materials such as graphene, semiconductors such as TiO_2, and quantum dots have recently been reported to work with metals for SERS, although they do not fit traditional definitions of SERS substrates.

SERS performance of our self-grown and solid-state silver nanowires (AgNWs) platform is evaluated by using commonly opted Rhodamine 6G (R6G) molecule as Raman probe. Concentrations of R6G dissolved in deionized water, used for the detection experiments, range from 10^{-3} M to 10^{-7} M. As shown in Figure 54, characteristic peaks of R6G are spotted at 612 cm^{-1}, 769 cm^{-1}, 1359 cm^{-1}, and 1649 cm^{-1} on AgNWs platform even for the lowest concentration of 10^{-7} M. It is clearly observed that, with the increase

in the concentration of R6G there is steep raise in the intensity of the mentioned peaks of R6G on the platform. The argument of the platform being chitosan polymer on which AgNWs are grown and its possible intervention with the detection process is supported by Raman research data. Where there are no reported data where chitosan Raman peaks are observed in the presence of any metal Nano structure. So, in our experiments too, we didn't find any polymer peaks intervening the Raman peaks of R6G. Sensitivity of the detection surface is calculated by linear plotting of detection range for all the concentrations, which is depicted in Figure 55. Graph for the sensitivity is plotted between log of concentrations and intensity of detection Raman peak 769 cm^{-1} intensity with respect to different R6G concentrations. The detection sensitivity obtained for our AgNWs platform is $R^2 = 0.9980$, which is in par with typical polyol-based AgNWs platform used for sensing applications.

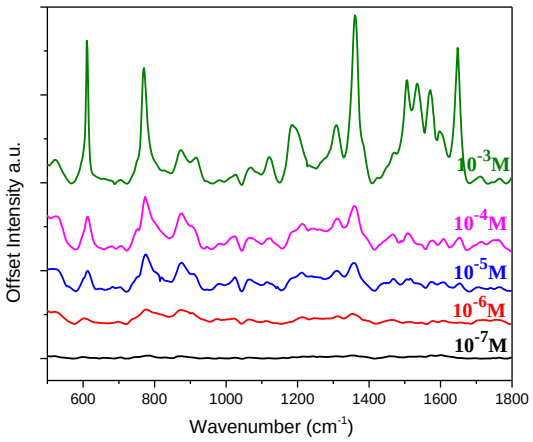

Figure 54. R6G Detection Peaks from Range of Concentrations Obtained from the Platform of AgNWs

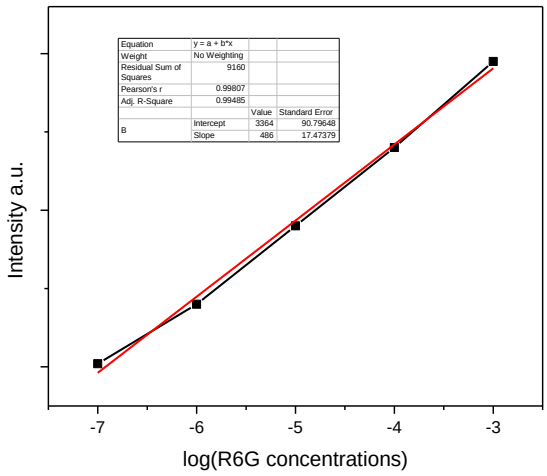

Figure 55. Sensitivity Plot of R6G Peak, 769 cm^{-1} and its Linear Fit

Additional to detection and sensitivity, we have verified the reproducibility of the AgNWs platform. Figure 56 shows the plots of intensity for R6G Raman peak 769 cm^{-1} taken from 20 different points on the platform. These plots are taken for two concentrations of R6G i.e. 10^{-3} and 10^{-5} M. Both the graph plots represent strong reproducible capability of the platform even at different concentrations.

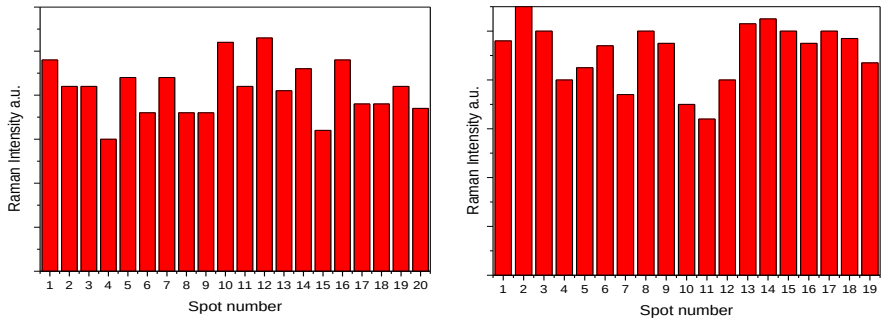

Figure 56. Raman Intensity Plot of R6G 769 cm^{-1} Peak at 10^{-3} M And at 10^{-5} M Concentrations

4.4 Discussion

In this section we present the key factors and conditions for the unique solid state AgNW growth. Three key conditions/factors have been investigated thoroughly. (1) Oxidative etching role on AgNW growth at solid state level is studied by over exposing the Ag-based composite film with oxygen or by covering the film with thin metal coating or with self-assembled polymer bead layer. This study is strongly supported by presented SEM images of the AgNW growth in temporal. (2) The role of NaCl is investigated on a par with the similar kind of investigations performed in solution process. Our results suggest that mixture of NaCl and $AgNO_3$ converts to AgCl nanocubes in the reaction process, which further form nucleation spots for the growth of AgNWs with a reduction process assisted by chitosan. EDS experiments shows the consumption of AgCl slowly with increase in the growth of AgNWs length with time. (3) Continual growth of AgNWs with respect to aging of the film is studied and presented with detailed analysis with the help of SEM images. The ability of AgNWs to grow outward from the polymer film up to a length of 28μm, shows the continuous supply of Ag^+ ions from within the film, like nutrient for a sprouted seed. This solid-state, bottom-up, AgCl nucleated and continual growth process of AgNWs is schematically depicted in Figure 57. The AgNW growth pathway resembles quite closely with the natural process of growth of sprouts and science behind its growth process from a seed. This process is a continual growth process, where the seed takes its “nutrient” source in the film and keep growing outward.

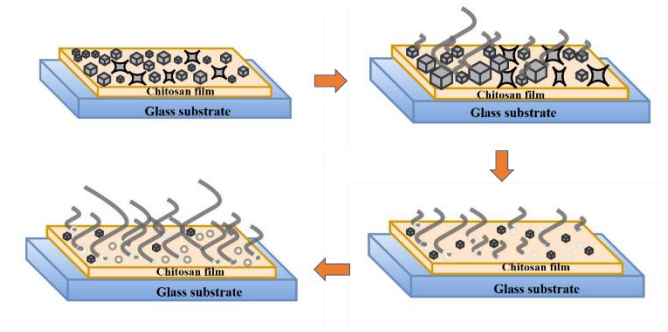

Figure 57. Schematic Depiction of Growth of AgNWs from Formation of AgNPs, AgCl Cubic Structures and Eventually to AgNWs

4.5 Conclusion

In this paper we describe factors that control the growth of AgNWs in a chitosan solid state medium. We show that like the solution-based AgNW synthetic processes that oxidative etching has a significant inhibitory role. Growth of nanowires is considered as new age nanotechnology research field. Where vertical bottom up growth of semiconductor nanowires research is being highly investigated because of its potential applications in the field of electronics. Solution processing of metal nanowires is well investigated by many researchers, especially in case of silver nanowires (AgNWs). However, vertical and bottom up growth of AgNW research is rare. This article presents such growth of AgNWs with unique self-growth property and mechanism of growing them at ambient conditions, unlike the use of complex and high vacuum-based equipment used to grow mentioned semiconducting NWs. The reported AgNW growth presents a new way of blocking oxidative etching effect on the growth by coating thin film at the Ag/Chitosan matrix film. The influence of Cl^- ions and AgCl NPs on the growth of AgNWs is examined. The edges of AgCl nanocubes are the nucleation sites for the

AgNWs. The Ag^+ in the film is the “nutrient” source for the “sprouted” AgNW with respect to the aging of the substrate film. With all the discussed conditions, this article stays as a foundation for a new avenue to bottom-up synthesis of AgNWs and a variety of potential applications.

CHAPTER V

PLASMONIC STUDY IN AU THIN FILMS/MOS_2 HETEROSTRUCTURES FOR SURFACE ENHANCED RAMAN SPECTROSCOPY APPLICATION

5.1 Introduction

Transition metal dichalcogenides (TMDs) are new age 2D materials drawing great attention in research field from past few years. These materials are mostly semiconductor and are atomically thin, with single layer thickness of 0.7nm [138]. MoS_2, is the most investigated TMD material due to its novel properties like having a tunable band gap property with a direct bandgap of 1.8ev in monolayer form and an indirect bandgap of 1.2ev in its bulk form. Due to this gap tuning property, MoS_2 is mostly investigated in research to apply in the fields of Electronics [104, 139], Photodetectors [140], SERS based sensors [141] and many other fields of research [142, 143]. Optical absorption and surface plasmon generation properties of MoS_2 has been widely investigated in terms of Raman peak enhancements due to incident light scattering with change in number of layers of MoS_2 [126]. Monolayer MoS_2 shows moderate SERS enhancement when compared to other 2 D materials like graphene and WeS2[144]. Recently, there is increase in research interest on improving the SERS property of semiconducting MoS_2, combining it with metal nanoparticles and nanostructures [115-117, 145], especially on understanding the behavior of MoS_2 when combined with Au metal [146, 147]. Many research findings claimed change in linear and non-linear properties, seen in monolayer

MoS_2 and Au heterostructures [109, 110]. But, there is still room in investigation on plasmons generated by Au thin film that are induced in few layers of MoS_2 both and their effect in MoS_2 optical properties related to Raman peak intensity change and in increasing SERS enhancement property associated with few layers of MoS_2.

In past three years optical analysis of MoS_2/Au thin film heterostructures became widely popular in understanding linear and non-linear optical behavior of MoS_2. Jia et al. investigated theoretically the behavior of MoS_2 on Au thin film under 20nm thickness reporting drastic modification in the excitonic optical properties of MoS_2 monolayer because of Au thin film[109]. Zeng et al. presented his research findings on Au thin film influence on secondary harmonic peak intensity raise of few layers MoS_2, which is due to strong localized field induced by Au thin film[110]. Photoluminescence (PL) is one of the important optical property of MoS_2 that is being constantly investigated for its intensity and quantum yield associated with direct bandgap monolayer MoS_2. Le Yu et al. claims that gap plasmons induced by their Au thin film and nanoparticle structure improved PL of monolayer MoS_2 by 4 times[111]. Haifeng Xu in his research report proved that with the inclusion of gold mirror layer between the dielectric layer and the substrate enhances overall PL intensity by 4 times of monolayer MoS_2 because of enhanced optical absorption[112]. Buscema et al. reports in detail the role and effect of the substrate on the PL and Raman signal of mono layer MoS_2. On all the studied substrates including Au thin film, single-layer MoS_2 shows a factor of ~4 enhancement of PL efficiency, relative to commonly used SiO_2 substrate. The observed phenomenon is reported due to radiative decay rates of neutral and charged excitons, which is different from previous claims[113].

Robison et al. with the help of Raman spectroscopy and scanning Kelvin probe microscopy (SKPM) investigated the effect of Au substrate on optical and electrostatic properties of monolayer MoS_2[114]. The increase in the Raman peak enhancement of monolayer MoS_2, when on Au thin film is claimed to be associated to SERS like enhancement shown by the nanoscale-textured metallic surfaces. Different shapes of Au nanostructures influence monolayer MoS_2 for enhance in optical absorption due to surface plasmons, shows ultrafast plasmonic hot electron transfer from Au nanostructures to MoS_2 and exhibits plasmonic pumping of excitonic photoluminescence. Other metal surfaces and nanostructures reported to induce plasmons into MoS_2 for change in its optical properties are Aluminum and Silver.

Raman peak intensities change is mostly influenced by number of layers of MoS_2 with raise in intensity is directly propositional to raise in number layers. This phenomenon is same for all preparation methods of MoS_2 and irrespective of substrate on which MoS_2 is deposited. The primary reason presented for this observation is the optical scattering taking place in the number of layers of the material, which is observed in the case of graphene too. Monolayer MoS_2 deposited on Au thin film and on insulating films like PVP, it observed to have higher Raman peak intensities compared to its deposition on semiconducting substrate like silicon. This phenomenon is supported by argument of electron transfer property taking place between Au and MoS_2 along with capability of band alignment induced by underneath Au film onto MoS_2.

Recent reports from 2014 shows employing MoS_2 in SERS enhancement applications [148], where it falls under same theory of enhancement generation as

graphene, where Raman enhancement results from chemical contact between a target molecule and the enhancing medium removing unwanted fluorescence (FL) is known as chemically enhanced Raman Scattering (CERS)[149]. 2D material Graphene supports the CERS process, which is named as GERS in case of Graphene. MoS_2 also show CERS with mediated by localized surface plasmon resonance (LSPR) which occurs in visible range rather than terahertz level like graphene. As a Raman enhancement substrate, MoS_2 has many advantages such as favorable biocompatibility, chemical stability, Flexural strength[127] etc. There are three most used ways to obtain few layers to monolayer MoS_2, that are primitive Mechanical exfoliation, Liquid Exfoliation and Chemical Vapor Deposition (CVD) in which I have opted for Mechanical exfoliation, since this method produces pristine level MoS_2 layers, it is simple process and is extremely comfortable method to opt for laboratory research and prototype design.

In this study we present a comprehensive report on influence of Au thin film on Raman peaks intensity raise in few layers MoS_2 deposited using mechanical exfoliation method on Au thin film. The plasmonic effect of Au film on the MoS_2 is validated by changing the thickness of Au film from 25nm to 200nm, where 150nm shows highest enhancement for respective Raman peaks. FDTD simulation results of plane Au films give similar results of highest plasmon field generation for 150nm Au surface. Importantly, it is verified that 150nm Au thin film gives highest SERS enhancement for the detection of R6G at 10^{-6}M concentration on few layers of MoS_2 along with mono layer when compared to other thicknesses of Au films.

This report shines light on applications involved with few layers MoS_2 when associated with Au thin film, as few layers deposition is much simpler than monolayer MoS_2.

5.2 Materials and Methods

Sample preparation of MoS_2 is done as follows. Few layers to mono layer MoS_2 are obtained by micro mechanical exfoliation of bulk MoS_2 (SPI supplies, 429ML-AB) using original matte finish invisible scotch tape (3M 810). Moreover, fabrication of heterostructures is done both on insulating and conducting substrates i.e. plane glass and Au thin film coated glass substrates. Single-, double-, and few-layer MoS_2 flakes were transferred on to the substrates using indirect method of transfer i.e. MoS_2 flakes are directly peeled from bulk using scotch tape and transferred onto a thermal tape. The thermal tape is made to stick on to the desired substrates and oven heated the same to 90^0C to make thermal tape self-release from the substrate. Au thin films of different thickness are fabricated using PVD with a 4nm Ti coating, which helps for the good adhesion of gold on to the base glass substrate. Prior to use, substrates were cleaned in piranha solution (3:1 concentrated H_2SO_4 to 30% H_2O_2) and dried using mild temperature and with N_2 air gun.

Optical characterizations are performed by Axio Imager Z2M upright Microscope, obtained images at 100X magnification. The source of the imaging is a white light and uniform brightness and contrast setting are maintained all thorough the experiments. To get the contrast profiles/grayscale values of the obtained optical images of MoS_2 flakes on different substrates, free software ImageJ.

Layer thinning of the obtained mechanical exfoliated MoS_2 flakes is performed by basic plasma cleaning procedure. MoS_2 transferred substrates are placed under vacuum of 200torr in South Bay Plasma Cleaner (O_2/Ar) and exposed to Ar plasma for 2 mins. The sample to plasma source distance is ~15cm. Plasma power of 90watts is maintained standard for all the samples.

Raman peaks measurements of MoS_2 are performed using a Horiba Jobin-Yvon Xplora confocal Raman equipment. A 532nm wavelength laser (2.33 eV excitation energy) was focused onto the sample through 50X objective lens. Focused laser point is of diameter 2µm with laser power used as 10% of total laser power, to avoid any noise signals due to thermal energy generated by using high power lasers. Raman system is auto calibrated using standard Si crystal, whose peak is obtained at 520 cm^{-1}. Standard Raman peaks of MoS_2 flakes $E_{2g}{}^1$ and A_{1g} are collected by specifically focusing laser point on desired flake, which is selected using confocal image. The Raman spectra were processed afterwards using Origin software (version 9).

Au thin film coatings of different thickness are obtained using PVD 75 Evaporation System, which is operated in clean room environment and at 10^{-6} torr pressure. Before the deposition of the gold films of varying thickness, a 4nm of titanium is deposited on the glass substrate to make gold film strongly adhere to the glass. For the thicknesses of the Au thin films employed in the experiments, similar conditions are maintained.

Plamonic study on the Au thin films is performed theoretically using Fourier transform time domain (FDTD) analysis software, obtained under individual license.

5.3 Mechanical Exfoliation of MoS_2 on to Different Substrates

5.3.1 Mechanical Exfoliation on Glass Substrate

Mechanical exfoliation is the first-generation method for obtaining few layers to monolayer of 2 D materials, which uses a scotch tape to peel of the layers from bulk material of the same. Here I have employed a modified mechanical exfoliation method for obtaining good ratio of few to monolayers and for effective transfer of the peeled MoS_2 from scotch tape to any desired substrate with strong adhesion of the same irrespective of the substrate. Additional to this process Argon plasma thinning of obtained few layers to convert the sample to mono layers is performed. The complete process is depicted step by step and effect of plasma thinning process are shown as below.

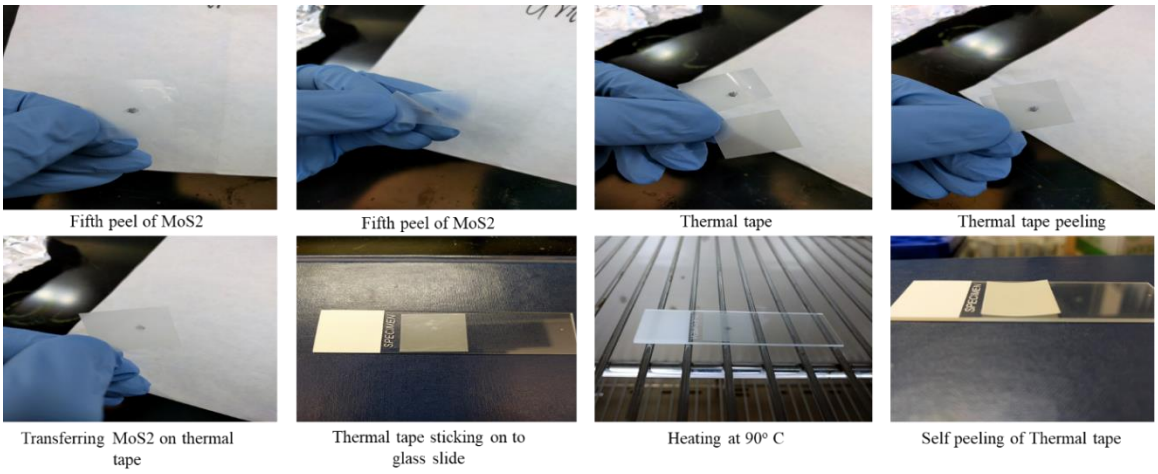

Figure 58. Mechanical Exfoliation of MoS_2 on Glass Substrate Using Scotch Tape and Thermal Tape

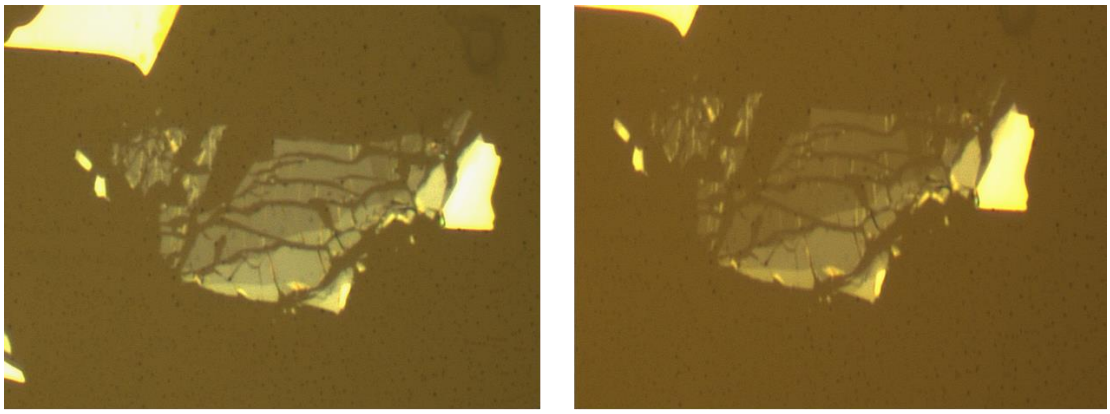

Figure 59. Plasma Thinning of MoS_2 Flakes Deposited on Glass Substrate

5.3.2 Mechanical Exfoliation on Au Substrate

Single layer of MoS_2 consists of single chain of Mo atoms sandwiched between two chains of So atoms, which combined have a thickness of 0.7nm. Many layers of MoS_2 consists of multiple single layers attached with each other due to the weak vandrawal forces between the layers. Mechanical exfoliation of MoS_2 exploits this property of multi-layer MoS_2 and with minimal force applied using a scotch tape, was able to peel of single layers from bulk and eventually transferred on to various substrates. But, the mechanical exfoliation reportedly has low throughput of obtaining few to mono layers MoS_2, when deposited on to the substrates like glass. Recent research findings of depositing MoS_2 on to Au thin films to form heterostructures has reported to obtain large are deposition of mono layers deposition on to the gold surface [93, 150]. This phenomenon is reported due to the strong electro affinity of sulfur to gold surface. The bottom layer of MoS_2 being a chain of sulfur atoms, which would be in direct contact with the surface when subjected to mechanical exfoliation process, binds strongly to the

gold surface and when peeled, top layers are removed, leaving single layer of MoS_2 on the surface of the gold film. In my experiments, I have used gold films of different thicknesses i.e. 25nm, 50nm, 100nm, 150nm and 200nm as substrates to deposit few layers of MoS_2. Similar, scotch tape peeling followed by thermal tape transfer method reported in previous section is employed for the deposition of few to mono layers of MoS_2 of gold thin films. Further layer thinning of the deposited MoS_2 flakes is performed using Ar plasma cleaner, below figures shows the optical images of the peeled MoS_2 flakes on Au thin film and plasma thinning of the same.

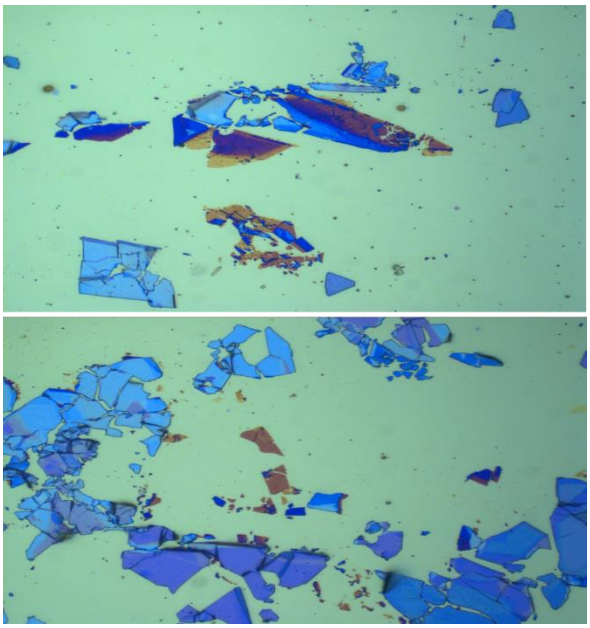

Figure 60. Optical Images of Deposition of MoS_2 on Au Thin Film

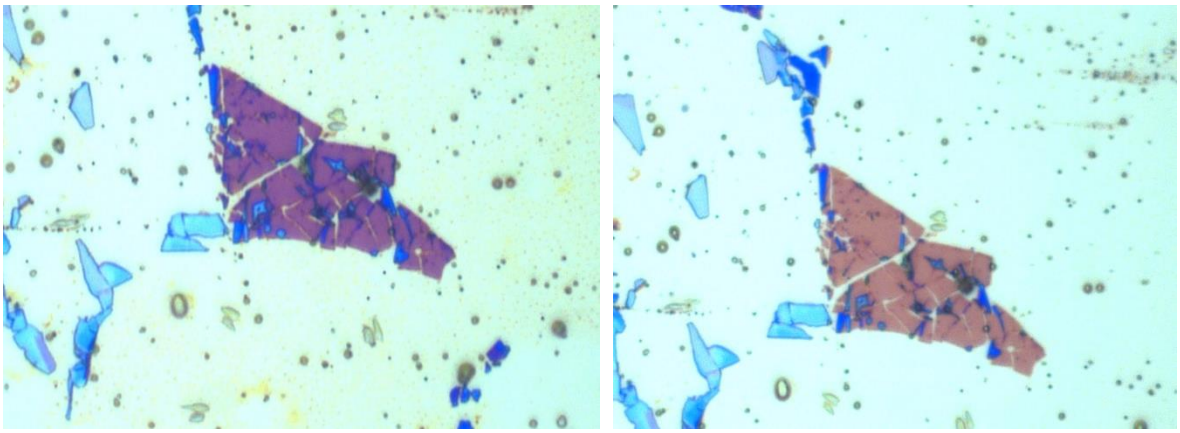

Figure 61. Plasma Thinning of MoS_2 on Au Thin Films

5.4 Results

5.4.1 Optical Analysis of MoS_2 Deposited on Different Substrates

Deposition of few layers to monolayer MoS_2 on the glass and Au thin film substrates need further characterizations to confirm the number of layers that had been deposited on the substrates. The count in the number of layers of MoS_2 are verified by various techniques like Optical observation of the change in color of the MoS_2 depending on the substrate used [110]. Raman analysis of the prominent Raman peaks associated with MoS_2 i.e. E_{2g}^1 and A_{1g}, where based on the difference between the wavenumber of the two peaks is matched to the number of layers associated with MoS_2. Photoluminescence (PL) analysis of bandgap associated with the change in number of layers of MoS_2, where for bulk, bandgap is around ~1.2eV, ~1.8eV for monolayer MoS_2 and for few layers of MoS_2 between 2 and 5, bandgap lies between ~1.2eV and ~1.8eV. Finally, AFM is used for direct imaging of the MoS_2 layers and it gives the thickness value of the flakes with respect to substrate.

Here in this section, I present a comprehensive study on the count of the number of layers based on the optical image color difference and based on the analytical analysis on contrast/grey values measurement of different number of MoS_2 layers deposited on the glass and Au thin film using imageJ software.

5.4.1.1 ImageJ Analysis of MoS_2 on Glass Substrate

Mechanical exfoliated MoS_2 flakes transferred on to the glass substrates are subjected to optical microscopy imaging as shown in Figure 59. This optical image is taken as the input file for ImageJ software to process the brightness values of desired flakes on the image. To evaluate the thickness of the desired flake and to confirm the layer thinning process, the contrast profile difference of the MoS_2 flake to the substrate is calculated. Brightness profile values are obtained from the original color image and grayscale images corresponding to R G B channels. Contrast difference values are plotted on the standard plot to present the change in number of layers of MoS_2 at different regions of the image depicted as shown in below Figure 62

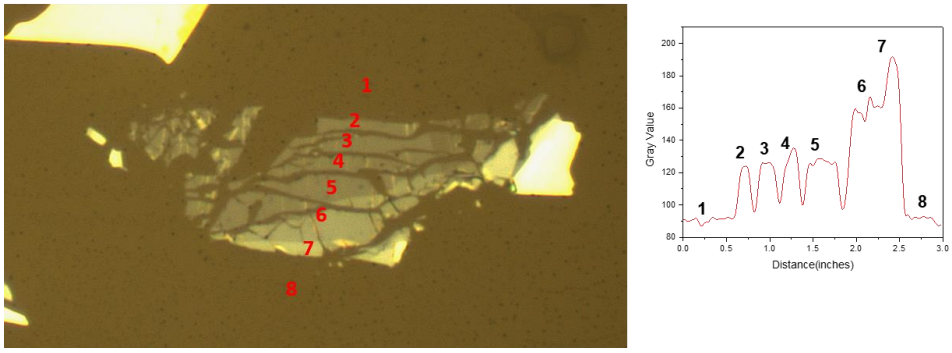

Figure 62. Optical Image of Mechanical Exfoliated MoS_2 Flakes Deposited onto the Glass, Inset Shows the Contrast Profile Plot

Contrast profile values of all the listed regions are plotted in the inset image of Figure 62. Substrate contrast is represented by C_s and MoS_2 flake contrast is denoted by C for calculating the contrast difference between the two, to know the thickness difference between the flakes in the image. The contrast difference C_d is given by difference between C and C_s. It is clearly seen from the Figure 62, with change in thickness of the flakes as seen visibly, the peaks of the contrast profile too raise to the highest value for the brighter flake and then drops down to lowest when plotted at the substrate level point. As discussed in the previous section, with Ar plasma exposure, thinning of MoS_2 flakes are reported. This report is verified using ImageJ contrast profile plotting of the thinning MoS_2 optical image. The results are shown in below Figure 63.

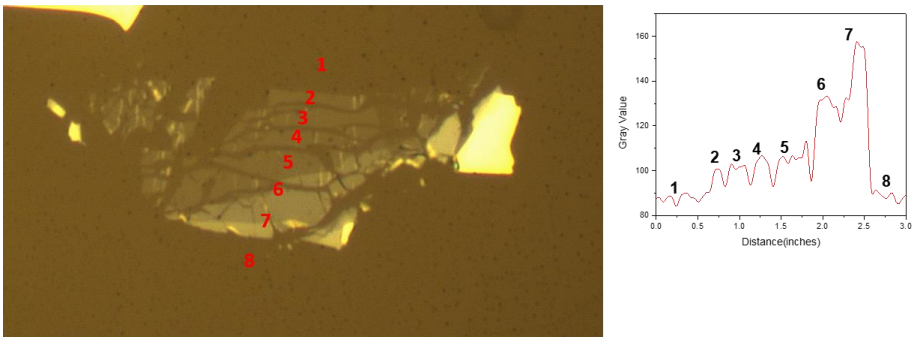

Figure 63. Optical Image of Plasma Thinning of MoS_2 Flakes, Inset Plot Shows the Contrast Profile

It is seen from the Figure 63 that, MoS_2 flakes have low contrast value plot when compared to that of the plot in Figure 62. This is due to the reported effect of the Ar plasma for further thinning of the few layer MoS_2 flakes. Gray values corresponding to the contrast profile plots shown in Figure 62 and 63 are summarized in below Table 5

Table 5. List of Gray Values Associated with MoS_2 Flakes for Before and After Plasma

Region	Before plasma	After plasma
1	90 (Cs)	90 (Cs)
2	130 (C)	105 (C)
3	130 (C)	105 (C)
4	130 (C)	105 (C)
5	130 (C)	105 (C)
6	160 (C)	130 (C)
7	200 (C)	160 (C)
8	90 (Cs)	90 (Cs)

Based on the above listed gray values at specific regions of MoS_2 flakes, it can be concluded that, this approach of validating the thickness of MoS_2 flakes using contrast values obtained from optical image is reliable and quick way. The contrast difference (Cd) between the substrate brightness and MoS_2 flakes at different thickness is plotted below in Figure 64. The difference in the Cd values for without and with plasma treated MoS_2 flakes, stays as potential proof of layer thinning.

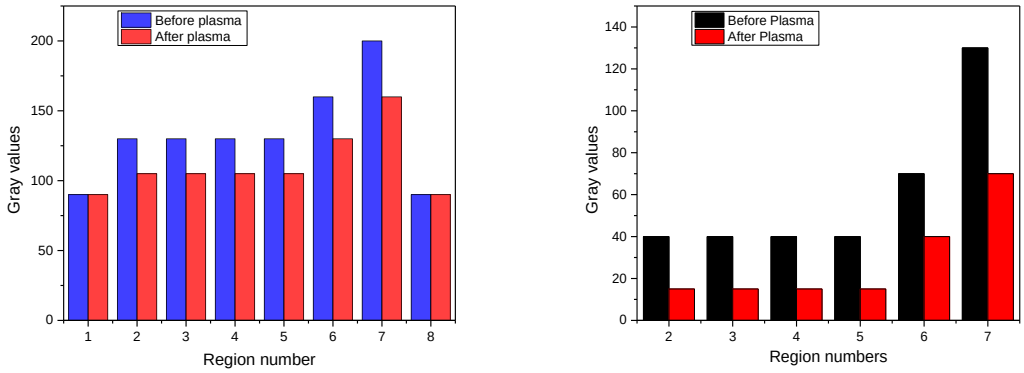

Figure 64. Contrast Plot of MoS_2 Flakes Without and With Plasma Exposure on the Left and Contrast Difference Plot of the Right

5.4.1.2 ImageJ Analysis of MoS_2 on Au Thin Film Substrate

Similar optical image analysis as presented in previous section is followed for the optical image of the MoS_2 flakes deposited on the Au thin film as shown in Figure 60. The only difference between previous analysis with glass substrate and present with Au thin film substrate is, the optical contrast values of the Au thin film are high when compared to the thin MoS_2 layers and when compared to the glass substrate. The optical image with specific marked regions and the contrast profile plots of the selected regions of interest are presented in below Figure 65.

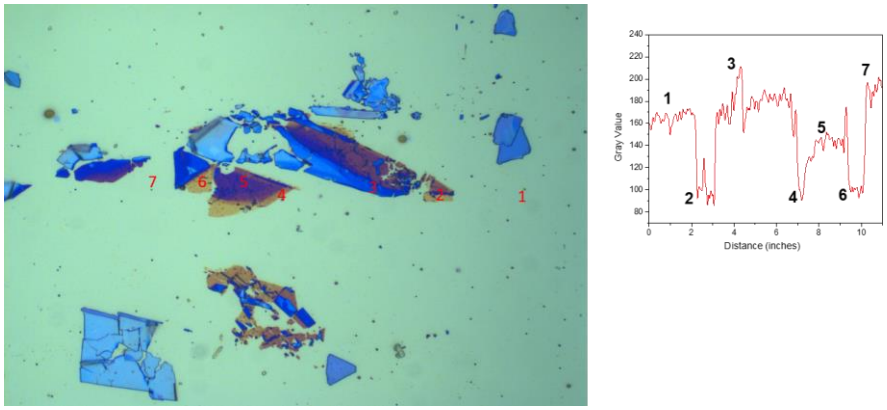

Figure 65. Optical Image of MoS_2 Flakes Deposited on Au Thin Film with Marked ROIs. Inset Figure Shows the Contrast Profile Plots of RIOs.

From the inset plot of Figure 65, it is seen that optical contrast of Au thin film substrate is of higher value when compared to thinner layers of MoS_2 as marked at regions '2', '4' and '6', also for the thicker flakes like at the region '3' the contrast value raises above the value of Au thin film itself. This clear differentiation in the optical contrast values when compared to the substrate values, adds to the advantages of employing Au thin film as a substrate to transfer few to mono layers of MoS_2. Comparing the optical images in Figure 59 and 60, optical color change of MoS_2 flakes with change in thickness is much differentiable in case of deposited films on Au thin film. The prime reason for this can be related to the highly reflective nature of the metal films when shined with light. The reflective light from the Au thin film scatters inside the few layers of MoS_2 and subjects to the change in absorption color of the flakes.

Additionally, optical contrast difference values of the MoS_2 flakes with respect to the gold substrate are calculated and plotted as shown in Figure 66. It is observed that, with the decrease in the thickness of the MoS_2 layers, there is drop in the value of Cd to

negative values, which is seen at regions ‘2’, ‘4’ and ‘6’ of the image. This negative optical contrast values are direct analytical proofs for layer thickness of the MoS_2 layers.

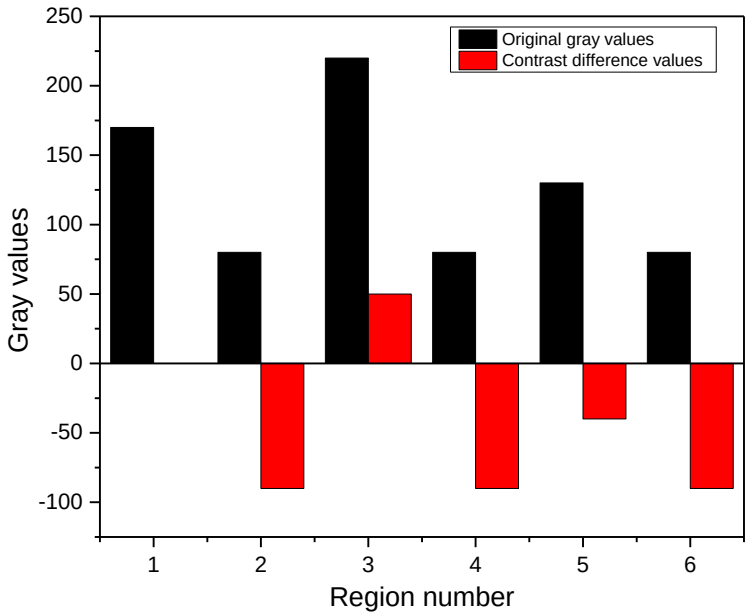

Figure 66. Plot of MoS_2 Optical Contrast and Contrast Difference Values

The regions shaded black in the plot, shows the real values of the contrast of the MoS_2 flakes on Au thin film. The regions shaded red in the plot, shows the contrast difference values of the MoS_2 flakes at the different regions, where the thin flakes give negative value, when compared to the contrast of base Au thin film.

5.4.2 Raman Analysis of Different Number of Layers on MoS_2 on Two Substrate Types

Thickness of MoS_2 flakes deposited on the substrate depends on the number of layers associated with the flake, with single layer of MoS_2 thickness is being around

0.7nm thick. Among all listed characterization tools available for the measurement of the thickness of the MoS_2, Raman spectroscopy is known for its non-destructive, non-invasive and quick way to provide the result. Two prominent Raman modes associated with MoS_2 are E_{2g}^1 vibrational mode generated from in plane vibration of two S atoms and one M atom of MoS_2 and A_{1g} vibrational mode generate from out of plane vibration of two S atoms in opposite direction. Change in these Raman modes w.r.t to frequency difference between the two modes, line width of the two modes, FWHM change of the two modes and intensity of the two modes results in different properties change in the material like change in thickness of the material, doping of the material, stress induced in the material and effects of the substrates.

In this section, we have concentrated on few factors affecting the Raman modes associated with the MoS_2 flakes, which are, sample thickness-based Raman mode frequency difference, intensity rise of the Raman peaks with change in thickness and effect on the intensity of the Raman modes with change in substrate on which the MoS_2 is deposited. Typically, Raman frequency modes E_{2g}^1 and A_{1g} of MoS_2 occur at 386 cm^{-1} and 404 cm^{-1} respectively. The difference in frequency of these two peaks determines the count of layers [108] like, if the difference is of ~19 cm^{-1} it corresponds to monolayer and further increase in this difference like 20 cm^{-1}, 21 cm^{-1}, 22 cm^{-1}, 23 cm^{-1} and 24 cm^{-1} corresponds to 2, 3, 4 layers respectively. If the difference of wavenumber is more than 25 the characterized MoS_2 is noted as bulk.

5.4.2.1 Raman Analysis of MoS_2 on Glass

Raman analysis of the MoS_2 flakes deposited on the glass substrate is performed for obtaining Raman mode frequencies related to different number of MoS_2 layers. Figure 67 shows Raman peaks of MoS_2 flakes of varying thickness ranging from mono layer to four layers. It is seen from the plots that, the frequency difference between E_{2g}^1 and A_{1g} widens with the change in layer number along with the rise in intensity of the peaks. This phenomenon is in line with the literature argument of red shifting of E_{2g}^1 peak and blue shift of A_{1g} peak with rise in number of layers of MoS_2. We have successfully obtained mono layer to few layers MoS_2 deposited on to the glass substrate with our proposed way of mechanical exfoliation method. Figure 68 shows associated optical images depicting the MoS_2 flakes associated with the Raman peaks plotted, Images are obtained from Raman confocal microscopy.

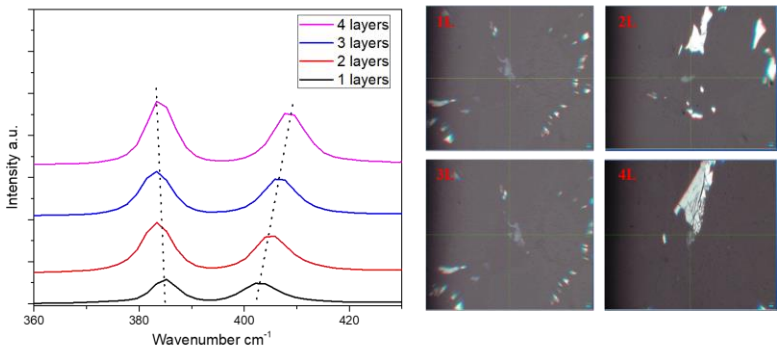

Figure 67. Raman Plots Displaying the Change in Frequency Difference and Intensity Rise

Change in the frequency of the both Raman peaks w.r.t change in layer number of MoS_2, as depicted in Figure 67 is plotted as shown in Figure 68. It is seen from the plot

that, E_{2g}^1 peak moves to lower frequency and A_{1g} peak moves to higher frequency, with increase in number of layers. Change in frequency is more evident in terms of A_{1g} peak rather than with E_{2g}^1 peaks, since the lattice vibrations addition to the addition of multiple layers effects A_{1g} peak more than E_{2g}^1 peak [107]. So, it is seen from the graph, that there is steady increase in the frequency for the A_{1g} peak, where with the E_{2g}^1 peak, from layer 2 to 4 there is no much change in the frequency is observed.

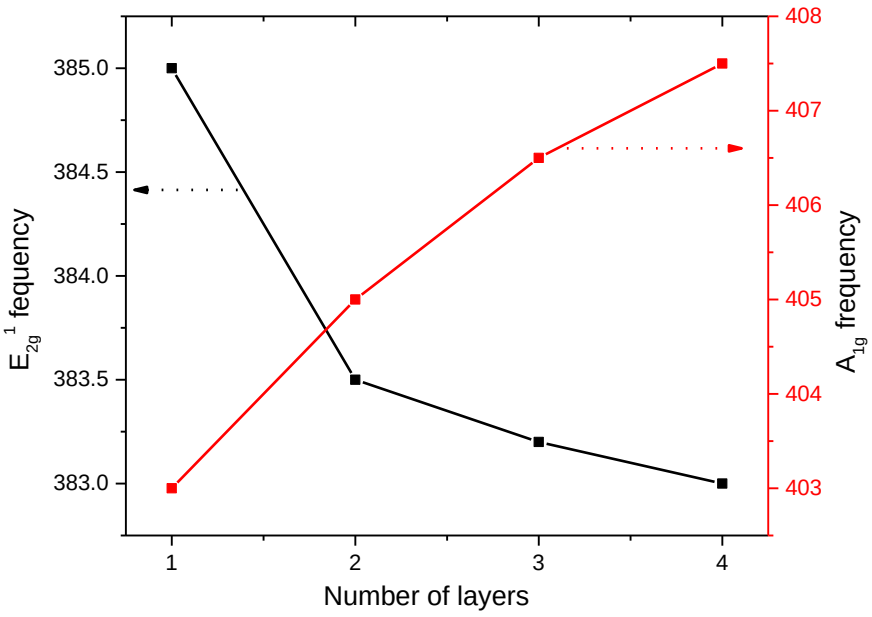

Figure 68. Raman Analysis Plot of E_{2g}^1 and A_{1g} Peaks w.r.t to Layer Change of MoS_2

Raman analysis of MoS_2 flakes deposited on the glass substrate and subjected to layer thinning process as shown in Figure 60 is presented in below Figure 69. It is seen that, based on the frequency difference of the E_{2g}^1 and A_{1g} peaks, Ar plasma exposure has successfully reduced the layer number of the deposited MoS_2 flakes. Before the plasma

exposure, the difference between the peaks is 23 cm^{-1} and after the plasma exposure it is reduced to 18 cm^{-1}, i.e. from 3 layers of as deposited MoS_2 flakes, Ar plasma exposure reduced it to mono layers MoS_2 flake.

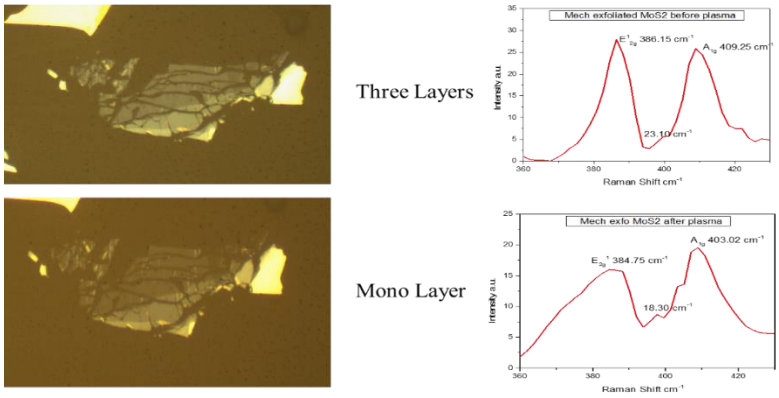

Figure 69. MoS_2 Flakes Deposited on Glass Substrate and Respective Raman Analysis

5.4.2.2 Raman Analysis of MoS_2 on Au Thin Film

Similar Raman analysis are carried out on the MoS_2 flakes that are deposited on the Au thin film. Here in this section, Au thin film of 100nm is employed as the substrate. Number of research articles based on the substrate effects on Raman peaks of MoS_2 are published, including Au thin film surface too. Proposed reasons for change in Raman peaks of MoS_2 due to the Au thin film are, band-gap alignment of MoS_2 and gold film, Electron and exciton transfer between conductive Au film and MoS_2 flakes, Second harmonic peak generation for MoS_2 deposited on the Au, and Surface plasmon effect of metal thin film on the MoS_2 flakes. All these reported studies are more concentrated on the mono-layer MoS_2 and on evaluation of its properties with the integration of Au thin film.

Here-in, we have investigated the Raman peak intensity change with change in number of layers, when MoS_2 is deposited on the gold film. As per the research findings and from our previous section, Raman peak intensity rises with increase in the number of layers till ~4 layers. This phenomenon is reported to be observed for any substrate [124]. But, in our research, when compared with the peak intensities of 4 layers MoS_2 on glass substrate, 4 layers of MoS_2 on gold substrate have seen to increase its intensity multifold. Figure 70 presents the combined plot of Raman peaks associated with different number of layers.

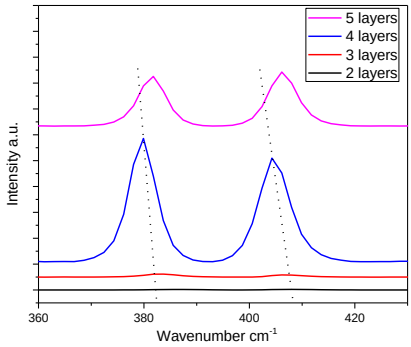

Figure 70. Raman Analysis of MoS_2 Flakes of Different Thickness Deposited on the Gold

Four layers of MoS_2 deposited on Au thin film is seen to have high rise in the intensity when compared to the intensities obtained for lower and higher thickness flakes of MoS_2. Additionally, Raman frequency of the $E_{2g}{}^1$ is seen to blue shift as observed in the case of MoS_2 on glass, but the peak A_{1g} associated with the out of plane vibrations of sulfur atoms tends to blue shift too. This is contradicting result compared to the MoS_2 behavior on glass substrate. This can be attributed to the effect of the Au substrate and

the binding effect of the gold surface with the MoS_2 flakes [107]. Individual plot of the change in frequencies of MoS_2 Raman peaks with change in number of layers is shown in below plot.

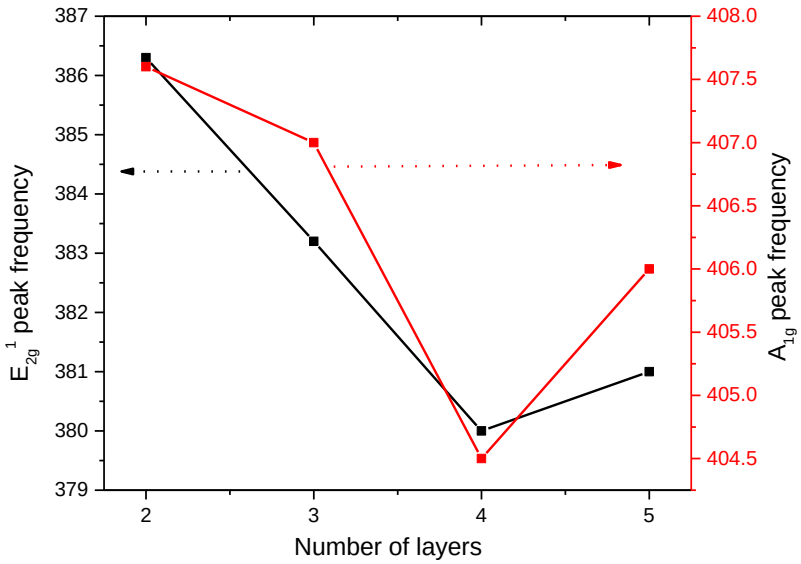

Figure 71. Raman Frequency Plot of E_{2g}^1 and A_{1g} Peaks w.r.t Number of Layers

The plot depicts, A_{1g} frequencies blue shifting and following the pattern of E_{2g}^1 peak frequencies plot. The unusual rise in the intensity of both the Raman peaks of MoS_2 when deposited on the gold film questions the role of gold film. Here, we propose the surface plasmon property of gold film is the reason for the rise in the intensity of MoS_2 Raman peaks. It is known that, this intensity dependence on the number layers of MoS_2 on glass substrate is attributed to the optical scattering inside multi layers leading to high optical absorption and reflectivity of the laser light shined on the substrate. But, in the

case of MoS/Au thin film heterostructure, along with optical scattering phenomenon, underneath Au film contributes to the generation of surface plasmons, which enhances the Raman peak intensities. To prove this proposal, we have used different thickness Au thin films, ranging from 25nm, 50nm, 100nm, 150nm and 200nm as substrates to deposit MoS_2 flakes. Detailed discussion on the experimental procedures and results in related to the plasmonic effect of the gold film thickness is discussed in next section.

5.4.3 Surface Plasmon Analysis of MoS_2/Au Heterostructures

Surface plasmon analysis of Au thin film is verified by employing different thickness of thin films for the deposition of MoS_2 flakes as discussed in previous section. Here, in this section we present the results of role of plasmons generated by Au film substrates using two different experimental analysis. One being, Raman characterization for peak intensity of E_{2g}^1 and A_{1g} modes of MoS_2 on different thickness Au thin films. Second one, being, FDTD simulation analysis of plane Au film deposited on the glass substrate with varying thickness for evaluating plasmon generation on the surface of the film.

MoS_2 flakes of few layers to mono layer are deposited on all selected thickness substrates of Au thin film, by the same procedure as mentioned in the previous sections. From each substrate, four layers thickness MoS_2 flake is selected for plasmon analysis. This selection of MoS_2 flake is done by optical color analysis, contrast analysis and Raman frequency difference analysis as discussed in previous sections. Figure 72 shows combined plot of Raman intensities obtained from four layers of MoS_2 flakes from different Au thickness thin film substrates.

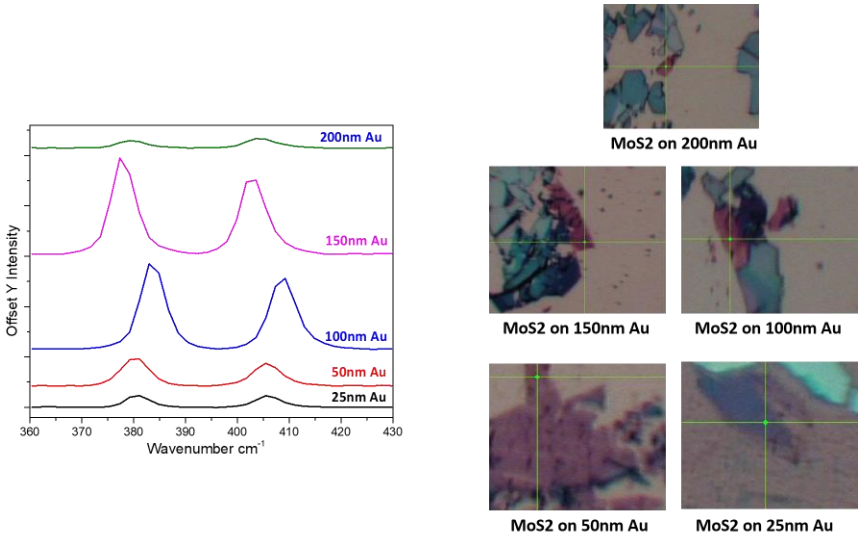

Figure 72. Raman Intensity Analysis of MoS_2 Peaks Associated with Four Layers Deposited on Different Thickness of Au Films

It is seen from the above figure that, there is steady rise in the intensity of four-layer MoS_2 flakes with the rise in the thickness of Au thin film. The rise intensity is stopped after 150nm, i.e. for 200nm the peak intensity is dropped to very low intensity count. With this result, we can confidently argue that, underneath Au thin film is playing significant role in rising the intensity of 4-layer MoS_2. Thickness dependence of Au thin film to generate plasmons, strong enough to influence the MoS_2 Raman peaks is presented. Where, 150nm thick Au film gives highest plasmon generation and in turn rise in the intensity of Raman peaks of MoS_2. The change in intensity values of E_{2g}^1 and A_{1g} peaks with change in Au film thickness are plotted in below Figure 73.

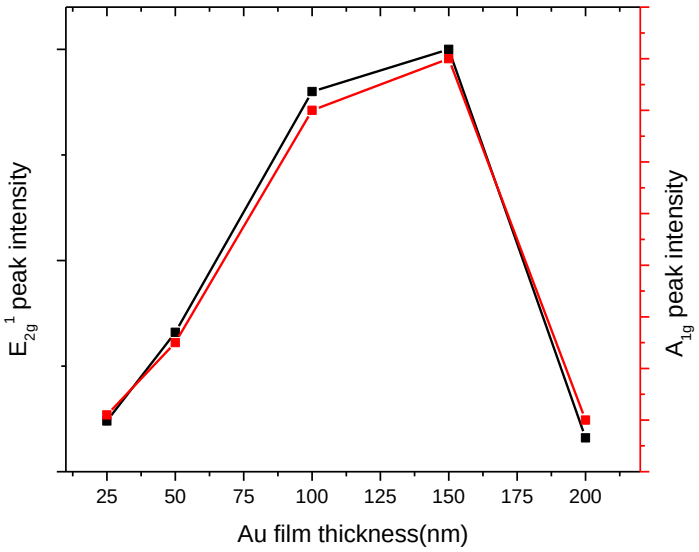

Figure 73. Raman Peak Intensity Analysis w.r.t to Thickness of Au Thin Film

From Figure 72, it is also observed that, there is blue and red shifts of E_{2g}^{1} and A_{1g} peaks depending on the thickness of the Au film. The related value plot is shown below in Figure 74.

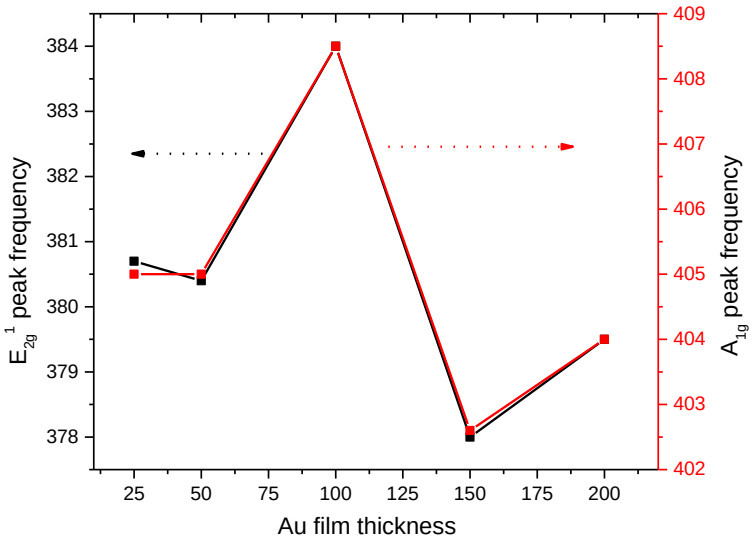

Figure 74. Raman Frequency Analysis Plot of E_{2g}^{1} and A_{1g} Peaks with Respect to the Change in Au Film Thickness

It is interesting to observe that, the frequency plots of two Raman peaks follow same pattern in blue and red shifting when MoS_2 is deposited on the Au substrates. It is seen that irrespective of Au thickness, binding of MoS_2 to Au is playing role in altering the peak positions of the MoS_2.

In second part of validating the plasmon generation on the surface of Au thin films, which in turn effect the rise in intensities of Raman peaks related to MoS_2. We have used FDTD simulation analysis to monitor the electromagnetic field distribution on the surface of the metal thin film, when shined with light (laser) source like in experimental conditions. Below Figure 75 shows the structure created in the FDTD software, with top layer being gold thin film, deposited on glass substrate. Simulation conditions subjected to the structure are, a PML layers in all directions, 532nm plane

wave source pointed towards the surface of the substrate, Reflective and transmission detectors placed above and below respectively, and Surface electric filed detector kept at few nanometers distance of the surface of the Au film. Thickness of Au thin film is varied for every simulation related to specific thickness of the film.

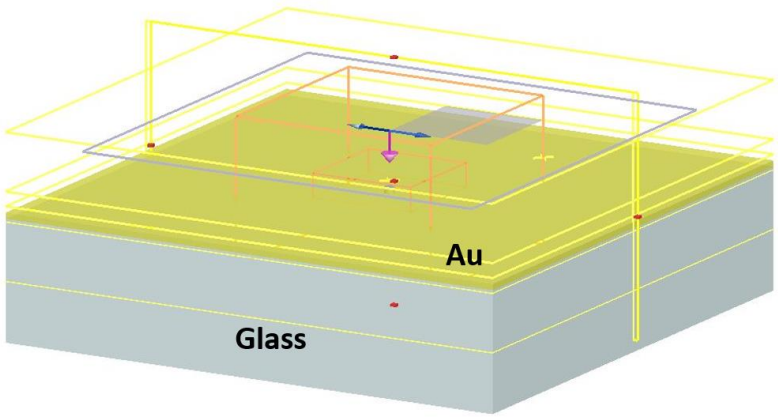

Figure 75. FDTD Simulation Structure for Surface Plasmon Analysis of the Au Thin Film with Varied Thickness of the Film

Simulated results of E field distribution over the surface of the thin film is shown in below Figure 76. Where, it is seen that, the field intensity of the surface plasmons generated, rises with rise in thickness of the Au film, till the point of 150nm and then decrease for 200nm thickness. Scale bar of the intensity value change can be seen beside each simulation result below. This result is perfectly in line with the experimental results shown in first part of the Raman experimental analysis performed to prove the role of surface plasmons and their influence on Raman peak intensity.

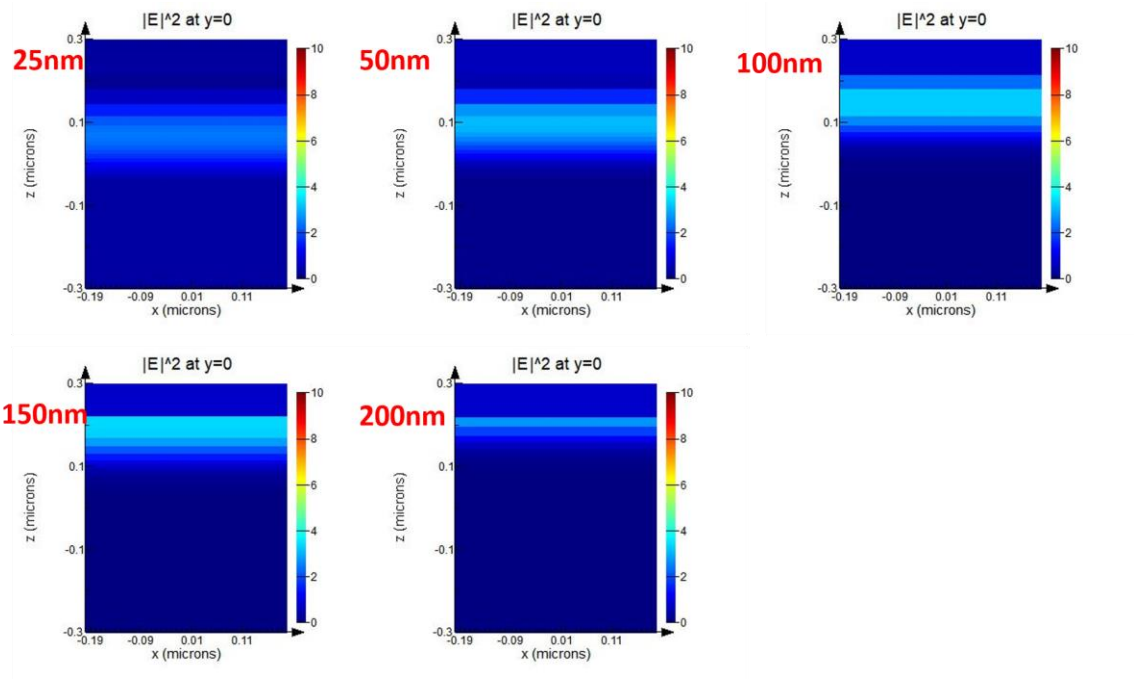

Figure 76. FDTD Simulation Analysis of Au Thin Film w.r.t Rise in the Thickness of Au Film

The E-filed strength distributed on the surface of the gold thin films of different thickness as seen in the Figure 76, is plotted in Figure 77 as shown below. This E field strength plot in Z axis shows the intensity of E field generated on the surface of Au thin film of different thicknesses. The plot shows similar result as discussed in previous section, where, MoS_2 deposited on 100nm and 150nm Au thin film is seen to have high enhancement of Raman signals associated with the same. The intensity graph plot of the E field strength with varying gold film thickness is presented in Figure 77. With this theoretical understanding of the effect of Au thin film plasmon generation with thickness dependence paves a way to support my experimental results observed in the case of MoS_2

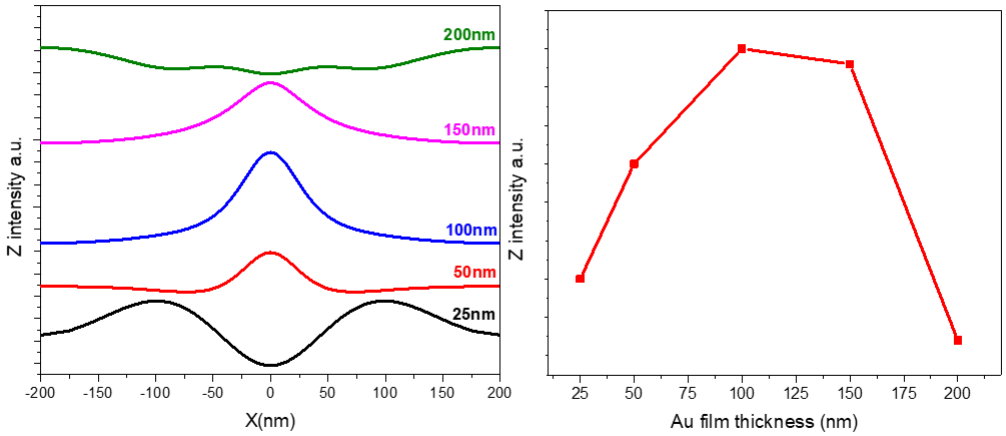

Figure 77. FDTD E-filed Strength Data Plot with Varying Thickness of Au Thin Film

5.4.4 SERS Property Evaluation of MoS_2/Au Heterostructures

Surface enhanced Raman spectroscopy (SERS) is prominent detection methodology employed with use of surface plasmons generated on surface of substrates. Free electrons on the surface of metal surfaces like Ag and Au tend to oscillate according to the frequency of light shined on the surface. This electro-magnetic wave travels along the surface of the metal and when in resonance with the Raman peaks associated with molecules of detection present on the surface, there can be seen rise in the Raman intensities of the detection molecule. This property of plasmon induced enhancement of the Raman peaks is named as surface enhanced Raman spectroscopy. Metal substrates generally show high enhancement of range of ~ 10^{10}. 2 D material, graphene which is atomically flat surface, have free flowing electrons on its surface like metal substrates and shows surface plasmons generation and there are number of reports [] claiming detection of bio-molecules on the surface of graphene with good enhancement factor. 2 D

material MoS_2 is a semiconductor material with tunable bandgap with not many free electrons on the surface of the materials. But, there are reports claiming SERS enhancement for monolayer MoS_2 material, which is seen to have less enhancement when compared to graphene material. Fabrication of monolayer MoS_2 is a complex process, even with using all the three existing methodologies of fabrication, which makes use of MoS_2 limited to the field of SERS based biosensors.

Here-in, we propose a simple and clean way of obtaining SERS enhancement even at the few layers of MoS_2 employed for bio-molecule detection even at low concentrations. Few-layer MoS_2 fabrication is much easier than mono-layer fabrication. With the presence of Au thin film underneath and at thickness (150nm) of the gold, we propose to obtain good Raman enhancement in our detection attempt of Raman probe molecule R6G. The proposed enhancement is compared with enhancement obtained from other thickness of Au films and from the MoS_2 few layers deposited on plane glass. Enhancement calculations are performed for all the detection results. The proposed MoS_2/Au thin film heterostructure platform is simple in making as, there are no nanostructures on the Au platform and few layers of MoS_2 are deposited using simple mechanical exfoliation method.

In this section, we present two experimental proofs and analysis for successfully finding the right combination of Au film thickness and number of MoS_2 layers for obtaining good enhancement in R6G detection signal. One is, evaluating the right thickness of Au thin film giving good plasmonic property and eventually good enhancement in the signal. Second is, Evaluating the proposed few layers MoS_2/ Au thin

film heterostructure platform used as an easy to fabricate detection platform.

Au thickness substrates as mentioned in previous sections have been immersed in rhodamine 6G (R6G) concentration of $2 * 10^{-2}$M for one hour of time, cleaned with Di water, dried in oven at low temperature and blown with N_2 gas before subjecting the substrates to Raman analysis. Raman laser of 532nm at low power of 10% of total laser power is employed for Raman analysis and 50X objective is used to visualize sample under Raman confocal microscope.

Figure 77 shows the R6G molecules specific Raman spectrum for different thickness of Au thin film. It is seen from the plot below that, with increase in the thickness of the Au thin film, there is seen rise in the intensity of Raman peaks associated with R6G. This rise intensity of Raman peaks is seen till 150nm thickness and for 200nm, the intensity drops drastically. This result of detection phenomenon using SERS under varying thickness of Au film is same as enhancement seen in the case of 4-layer MoS_2 Raman peaks due to Au film thickness. To compare the results of Figure 73, here we plot dominant R6G peak 765 cm^{-1} intensity w.r.t thickness of Au thin film as seen in Figure 78. The both plots of Figure 73 and 78 matches exactly proving the influence of Au thin film on the Raman peaks irrespective of the material that is deposited on the film, in our case it is MoS_2, as shown in Figure 72 and R6G, as shown in Figure 77.

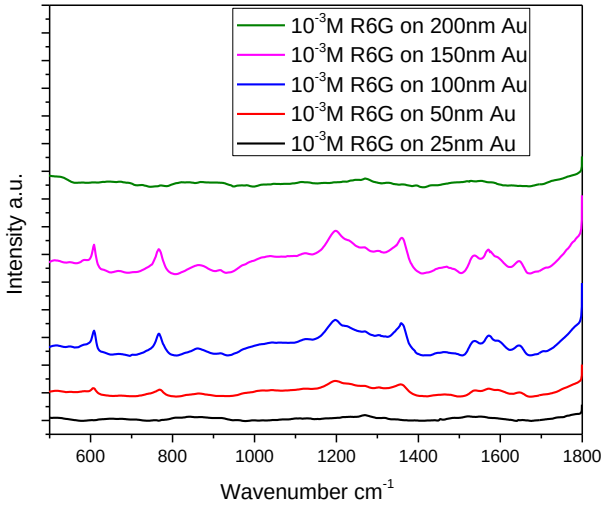

Figure 78. R6G Detection at Higher Concentration on Different Thickness of Au Thin Films

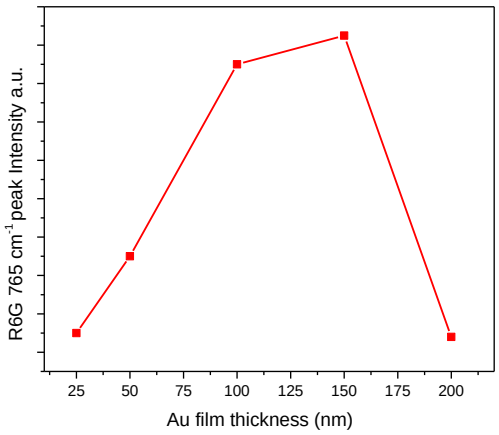

Figure 79. R6G Peak 765 cm^{-1} Intensity Plot w.r.t Thickness of Au Thin Film

With above analysis, it is found that Au film of thickness of 150nm is playing dominant role in enhancing the Raman signals of the material that is deposited on the film.

Further, R6G detection enhancement of MoS_2 material is verified with and without integration of Au thin film.

MoS_2 flakes deposited on the plane glass slide using out mechanical exfoliation method is chosen for the detection analysis. R6G concentration of 10^{-6}M is used in the analysis. MoS_2/glass slide is immersed in R6G solution for an hour and cleaned before using it for Raman analysis. Figure 79 presents the comparison of R6G Raman peaks obtained when deposited on MoS_2/glass slide and on plane glass slide. It is to be noted that, for plane glass, we used higher concentration of R6G solution.

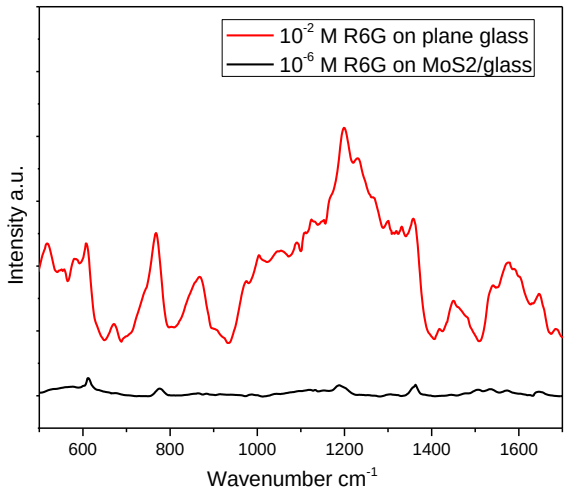

Figure 80. R6G Detection on Plane Glass with Higher Concentration Compared to Detection on MoS_2/Glass at Lower Concentration

It is observed from the above plot that, irrespective of the intensity change, R6G peaks on plane glass lost their structure stability when compared to the peaks obtained when deposited on Au thin films.

Enhancement factor (EF) for detection of R6G molecules on MoS_2/glass substrate is calculated for 765 cm^{-1} peak at concentration of 10^{-6}M. Formula used for the calculation is shown below

$$EF = (I_{SERS}*C_{SR})/(I_{SR}*C_{SERS})$$

Where, I_{SERS} is intensity of R6G peak on MoS_2, I_{SR} is intensity of R6G on glass substrate, C_{SERS} is concentration of R6G used for detection on MoS_2 and C_{SR} is concentration of R6G used on plane glass substrate. With values obtained from Figure 79, calculated EF for MoS_2 on glass is ~10^2, which is same as reported values of detection capability of plane MoS_2 film [144].

R6G detection of MoS_2/Au thin film heterostructure platform is performed on Au thickness films 50nm, 100nm and 150nm, since these three were the films which shown good detection peaks of R6G at higher concentration, in Figure 77. MoS_2 deposited Au films are immersed in 10^{-6}M concentration of R6G for an hour and cleaned before detection analysis. Figure 80 shows the detection peaks of R6G molecule on MoS_2/Au thin film substrates, whereas discussed before 150nm Au thin/ MoS_2 substrate gives good enhanced peaks compared to other Au thickness platforms as shown in Figure 80 below. With the values of peak intensities obtained in Figure 77, EF is calculated for detection of R6G on MoS_2/Au thin film substrates.

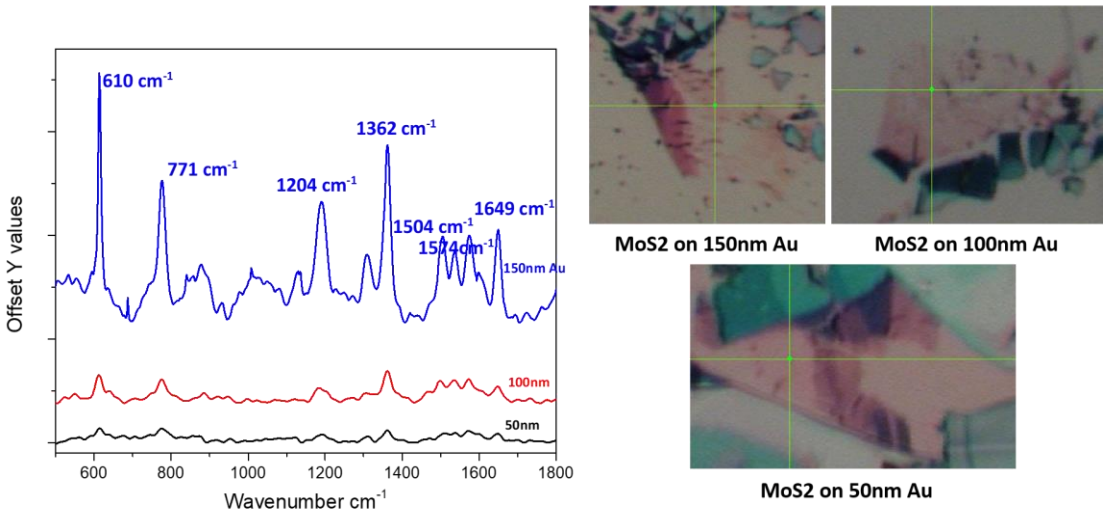

Figure 81. R6G Detection Analysis on MoS_2/Au Thin Film Substrates with Varying Film Thickness

EF obtained for 50nm thin film is similar to the EF obtained for MoS_2/glass substrate i.e. ~10^2, but calculated EF for thin films 100nm and 150nm is seen to increase to ~ $2*10^3$ and ~$3*10^4$ respectively. So from all the results obtained for the combination of MoS_2/Au thin film heterostructure platforms, its is proved that Au thin film of 150nm is having highest generation of plasmons and eventually helping in high SERS property, when integrated with Au thin film. Additionally, it is seen from the figure 80, that the structure of Raman peaks associated with R6G is much sharper when deposited on MoS_2/Au thin film substrates.

Based on the high plasmonic generation seen on the surface of 150nm Au thin film, we have investigated the detection of R6G at 10^{-6}M concentration on Few layers of MoS_2 as shown in Figure 81. It is observed that, with rise in the thickness of the MoS_2 flakes, determined based on the optical color contrast analysis and Raman analysis, the

R6G detection capability is decreased. The intensity drops of R6G Raman peaks w.r.t to brightness of the MoS_2 flakes is shown in Figure 81. But, when compared to R6G detection on mono-layer MoS_2/glass substrate, it is seen that, few-layer MoS_2/Au thin film substrates give better enhancement at low concentrations of R6G. The difference is seen both in peak intensity change and in the sharper shape structure obtained for R6G peaks on Au thin film.

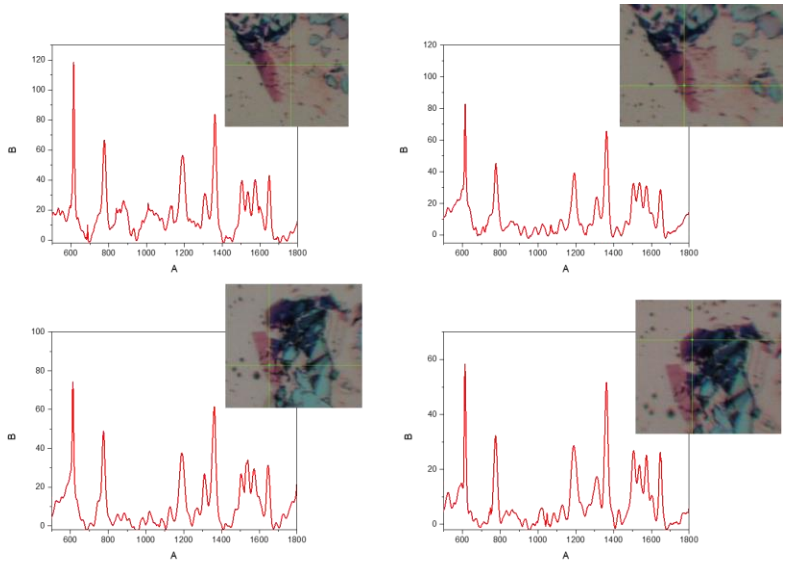

Figure 82. R6G Detection Plots on Few-Layer MoS_2/Au Thin Film (150nm) Substrates

5.5 Discussion

Key observations presented in this work are: 1. Obtained layer thickness of mechanical exfoliated MoS_2 flakes deposited on glass and Au thin film substrates using thermal tape peeling method is seen to further thinned using mild Ar plasma exposure for 2min of time. 2. Optical contrast difference calculations are performed between contrast value of MoS_2 flake when compared with contrast value of substrate on which the MoS_2

flakes are deposited. This analysis proves the reduction in layer thickness compared to the observation in the color change of the flakes. 3. Raman peak intensity of MoS_2 is varied with rise in the thickness of the material. This enhancement of intensity is multi-folded when MoS_2 flakes of different thickness are deposited on Au thin films. This phenomenon is attributed to the plasmons generation on the surface of Au thin film. 4. With support of FDTD analysis, R6G detection analysis (both on plane Au thin film and MoS_2/Au thin films) its proven that 150nm thick Au film gives highest enhancement for the detection with EF of ~$3*10^4$.

In present work, through Raman analysis of MoS_2 flakes with different thickness deposited on two different substrates (glass and gold film) is presented. It is understood from the analysis that Au thin film plays role in affecting the Raman peaks both in intensity rise and in frequency shift. Frequency shift of the Raman peaks is attributed to the strong binding of the MoS_2 flakes to the Au thin film substrate. Intensity rise of Raman peaks is seen to have significantly high value at 4-layers of MoS_2 deposited on Au thin film. This phenomenon is further verified for the plasmonic effect of the underneath Au thin film by varying the thickness of Au thin film and performing Raman analysis on the same. From the results it is seen that, Au thin film of thickness 150nm is having highest enhancement generation capability, which is proved by FDTD simulation results and R6G detection results on plane gold film substrates and on MoS_2/Au thin film heterostructure substrates.

This work presents new way of obtaining good enhancement in detection signal of a molecule, in this case R6G, when deposited on few layers of MoS_2. Since, few- layer

MoS_2 have very less enhancement capability as such. Integrating few-layer MoS_2 with right thickness of Au thin film, we can design an easy way to fabricate platform for SERS based bio-sensor applications.

CHAPTER VI

CONCLUSION

In summary to my thesis work, two proposed projects on design, understanding and development of novel new age platforms for surface enhanced Raman spectroscopy (SERS) applications are completed.

Solid-state silver nanowires are new to the research fields that are working on silver nanowires for various applications. In the past decade of the metal nanowire research, there are very rare attempts to grow the wires in bottom-up and solid-state form. Till now only semiconducting nanowires are proved to be grown in such manner. Here, in the first section of my work, I have presented a methodology, where silver nanowires can be growth in bottom-up and solid-state mode from a polymer substrate. Importantly, this process of growth is attempted through 'green' chemistry manner and performed at room temperature.

Ag nanoparticles are synthesized from chitosan polymer solution and silver precursor $AgNO_3$ mixture, when subjected to ultrasonication. Here, polymer acts as both reducing and stabilizing agent for forming Ag nanoparticles. Silver nanowires (AgNWs) growth is attempted with the formation of Ag/Chitosan solution into thin films by drop-casting the same on PET substrates. Three main conditions influencing the solid-state growth of proposed Ag NWs are: 1. Oxidative etching, which is commonly seen in solution processing, where oxygen from the environment reacts with Ag atoms, which are

favorable to form Ag NWs and dissociates them to form spherical Ag NPs. In our work, the blocking of oxygen is not attempted during the formation of Ag NPs in the solution but, is blocked when the Ag/chitosan solution is made into films. A thin film of Au/Pd is sputter coated on to the film to avoid oxygen interaction over the surface of the film. This proposed mechanism of blocking oxygen is new of its kind and successfully proved to have worked in helping the self-growth of Ag NWs. 2. Role of Cl^- ion is studied in terms of formation of AgCl nano-cubes, which eventually servers as a source of growth of solid-state Ag NWs from the polymer base. Different concentrations of NaCl additive is added to the reaction solution, to form equally different concentrations of AgCl nanoparticles. With the help of different characterization techniques, I have successfully deduced the right concentration of NaCl that initiates the growth of Ag NWs, which further grown into high aspect ratio wires. 3. Time analysis for the change in length and width of the nanowire is performed on the Ag/Chitosan films using SEM. It is observed that our proposed self-growth Ag NWs, have energy and enough source in the polymer base to grow to a length of 30µm and a width of 500nm in a period of seven weeks. Based on the above three important growth factor analysis, Perfect platform of large area grown solid-state silver nanowires is obtained. This platform is attempted to be used for SERS application for the detection of Raman probe molecule R6G. The results showed prominent detection capability of the platform, extending the detection limit to 10^{-7}M with a sensitivity recorded as $R^2 = 0.9986$.

MoS_2 and its use for SERS applications is studied thoroughly is many previous research articles. MoS_2 is studied to have very low detection capability (<100) for any

molecules deposited on its surface. Further, research findings state that, only mono-layer MoS_2 can be used for enhancement studies, as with the increase in the number of layers, the MoS_2 moves to indirect band gap, which don't show any free electron oscillations. Growth of mono-layer MoS_2 is a complex process, in all the three existing ways of fabricating compared to growth of few-layer MoS_2. So, there is an urgent need in a system where, with employing few layers of MoS_2, detection of molecules is achieved at low concentrations.

In this part of my work, I have designed a heterostructure platform consisting of few-layer MoS_2 and Au thin film for its use in SERS application to detect R6G molecule at low concentration of 10^{-6}M. This proposed method is easy to fabricate and quick in its detection procedure. The designed platform is validated using Optical microscopy and Raman spectroscopy for detection of thickness of MoS_2 flakes deposited on the substrates. ImageJ software is extensively used to validate the layer thinning procedure attempted in our study for obtaining thin flakes of MoS_2. Raman spectroscopy is proven sensitive tool which gives thickness of MoS_2 flakes based on the frequency difference between two dominant Raman peaks along with intensity change of the peaks. These two methods are made use to validate our platform of MoS_2 deposited on Au thin film. From Raman analysis of MoS_2 on gold, it is observed that, there is rise in the peak intensity of Raman peaks of MoS_2, especially for ~4 layers of MoS_2. This phenomenon is investigated by change in the thickness of Au thin film, which has given result of dependence of Au thin film thickness for the reason for increase in Raman peak intensity. Further, this phenomenon is assumed due to surface plasmon generation on the surface of

the film, which is validated using FDTD simulation analysis on all different thickness Au films. The result of FDTD analysis showed 150nm thickness is giving high plasmon generation. Further, integrating few-layers of MoS_2 on to the 150nm Au thin film and detecting R6G molecule at low concentration is performed to give an enhancement capability of ~10^4 when compared to ~100 enhancement of mono-layer MoS_2 deposited on the glass.

REFERENCES

[1] S. Coskun, B. Aksoy, and H. E. Unalan, "Polyol Synthesis of Silver Nanowires: An Extensive Parametric Study," *Crystal Growth & Design,* vol. 11, pp. 4963-4969, 2011/11/02 2011.

[2] W. M. Schuette and W. E. Buhro, "Polyol Synthesis of Silver Nanowires by Heterogeneous Nucleation; Mechanistic Aspects Influencing Nanowire Diameter and Length," *Chemistry of Materials,* vol. 26, pp. 6410-6417, 2014/11/25 2014.

[3] H. Xie, X. Yang, D. Du, Y. Zhao, and Y. Wang, "Flexible Transparent Conductive Film Based on Random Networks of Silver Nanowires," *Micromachines,* vol. 9, p. 295, 2018.

[4] H. Chevva, R. Chandran, D. LaJeunesse, and J. Wei, "Solid-state growth of Ag nanowires and analysis of the self-growing process on a bio-polymer chitosan film," *New Journal of Chemistry,* 2019.

[5] D. Elieh-Ali-Komi and M. R. Hamblin, "Chitin and Chitosan: Production and Application of Versatile Biomedical Nanomaterials," *International journal of advanced research,* vol. 4, pp. 411-427, 2016.

[6] X. Li and H. Zhu, "Two-dimensional MoS2: Properties, preparation, and applications," *Journal of Materiomics,* vol. 1, pp. 33-44, 2015/03/01/ 2015.

[7] J. Kang, L. Zhang, and S.-H. Wei, "A Unified Understanding of the Thickness-Dependent Bandgap Transition in Hexagonal Two-Dimensional Semiconductors," *The Journal of Physical Chemistry Letters,* vol. 7, pp. 597-602, 2016/02/18 2016.

[8] Y.-H. Lee, X.-Q. Zhang, W. Zhang, M.-T. Chang, C.-T. Lin, K.-D. Chang, *et al.*, "Synthesis of Large-Area MoS2 Atomic Layers with Chemical Vapor Deposition," *Advanced Materials,* vol. 24, pp. 2320-2325, 2012.

[9] X. Fan, P. Xu, D. Zhou, Y. Sun, Y. C. Li, M. A. T. Nguyen, *et al.*, "Fast and Efficient Preparation of Exfoliated 2H MoS2 Nanosheets by Sonication-Assisted Lithium Intercalation and Infrared Laser-Induced 1T to 2H Phase Reversion," *Nano Letters,* vol. 15, pp. 5956-5960, 2015/09/09 2015.

[10] H. Li, J. Wu, Z. Yin, and H. Zhang, "Preparation and Applications of Mechanically Exfoliated Single-Layer and Multilayer MoS2 and WSe2 Nanosheets," *Accounts of Chemical Research,* vol. 47, pp. 1067-1075, 2014/04/15 2014.

[11] S. Marpu, S. S. Kolailat, D. Korir, B. L. Kamras, R. Chaturvedi, A. Joseph, *et al.*, "Photochemical formation of chitosan-stabilized near-infrared-absorbing silver Nanoworms: A “Green” synthetic strategy and activity on Gram-negative pathogenic bacteria," *Journal of Colloid and Interface Science,* vol. 507, pp. 437-452, 2017.

[12] T. K. Sau and A. L. Rogach, "Nonspherical noble metal nanoparticles: Colloid-chemical synthesis and morphology control," *Advanced Materials,* vol. 22, pp. 1781-1804, 2010.

[13] X. Lu, M. Rycenga, S. E. Skrabalak, B. Wiley, and Y. Xia, "Chemical synthesis of novel plasmonic nanoparticles," in *Annual Review of Physical Chemistry* vol. 60, ed, 2009, pp. 167-192.

[14] S. Guo and E. Wang, "Noble metal nanomaterials: Controllable synthesis and application in fuel cells and analytical sensors," *Nano Today,* vol. 6, pp. 240-264, 2011.

[15] A. Haider and I. K. Kang, "Preparation of silver nanoparticles and their industrial and biomedical applications: A comprehensive review," *Advances in Materials Science and Engineering,* vol. 2015, 2015.

[16] R. Jin, "Atomically precise metal nanoclusters: Stable sizes and optical properties," *Nanoscale,* vol. 7, pp. 1549-1565, 2015.

[17] Q. Zhou, J. Lv, Y. Ren, J. Chen, D. Gao, Z. Lu, *et al.*, "A green in situ synthesis of silver nanoparticles on cotton fabrics using Aloe vera leaf extraction for durable ultraviolet protection and antibacterial activity," *Textile Research Journal,* vol. 87, pp. 2407-2419, 2017.

[18] N. I. Hulkoti and T. C. Taranath, "Biosynthesis of nanoparticles using microbes-A review," *Colloids and Surfaces B: Biointerfaces,* vol. 121, pp. 474-483, 2014.

[19] V. K. Sharma, R. A. Yngard, and Y. Lin, "Silver nanoparticles: Green synthesis and their antimicrobial activities," *Advances in Colloid and Interface Science,* vol. 145, pp. 83-96, 2009.

[20] K. Peppler and J. Janek, "Template assisted solid state electrochemical growth of silver micro- and nanowires," *Electrochimica Acta,* vol. 53, pp. 319-323, 2007/12/01/ 2007.

[21] M. Rycenga, C. M. Cobley, J. Zeng, W. Li, C. H. Moran, Q. Zhang, *et al.*, "Controlling the Synthesis and Assembly of Silver Nanostructures for Plasmonic Applications," *Chemical Reviews,* vol. 111, pp. 3669-3712, 2011/06/08 2011.

[22] K. Zou, X. H. Zhang, X. F. Duan, X. M. Meng, and S. K. Wu, "Seed-mediated synthesis of silver nanostructures and polymer/silver nanocables by UV irradiation," *Journal of Crystal Growth,* vol. 273, pp. 285-291, 2004/12/17/ 2004.

[23] H.-H. Park, X. Zhang, Y.-J. Choi, H.-H. Park, and R. H. Hill, "Synthesis of Ag Nanostructures by Photochemical Reduction Using Citrate-Capped Pt Seeds," *Journal of Nanomaterials,* vol. 2011, p. 7, 2011.

[24] D. Kim, S. Jeong, and J. Moon, "Synthesis of silver nanoparticles using the polyol process and the influence of precursor injection," *Nanotechnology,* vol. 17, pp. 4019-4024, 2006/07/14 2006.

[25] M. R. Johan, N. A. K. Aznan, S. T. Yee, I. H. Ho, S. W. Ooi, N. Darman Singho, *et al.*, "Synthesis and Growth Mechanism of Silver Nanowires through Different Mediated Agents (CuCl2 and NaCl) Polyol Process," *Journal of Nanomaterials,* vol. 2014, p. 7, 2014.

[26] Y. Sun, B. Mayers, T. Herricks, and Y. Xia, "Polyol Synthesis of Uniform Silver Nanowires: A Plausible Growth Mechanism and the Supporting Evidence," *Nano Letters,* vol. 3, pp. 955-960, 2003/07/01 2003.

[27] X. Xu, S. He, C. Zhou, X. Xia, L. Xu, H. Chen, *et al.*, "Largely-increased length of silver nanowires by controlled oxidative etching processes in solvothermal reaction and the application in highly transparent and conductive networks," *RSC Advances,* vol. 6, pp. 105895-105902, 2016.

[28] T. Haggren, V. Khayrudinov, V. Dhaka, H. Jiang, A. Shah, M. Kim, *et al.*, "III–V nanowires on black silicon and low-temperature growth of self-catalyzed rectangular InAs NWs," *Scientific Reports,* vol. 8, p. 6410, 2018/04/23 2018.

[29] G. Pozina, A. R. Gubaydullin, M. I. Mitrofanov, M. A. Kaliteevski, I. V. Levitskii, G. V. Voznyuk, *et al.*, "Approach to high quality GaN lateral nanowires and planar cavities fabricated by focused ion beam and metal-organic vapor phase epitaxy," *Scientific Reports,* vol. 8, p. 7218, 2018/05/08 2018.

[30] Z.-x. Yang, Y. Yin, J. Sun, L. Bian, N. Han, Z. Zhou, *et al.*, "Chalcogen passivation: an in-situ method to manipulate the morphology and electrical property of GaAs nanowires," *Scientific Reports,* vol. 8, p. 6928, 2018/05/02 2018.

[31] F. Hayee, T. C. Narayan, N. Nadkarni, A. Baldi, A. L. Koh, M. Z. Bazant, *et al.*, "In-situ visualization of solute-driven phase coexistence within individual nanorods," *Nature Communications,* vol. 9, p. 1775, 2018/05/02 2018.

[32] Y. Robin, S. Y. Bae, T. V. Shubina, M. Pristovsek, E. A. Evropeitsev, D. A. Kirilenko, *et al.*, "Insight into the performance of multi-color InGaN/GaN nanorod light emitting diodes," *Scientific Reports,* vol. 8, p. 7311, 2018/05/09 2018.

[33] W. Ning, F. Kong, Y. Han, H. Du, J. Yang, M. Tian, *et al.*, "Robust surface state transport in thin bismuth nanoribbons," *Scientific Reports,* vol. 4, p. 7086, 11/18/online 2014.

[34] L. Zhang, G. Wu, F. Gu, and H. Zeng, "Single MoO3 nanoribbon waveguides: good building blocks as elements and interconnects for nanophotonic applications," *Scientific Reports,* vol. 5, p. 17388, 11/27/online 2015.

[35] J. I. Cerdá, J. Sławińska, G. Le Lay, A. C. Marele, J. M. Gómez-Rodríguez, and M. E. Dávila, "Unveiling the pentagonal nature of perfectly aligned single-and double-strand Si nano-ribbons on Ag(110)," *Nature Communications,* vol. 7, p. 13076, 10/06/online 2016.

[36] K. C. Goddeti, C. Lee, Y. K. Lee, and J. Y. Park, "Three-dimensional hot electron photovoltaic device with vertically aligned TiO2 nanotubes," *Scientific Reports,* vol. 8, p. 7330, 2018/05/09 2018.

[37] A. N. Filippin, M. Macias-Montero, Z. Saghi, J. Idígoras, P. Burdet, A. Barranco, *et al.*, "Vacuum template synthesis of multifunctional nanotubes with tailored nanostructured walls," *Scientific Reports,* vol. 6, p. 20637, 02/10/online 2016.

[38] N. A. Lanzillo, N. Kharche, and S. K. Nayak, "Substrate-induced Band Gap Renormalization in Semiconducting Carbon Nanotubes," *Scientific Reports,* vol. 4, p. 3609, 01/09/online 2014.

[39] W.-H. Xu, L. Wang, Z. Guo, X. Chen, J. Liu, and X.-J. Huang, "Copper Nanowires as Nanoscale Interconnects: Their Stability, Electrical Transport, and Mechanical Properties," *ACS Nano,* vol. 9, pp. 241-250, 2015/01/27 2015.

[40] L. Mai, X. Tian, X. Xu, L. Chang, and L. Xu, "Nanowire Electrodes for Electrochemical Energy Storage Devices," *Chemical Reviews,* vol. 114, pp. 11828-11862, 2014/12/10 2014.

[41] K. Dawson, J. Strutwolf, K. P. Rodgers, G. Herzog, D. W. M. Arrigan, A. J. Quinn, *et al.*, "Single Nanoskived Nanowires for Electrochemical Applications," *Analytical Chemistry,* vol. 83, pp. 5535-5540, 2011/07/15 2011.

[42] M. S. AlSalhi, M. Atif, A. A. Ansari, K. Khun, Z. H. Ibupoto, and M. Willander, "Growth and characterization of ZnO nanowires for optical applications," *Laser Physics,* vol. 23, p. 065602, 2013.

[43] F. Xu, Z.-x. Wu, and Y.-q. Lu, "Nonlinear optics in optical-fiber nanowires and their applications," *Progress in Quantum Electronics,* vol. 55, pp. 35-51, 2017/09/01/ 2017.

[44] Y. Wu and P. Yang, "Direct Observation of Vapor−Liquid−Solid Nanowire Growth," *Journal of the American Chemical Society,* vol. 123, pp. 3165-3166, 2001/04/01 2001.

[45] C. Zhang, X. Miao, P. K. Mohseni, W. Choi, and X. Li, "Site-Controlled VLS Growth of Planar Nanowires: Yield and Mechanism," *Nano Letters,* vol. 14, pp. 6836-6841, 2014/12/10 2014.

[46] M. Siwei and H. K. Adrian, "ZnO nanowire growth by chemical vapor deposition with spatially controlled density on Zn 2 GeO 4 :Mn polycrystalline substrates," *Materials Research Express,* vol. 4, p. 065012, 2017.

[47] P. Li and J. Zhang, "CVD Growth of Carbon Nanotube Forest with Selective Wall-Number from Fe–Cu Catalyst," *The Journal of Physical Chemistry C,* vol. 120, pp. 11163-11169, 2016/05/26 2016.

[48] F. Grace, P. Kumaranand, S. Martin, K. Tadhg, and M. R. Kevin, "Solution synthesis of lead seeded germanium nanowires and branched nanowire networks and their application as Li-ion battery anodes," *Nanotechnology,* vol. 28, p. 255603, 2017.

[49] P. Pertl, M. S. Seifner, C. Herzig, A. Limbeck, M. Sistani, A. Lugstein, *et al.*, "Solution-based low-temperature synthesis of germanium nanorods and nanowires," *Monatshefte für Chemie - Chemical Monthly,* May 02 2018.

[50] X. Li, L. Sun, H. Wang, K. Xie, Q. Long, X. Lai, *et al.*, "Synthesis of cobalt nanowires in aqueous solution under an external magnetic field," *Beilstein Journal of Nanotechnology*, vol. 7, pp. 990-994, 2016.

[51] H. K. Yu and J.-L. Lee, "Growth mechanism of metal-oxide nanowires synthesized by electron beam evaporation: A self-catalytic vapor-liquid-solid process," *Scientific Reports,* vol. 4, p. 6589, 10/10/online 2014.

[52] P. Zhang, I. Wyman, J. Hu, S. Lin, Z. Zhong, Y. Tu, *et al.*, "Silver nanowires: Synthesis technologies, growth mechanism and multifunctional applications," *Materials Science and Engineering: B,* vol. 223, pp. 1-23, 2017/09/01/ 2017.

[53] S. E. H. Murph, C. J. Murphy, A. Leach, and K. Gall, "A Possible Oriented Attachment Growth Mechanism for Silver Nanowire Formation," *Crystal Growth & Design,* vol. 15, pp. 1968-1974, 2015/04/01 2015.

[54] N. O. Weiss and X. Duan, "A guide for nanowire growth," *Proceedings of the National Academy of Sciences,* vol. 110, pp. 15171-15172, 2013.

[55] R. G. Hobbs, N. Petkov, and J. D. Holmes, "Semiconductor Nanowire Fabrication by Bottom-Up and Top-Down Paradigms," *Chemistry of Materials,* vol. 24, pp. 1975-1991, 2012/06/12 2012.

[56] X. Y., Y. P., S. Y., W. Y., M. B., G. B., *et al.*, "One-Dimensional Nanostructures: Synthesis, Characterization, and Applications," *Advanced Materials,* vol. 15, pp. 353-389, 2003.

[57] J. Yao, Y. Wang, K.-T. Tsai, Z. Liu, X. Yin, G. Bartal, *et al.*, "Design, fabrication and characterization of indefinite metamaterials of nanowires," *Philosophical Transactions of the Royal Society A: Mathematical, Physical and Engineering Sciences,* vol. 369, pp. 3434-3446, 2011.

[58] H.-W. Jang, B.-Y. Hwang, K.-W. Lee, Y.-M. Kim, and J.-Y. Kim, "Controlling the size of silver nanowires produced by a tetrabutylammonium dichlorobromide salt-based polyol process: Kinetics of silver crystal growth," *AIP Advances,* vol. 8, p. 025303, 2018.

[59] M. Heiss, Y. Fontana, A. Gustafsson, G. Wüst, C. Magen, D. D. O'Regan, *et al.*, "Self-assembled quantum dots in a nanowire system for quantum photonics," *Nature Materials,* vol. 12, p. 439, 02/03/online 2013.

[60] T. Z. and K. N. A., "One-Dimensional Assemblies of Nanoparticles: Preparation, Properties, and Promise," *Advanced Materials,* vol. 17, pp. 951-962, 2005.

[61] M.-C. Sun, G. Kim, J. H. Lee, H. Kim, S. W. Kim, H. W. Kim, *et al.*, "Patterning of Si nanowire array with electron beam lithography for sub-22nm Si nanoelectronics technology," *Microelectronic Engineering,* vol. 110, pp. 141-146, 2013/10/01/ 2013.

[62] N. F. Za'bah, K. S. K. Kwa, L. Bowen, B. Mendis, and A. O'Neill, "Top-down fabrication of single crystal silicon nanowire using optical lithography," *Journal of Applied Physics,* vol. 112, p. 024309, 2012.

[63] S. F. A. Rahman, N. A. Yusof, M. N. Hamidon, R. M. Zawawi, and U. Hashim, "Top-down fabrication of silicon nanowire sensor using electron beam and optical mixed lithography," in *2014 IEEE International Conference on Semiconductor Electronics (ICSE2014),* 2014, pp. 64-67.

[64] G. Pennelli, "Top down fabrication of long silicon nanowire devices by means of lateral oxidation," *Microelectronic Engineering,* vol. 86, pp. 2139-2143, 2009/11/01/ 2009.

[65] G.-C. He, M.-L. Zheng, X.-Z. Dong, F. Jin, J. Liu, X.-M. Duan, *et al.*, "The Conductive Silver Nanowires Fabricated by Two-beam Laser Direct Writing on the Flexible Sheet," *Scientific Reports,* vol. 7, p. 41757, 02/02/online 2017.

[66] H. Oh, J. Lee, J.-H. Kim, J.-W. Park, and M. Lee, "Fabrication of Invisible Ag Nanowire Electrode Patterns Based on Laser-Induced Rayleigh Instability," *The Journal of Physical Chemistry C,* vol. 120, pp. 20471-20477, 2016/09/15 2016.

[67] J. Huang, D. Fan, Y. Ekinci, and C. Padeste, "Fabrication of ultrahigh resolution metal nanowires and nanodots through EUV interference lithography," *Microelectronic Engineering,* vol. 141, pp. 32-36, 2015/06/15/ 2015.

[68] A. Wolfsteller, N. Geyer, T. K. Nguyen-Duc, P. Das Kanungo, N. D. Zakharov, M. Reiche, *et al.*, "Comparison of the top-down and bottom-up approach to fabricate nanowire-based silicon/germanium heterostructures," *Thin Solid Films,* vol. 518, pp. 2555-2561, 2010/02/26/ 2010.

[69] X. Niu, S. Liu, R. Xing, X. Wang, B. Zhang, J. Chen, *et al.*, "Synthesis of single-crystalline silver sulfide nanowires by diffusion in porous anodic aluminium oxide template," *Materials Letters,* vol. 61, pp. 5098-5101, 2007/12/01/ 2007.

[70] M. Oh, W.-Y. Jin, H. Jun Jeong, M. S. Jeong, J.-W. Kang, and H. Kim, "Silver Nanowire Transparent Conductive Electrodes for High-Efficiency III-Nitride Light-Emitting Diodes," *Scientific Reports,* vol. 5, p. 13483, 09/03/online 2015.

[71] J. Li, W. Zhang, Q. Li, and B. Li, "Excitation of surface plasmons from silver nanowires embedded in polymer nanofibers," *Nanoscale,* vol. 7, pp. 2889-2893, 2015.

[72] H. Wei, D. Pan, and H. Xu, "Routing of surface plasmons in silver nanowire networks controlled by polarization and coating," *Nanoscale,* vol. 7, pp. 19053-19059, 2015.

[73] Q. Li and M. Qiu, "Plasmonic wave propagation in silver nanowires: guiding modes or not?," *Optics Express,* vol. 21, pp. 8587-8595, 2013/04/08 2013.

[74] G. Lu, H. Yuan, L. Su, B. Kenens, Y. Fujita, M. Chamtouri, *et al.*, "Plasmon-Mediated Surface Engineering of Silver Nanowires for Surface-Enhanced Raman Scattering," *The Journal of Physical Chemistry Letters,* vol. 8, pp. 2774-2779, 2017/07/06 2017.

[75] J.-M. Renoirt, M. Debliquy, J. Albert, A. Ianoul, and C. Caucheteur, "Surface Plasmon Resonances in Oriented Silver Nanowire Coatings on Optical Fibers," *The Journal of Physical Chemistry C,* vol. 118, pp. 11035-11042, 2014/05/22 2014.

[76] H. Ditlbacher, A. Hohenau, D. Wagner, U. Kreibig, M. Rogers, F. Hofer, *et al.*, "Silver Nanowires as Surface Plasmon Resonators," *Physical Review Letters,* vol. 95, p. 257403, 12/16/ 2005.

[77] R. S. Jones, R. R. Draheim, and M. Roldo, "Silver Nanowires: Synthesis, Antibacterial Activity and Biomedical Applications," *Applied Sciences,* vol. 8, p. 673, 2018.

[78] S. E. Hunyadi and C. J. Murphy, "Bimetallic silver–gold nanowires: fabrication and use in surface-enhanced Raman scattering," *Journal of Materials Chemistry,* vol. 16, pp. 3929-3935, 2006.

[79] Y. Song, D. Luo, S. Ye, H. Hou, and L. Wang, "Facile fabrication of SERS-active substrates based on discarded silver compact disks," *Applied Surface Science,* vol. 258, pp. 2584-2590, 2012/01/15/ 2012.

[80] C. Song, J. Chen, Y. Zhao, and L. Wang, "Gold-modified silver nanorod arrays for SERS-based immunoassays with improved sensitivity," *Journal of Materials Chemistry B,* vol. 2, pp. 7488-7494, 2014.

[81] C. Marambio-Jones and E. M. V. Hoek, "A review of the antibacterial effects of silver nanomaterials and potential implications for human health and the

environment," *Journal of Nanoparticle Research,* vol. 12, pp. 1531-1551, 2010/06/01 2010.

[82] Z. Zeng, Z. Yin, X. Huang, H. Li, Q. He, G. Lu, *et al.*, "Single-Layer Semiconducting Nanosheets: High-Yield Preparation and Device Fabrication," *Angewandte Chemie International Edition,* vol. 50, pp. 11093-11097, 2011.

[83] Z. Yin, H. Li, H. Li, L. Jiang, Y. Shi, Y. Sun, *et al.*, "Single-Layer MoS2 Phototransistors," *ACS Nano,* vol. 6, pp. 74-80, 2012/01/24 2012.

[84] M. R. Laskar, L. Ma, S. Kannappan, P. S. Park, S. Krishnamoorthy, D. N. Nath, *et al.*, "Large area single crystal (0001) oriented MoS2," *Applied Physics Letters,* vol. 102, p. 252108, 2013.

[85] C. Muehlethaler, C. R. Considine, V. Menon, W.-C. Lin, Y.-H. Lee, and J. R. Lombardi, "Ultrahigh Raman Enhancement on Monolayer MoS2," *ACS Photonics,* vol. 3, pp. 1164-1169, 2016/07/20 2016.

[86] L. Sun, H. Hu, D. Zhan, J. Yan, L. Liu, J. S. Teguh, *et al.*, "Plasma Modified MoS2 Nanoflakes for Surface Enhanced Raman Scattering," *Small,* vol. 10, pp. 1090-1095, 2014.

[87] I. Song, C. Park, and H. C. Choi, "Synthesis and properties of molybdenum disulphide: from bulk to atomic layers," *RSC Advances,* vol. 5, pp. 7495-7514, 2015.

[88] K. S. Novoselov, D. Jiang, F. Schedin, T. J. Booth, V. V. Khotkevich, S. V. Morozov, *et al.*, "Two-dimensional atomic crystals," *Proceedings of the National Academy of Sciences of the United States of America,* vol. 102, pp. 10451-10453, July 26, 2005 2005.

[89] G. Zhang, H. Liu, J. Qu, and J. Li, "Two-dimensional layered MoS2: rational design, properties and electrochemical applications," *Energy & Environmental Science,* vol. 9, pp. 1190-1209, 2016.

[90] Y.-C. Lin, D. O. Dumcenco, Y.-S. Huang, and K. Suenaga, "Atomic mechanism of the semiconducting-to-metallic phase transition in single-layered MoS2," *Nature Nanotechnology,* vol. 9, p. 391, 04/20/online 2014.

[91] Z. Li, Meng, Xiangchao, Zhang, Zisheng, "Recent development on MoS 2 -based photocatalysis: A review," *Journal of Photochemistry and Photobiology C: Photochemistry Reviews,* vol. 35, pp. 1389-5567, 2018.

[92] L. Ottaviano, S. Palleschi, F. Perrozzi, G. D'Olimpio, F. Priante, M. Donarelli, *et al.*, "Mechanical exfoliation and layer number identification of MoS2 revisited," *2D Materials*, vol. 4, p. 045013, 2017/09/08 2017.

[93] G. Z. Magda, J. Pető, G. Dobrik, C. Hwang, L. P. Biró, and L. Tapasztó, "Exfoliation of large-area transition metal chalcogenide single layers," *Scientific Reports*, vol. 5, p. 14714, 10/07/online 2015.

[94] A. Gupta, V. Arunachalam, and S. Vasudevan, "Liquid-Phase Exfoliation of MoS2 Nanosheets: The Critical Role of Trace Water," *The Journal of Physical Chemistry Letters*, vol. 7, pp. 4884-4890, 2016/12/01 2016.

[95] A. Jawaid, D. Nepal, K. Park, M. Jespersen, A. Qualley, P. Mirau, *et al.*, "Mechanism for Liquid Phase Exfoliation of MoS2," *Chemistry of Materials*, vol. 28, pp. 337-348, 2016/01/12 2016.

[96] S. K. Tuteja, T. Duffield, and S. Neethirajan, "Liquid exfoliation of 2D MoS2 nanosheets and their utilization as a label-free electrochemical immunoassay for subclinical ketosis," *Nanoscale*, vol. 9, pp. 10886-10896, 2017.

[97] W. Zhang, X. Xiao, Y. Li, X. Zeng, L. Zheng, and C. Wan, "Liquid-exfoliation of layered MoS2 for enhancing photocatalytic activity of TiO2/g-C3N4 photocatalyst and DFT study," *Applied Surface Science*, vol. 389, pp. 496-506, 12/15/ 2016.

[98] L. Samad, S. M. Bladow, Q. Ding, J. Zhuo, R. M. Jacobberger, M. S. Arnold, *et al.*, "Layer-Controlled Chemical Vapor Deposition Growth of MoS2 Vertical Heterostructures via van der Waals Epitaxy," *ACS Nano*, vol. 10, pp. 7039-7046, 2016/07/26 2016.

[99] A. Özden, F. Ay, C. Sevik, and N. K. Perkgöz, "CVD growth of monolayer MoS2: Role of growth zone configuration and precursors ratio," *Japanese Journal of Applied Physics*, vol. 56, p. 06GG05, 2017/05/08 2017.

[100] Y. Xie, Z. Wang, Y. Zhan, P. Zhang, R. Wu, T. Jiang, *et al.*, "Controllable growth of monolayer MoS2by chemical vapor deposition via close MoO2precursor for electrical and optical applications," *Nanotechnology*, vol. 28, p. 084001, 2017/01/18 2017.

[101] H. Bergeron, V. K. Sangwan, J. J. McMorrow, G. P. Campbell, I. Balla, X. Liu, *et al.*, "Chemical vapor deposition of monolayer MoS2 directly on ultrathin Al2O3 for low-power electronics," *Applied Physics Letters*, vol. 110, p. 053101, 2017.

[102] H. F. Liu, S. L. Wong, and D. Z. Chi, "CVD Growth of MoS2-based Two-dimensional Materials," *Chemical Vapor Deposition,* vol. 21, pp. 241-259, 2015.

[103] S. Balendhran, S. Walia, H. Nili, J. Z. Ou, S. Zhuiykov, R. B. Kaner, *et al.*, "Two-Dimensional Molybdenum Trioxide and Dichalcogenides," *Advanced Functional Materials,* vol. 23, pp. 3952-3970, 2013.

[104] B. Radisavljevic, A. Radenovic, J. Brivio, V. Giacometti, and A. Kis, "Single-layer MoS2 transistors," *Nature Nanotechnology,* vol. 6, p. 147, 01/30/online 2011.

[105] G. Deokar, D. Vignaud, R. Arenal, P. Louette, and J. F. Colomer, "Synthesis and characterization of MoS2nanosheets," *Nanotechnology,* vol. 27, p. 075604, 2016/01/20 2016.

[106] Y. Gong, J. Lin, X. Wang, G. Shi, S. Lei, Z. Lin, *et al.*, "Vertical and in-plane heterostructures from WS2/MoS2 monolayers," *Nature Materials,* vol. 13, p. 1135, 09/28/online 2014.

[107] H. Li, Q. Zhang, C. C. R. Yap, B. K. Tay, T. H. T. Edwin, A. Olivier, *et al.*, "From Bulk to Monolayer MoS2: Evolution of Raman Scattering," *Advanced Functional Materials,* vol. 22, pp. 1385-1390, 2012.

[108] S. Xiao, P. Xiao, X. Zhang, D. Yan, X. Gu, F. Qin, *et al.*, "Atomic-layer soft plasma etching of MoS2," *Scientific Reports,* vol. 6, p. 19945, 01/27/online 2016.

[109] G. Yi Jia, Q. Zhang, Z. Xian Huang, S. Bin Huang, and J. Xu, "Ultrathin gold film modified optical properties of excitons in monolayer MoS2," *Physical Chemistry Chemical Physics,* vol. 19, pp. 27259-27265, 2017.

[110] J. Zeng, M. Yuan, W. Yuan, Q. Dai, H. Fan, S. Lan, *et al.*, "Enhanced second harmonic generation of MoS2 layers on a thin gold film," *Nanoscale,* vol. 7, pp. 13547-13553, 2015.

[111] L. Yu, D. Liu, X.-Z. Qi, X. Xiong, L.-T. Feng, M. Li, *et al.*, "Gap plasmon-enhanced photoluminescence of monolayer MoS2 in hybrid nanostructure," *Chinese Physics B,* vol. 27, p. 047302, 2018/04 2018.

[112] H. Xu, "Enhanced light–matter interaction of a MoS2 monolayer with a gold mirror layer," *RSC Advances,* vol. 7, pp. 23109-23113, 2017.

[113] M. Buscema, G. A. Steele, H. S. J. van der Zant, and A. Castellanos-Gomez, "The effect of the substrate on the Raman and photoluminescence emission of single-layer MoS2," *Nano Research,* vol. 7, pp. 561-571, April 01 2014.

[114] B. J. Robinson, C. E. Giusca, Y. T. Gonzalez, N. D. Kay, O. Kazakova, and O. V. Kolosov, "Structural, optical and electrostatic properties of single and few-layers MoS2: effect of substrate," *2D Materials*, vol. 2, p. 015005, 2015/02/20 2015.

[115] J. Song, L. Lu, Q. Cheng, and Z. Luo, "Surface plasmon-enhanced optical absorption in monolayer MoS2 with one-dimensional Au grating," *Journal of Quantitative Spectroscopy and Radiative Transfer*, vol. 211, pp. 138-143, 2018/05/01/ 2018.

[116] Y. Yu, Z. Ji, S. Zu, B. Du, Y. Kang, Z. Li, *et al.*, "Ultrafast Plasmonic Hot Electron Transfer in Au Nanoantenna/MoS2 Heterostructures," *Advanced Functional Materials*, vol. 26, pp. 6394-6401, 2016.

[117] S. Najmaei, A. Mlayah, A. Arbouet, C. Girard, J. Léotin, and J. Lou, "Plasmonic Pumping of Excitonic Photoluminescence in Hybrid MoS2–Au Nanostructures," *ACS Nano*, vol. 8, pp. 12682-12689, 2014/12/23 2014.

[118] L. Hailong, Z. Bing, G. Tian, C. Fayi, and W. Xijun, "Weak plasmon–exciton coupling between monolayer molybdenum disulfide and aluminum disks," *Optics Letters*, vol. 43, pp. 3204-3207, 2018/07/15 2018.

[119] S. Zu, B. Li, Y. Gong, Z. Li, P. M. Ajayan, and Z. Fang, "Active Control of Plasmon–Exciton Coupling in MoS2–Ag Hybrid Nanostructures," *Advanced Optical Materials*, vol. 4, pp. 1463-1469, 2016.

[120] B. Chakraborty, H. S. S. R. Matte, A. K. Sood, and C. N. R. Rao, "Layer-dependent resonant Raman scattering of a few layer MoS2," *Journal of Raman Spectroscopy*, vol. 44, pp. 92-96, 2013.

[121] Q. Qian, Z. Zhang, and K. J. Chen, "Layer-dependent second-order Raman intensity of $\mathrm{Mo}{\mathrm{S}}_{2}$ and $\mathrm{WS}{\mathrm{e}}_{2}$: Influence of intervalley scattering," *Physical Review B*, vol. 97, p. 165409, 04/09/ 2018.

[122] R. Saito, Y. Tatsumi, S. Huang, X. Ling, and M. S. Dresselhaus, "Raman spectroscopy of transition metal dichalcogenides," *Journal of Physics: Condensed Matter*, vol. 28, p. 353002, 2016/07/07 2016.

[123] X.-L. Li, X.-F. Qiao, W.-P. Han, X. Zhang, Q.-H. Tan, T. Chen, *et al.*, "Determining layer number of two-dimensional flakes of transition-metal dichalcogenides by the Raman intensity from substrates," *Nanotechnology*, vol. 27, p. 145704, 2016/02/24 2016.

[124] S.-L. Li, H. Miyazaki, H. Song, H. Kuramochi, S. Nakaharai, and K. Tsukagoshi, "Quantitative Raman Spectrum and Reliable Thickness Identification for Atomic Layers on Insulating Substrates," *ACS Nano,* vol. 6, pp. 7381-7388, 2012/08/28 2012.

[125] Y. Y. Wang, Z. H. Ni, Z. X. Shen, H. M. Wang, and Y. H. Wu, "Interference enhancement of Raman signal of graphene," *Applied Physics Letters,* vol. 92, p. 043121, 2008.

[126] M. Sakamoto and K.-i. Saitow, "Field enhancement of MoS2: visualization of the enhancement and effect of the number of layers," *Nanoscale,* vol. 10, pp. 22215-22222, 2018.

[127] Y. Y. Xu, C. Yang, S. Z. Jiang, B. Y. Man, M. Liu, C. S. Chen, *et al.*, "Layer-controlled large area MoS2 layers grown on mica substrate for surface-enhanced Raman scattering," *Applied Surface Science,* vol. 357, pp. 1708-1713, 2015/12/01/ 2015.

[128] J. Li, W. Zhang, H. Lei, and B. Li, "Ag nanowire/nanoparticle-decorated MoS2 monolayers for surface-enhanced Raman scattering applications," *Nano Research,* vol. 11, pp. 2181-2189, 2018/04/01 2018.

[129] T. D. Sargeant, M. O. Guler, S. M. Oppenheimer, A. Mata, R. L. Satcher, D. C. Dunand, *et al.*, "Hybrid bone implants: Self-assembly of peptide amphiphile nanofibers within porous titanium," *Biomaterials,* vol. 29, pp. 161-171, 2008/01/01/ 2008.

[130] P. Sarkar, C. Parameswaran, C. Harish, M. B. Chandra, and A. N. Grace, "Kinetics of Silver Nanoparticle Growth Using DMF as Reductant – Effect of Surfactants," *Advanced Materials Research,* vol. 938, pp. 30-35, 2014.

[131] H. Chevva, R. Chandran, D. LaJeunesse, and J. Wei, "Silver nanowires (AgNWs) growth in-situ on chitosan polymer matrix film for SERS application," in *2017 IEEE 17th International Conference on Nanotechnology (IEEE-NANO)*, 2017, pp. 885-889.

[132] R. Long, S. Zhou, B. J. Wiley, and Y. Xiong, "Oxidative etching for controlled synthesis of metal nanocrystals: atomic addition and subtraction," *Chemical Society Reviews,* vol. 43, pp. 6288-6310, 2014.

[133] K. E. Korte, S. E. Skrabalak, and Y. Xia, "Rapid synthesis of silver nanowires through a CuCl- or CuCl2-mediated polyol process," *Journal of Materials Chemistry,* vol. 18, pp. 437-441, 2008.

[134] G. Deignan and I. A. Goldthorpe, "The dependence of silver nanowire stability on network composition and processing parameters," *RSC Advances,* vol. 7, pp. 35590-35597, 2017.

[135] R. Chandran, K. Nowlin, and D. R. LaJeunesse, "Nanosphere Lithography of Chitin and Chitosan with Colloidal and Self-Masking Patterning," *Polymers,* vol. 10, p. 218, 2018.

[136] R. Chandran, H. Chevva, Z. Zeng, Y. Liu, W. Zhang, J. Wei, *et al.*, "Solid-state synthesis of silver nanowires using biopolymer thin films," *Materials Today Nano,* vol. 1, pp. 22-28, 2018/03/01/ 2018.

[137] H. Chevva, R. Chandran, D. LaJeunesse, and J. Wei, "Solid-state growth of Ag nanowires and analysis of the self-growing process on a bio-polymer chitosan film," *New Journal of Chemistry,* vol. 43, pp. 3529-3535, 2019.

[138] R. J. Wu, M. L. Odlyzko, and K. A. Mkhoyan, "Determining the thickness of atomically thin MoS2 and WS2 in the TEM," *Ultramicroscopy,* vol. 147, pp. 8-20, 2014/12/01/ 2014.

[139] N. Choudhary, M. D. Patel, J. Park, B. Sirota, and W. Choi, "Synthesis of large scale MoS2 for electronics and energy applications," *Journal of Materials Research,* vol. 31, pp. 824-831, 2016.

[140] H. Wang, C. Li, P. Fang, Z. Zhang, and J. Z. Zhang, "Synthesis, properties, and optoelectronic applications of two-dimensional MoS2 and MoS2-based heterostructures," *Chemical Society Reviews,* vol. 47, pp. 6101-6127, 2018.

[141] S. Jiang, J. Guo, C. Zhang, C. Li, M. Wang, Z. Li, *et al.*, "A sensitive, uniform, reproducible and stable SERS substrate has been presented based on MoS2@Ag nanoparticles@pyramidal silicon," *RSC Advances,* vol. 7, pp. 5764-5773, 2017.

[142] W. Zhang, P. Zhang, Z. Su, and G. Wei, "Synthesis and sensor applications of MoS2-based nanocomposites," *Nanoscale,* vol. 7, pp. 18364-18378, 2015.

[143] T. Liu and Z. Liu, "2D MoS2 Nanostructures for Biomedical Applications," *Advanced Healthcare Materials,* vol. 7, p. 1701158, 2018.

[144] X. Ling, W. Fang, Y.-H. Lee, P. T. Araujo, X. Zhang, J. F. Rodriguez-Nieva, *et al.*, "Raman Enhancement Effect on Two-Dimensional Layered Materials: Graphene, h-BN and MoS2," *Nano Letters,* vol. 14, pp. 3033-3040, 2014/06/11 2014.

[145] J. Miao, W. Hu, Y. Jing, W. Luo, L. Liao, A. Pan, *et al.*, "Surface Plasmon-Enhanced Photodetection in Few Layer MoS2 Phototransistors with Au Nanostructure Arrays," *Small,* vol. 11, pp. 2392-2398, 2015.

[146] B. Mukherjee, N. Kaushik, R. P. N. Tripathi, A. M. Joseph, P. K. Mohapatra, S. Dhar, *et al.*, "Exciton Emission Intensity Modulation of Monolayer MoS(2) via Au Plasmon Coupling," *Scientific reports,* vol. 7, pp. 41175-41175, 2017.

[147] S. G. Sørensen, H. G. Füchtbauer, A. K. Tuxen, A. S. Walton, and J. V. Lauritsen, "Structure and Electronic Properties of In Situ Synthesized Single-Layer MoS2 on a Gold Surface," *ACS Nano,* vol. 8, pp. 6788-6796, 2014/07/22 2014.

[148] M. Chhowalla, H. S. Shin, G. Eda, L.-J. Li, K. P. Loh, and H. Zhang, "The chemistry of two-dimensional layered transition metal dichalcogenide nanosheets," *Nature Chemistry,* vol. 5, p. 263, 03/20/online 2013.

[149] Y. Lee, H. Kim, J. Lee, S. H. Yu, E. Hwang, C. Lee, *et al.*, "Enhanced Raman Scattering of Rhodamine 6G Films on Two-Dimensional Transition Metal Dichalcogenides Correlated to Photoinduced Charge Transfer," *Chemistry of Materials,* vol. 28, pp. 180-187, 2016/01/12 2016.

[150] M. Velický, G. E. Donnelly, W. R. Hendren, S. McFarland, D. Scullion, W. J. I. DeBenedetti, *et al.*, "Mechanism of Gold-Assisted Exfoliation of Centimeter-Sized Transition-Metal Dichalcogenide Monolayers," *ACS Nano,* vol. 12, pp. 10463-10472, 2018/10/23 2018.